University of Alberta

PARTICLE CAPTURE FROM NON-AQUEOUS MEDIA ON PACKED BEDS

by

RASHMI NARAYAN ©

A thesis submitted to the Faculty of Graduate Studies and Research in partial fulfillment of the requirements for the degree of **MASTER OF SCIENCE**

Department of Chemical and Materials Engineering

Edmonton, Alberta

Fall 1996

University of Alberta

Release Form

Name of Author	:	Rashmi Narayan
Title of Thesis	:	Particle Capture from Non-Aqueous Media on Packed Beds
Degree	:	Master of Science
Year This Degree Granted	:	1996

Permission is hereby granted to the University of Alberta Library to reproduce single copies of this thesis and to lend or sell such copies for private, scholarly, or scientific research purposes only.

The author reserves all other publications and other rights in association with the copyright in the thesis, and except as hereinbefore provided, neither the thesis nor any substantial thereof may be printed or otherwise reproduced in any material form whatever without the author's prior written permission.

VI/9, KEYUR

RCF Colony, Chembur

Mumbai 400 074
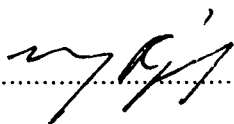
India

September 17, 1996
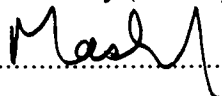
UNIVERSITY OF ALBERTA

FACULTY OF GRADUATE STUDIES AND RESEARCH
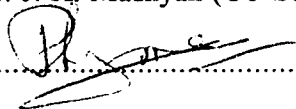
The undersigned certify that they have read, and recommended to the Faculty of Graduate Studies and Research for acceptance, a thesis entitled **PARTICLE CAPTURE FROM NON-AQUEOUS MEDIA ON PACKED BEDS** submitted by **RASHMI NARAYAN** in partial fulfillment of the requirements for the degree of **MASTER OF SCIENCE**.
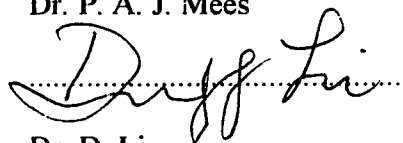
....
Dr. M. R. Gray (Co-Supervisor)

....
Dr. J. H. Masliyah (Co-Supervisor)

....
Dr. P. A. J. Mees

....
Dr. D. Li

Date : 18 Sep '96

Abstract

Hydrotreaters are fixed bed catalytic reactors with cocurrent downflow of hydrocarbon liquid and hydrogen. It was observed that these reactors show excessive pressure build up due to accumulation of fines in the bed, leading to premature shutdown of the reactors. The motivation for this work can be credited to research undertaken at Syncrude Canada Ltd. to study plugging of these reactors.

In order to understand the fundamentals of particle removal in these reactors, we decided to take a step back and study filtration for a single phase hydrocarbon system. The experiments involved studying the capture of carbon black particles from a suspension in kerosene onto a packed bed. Glass beads and catalyst were used as packing. Capture efficiencies and pressure drop build up for both upward and downward flow were monitored during the course of the experiment.

The capture efficiency was found to be independent of the concentration of the suspension for a given set of conditions. With increasing velocity, capture efficiency showed a decrease in value. The capture efficiency, for corresponding velocities, was found to be higher for downward flow as compared to upward flow of the suspension through the packed bed.

An attempt to model the pressure drop build-up across the bed using Ergun's equation proved to be inadequate. Hence this work attempts to predict the anomalous pressure drop build-up by the 'hydraulic diameter' model. However, it was also observed that the pressure drop build-up decreased with increasing velocity of the liquid stream. Photographs obtained of the deposit within the pores of the bed help explain this observation.

Acknowledgements

Table of Contents

drop increase

List of Figures

List of Tables

Nomenclature

a_c	radius of collector, m
a_p	radius of particle, m
A	cross-sectional area of packed bed, m^2
A	absorbance (for spectrophotometry)
A_s	Happel's parameter to account for the bed of spheres
c	volume fraction of deposit within pores
c_s	Cunningham correction factor
C	concentration of particles in fluid stream, kg/m^3
C_i	concentration of particles in fluid stream at the inlet to the packed bed, kg/m^3
C_o	concentration of particles in fluid stream at the outlet from the packed bed, kg/m^3
C_∞	concentration of particles in fluid stream far away from the collector, kg/m^3
d_c	diameter of collector, m
d_{co}	diameter of collector before deposition commences, m
d_p	diameter of particle, m
D_{BM}	Brownian diffusivity ($c_s kT/3\pi\mu d_p$), m^2/s
D_{col}	diameter of packed bed, m
e	elementary charge, C
ΔE	streaming potential, V
E_∞	electric field strength, V/m
g	acceleration due to gravity, m/s^2
H	Hamaker constant, J
I	mass flux of particles over a collector, kg/s
I_i	Intensity of incident light
I_t	Intensity of transmitted light
k	Boltzmann constant, J/K
k_d	permeability of deposit

k_{cell}	cell constant of packed bed, m^{-1}
k_L	mass transfer coefficient, m/s
L	length of packed bed, m
n	number of particles per collector
n_{io}	i^{th} ionic number concentration at time t = 0, m^{-3}
N	number of collectors in bed
N_{ADS}	Adhesion number ($Ha_c^2/9\pi\mu A_s a_p^4 U_\infty$)
N_G	Gravity number ($2a_p^2(\rho_p-\rho)g/9\mu U_\infty$)
$N_{G,S}$	Gravity number as defined by Spielman-Fitzpatrick ($N_G/A_S N_R^2$)
N_{Lo}	London number ($N_{ADS}A_S N_R^2$)
N_{Pe}	Peclet number ($d_c U_\infty/D_{BM}$)
N_R	relative size parameter (d_p/d_c)
N_{Sh}	Sherwood number ($k_L \delta/D_{BM}$)
ΔP	pressure drop across packed bed, N/m^2
$(\Delta P)_o$	pressure drop across packed bed before deposition commences, N/m^2
$(\Delta P)_{packing}$	pressure drop across packed bed before deposition commences, N/m^2
$(\Delta P)_{deposit}$	pressure drop due to deposit, N/m^2
Q	flow rate of fluid stream, m^3/s
Re	Reynolds number ($d_c U_\infty \rho/\mu$)
R_{KCl}	resistance of KCl solution in column, Ω
R_{ker}	resistance of kerosene in column, Ω
R_p	resistance of kerosene solution in column when packed, Ω
St	Stokes number ($2c_s\rho_p U_\infty a_p^2/9\mu a_c$)
t	time, s or h
T	temperature, K
U	electrophoretic velocity, m/s
U_∞	superficial velocity of fluid stream/ empty bed velocity, m/s
V_S	settling velocity of particles, m/s
x	distance from a charged surface, m

x	distance along a packed bed, m
z_i	absolute value of the valency for a (z:z) electrolyte
α	occlusion parameter
β	inverse dependence of filter coefficient on superficial velocity
δ_f	thickness of a film, m
χ	specific conductivity, Ω^{-1} m^{-1}
χ_B	bulk specific conductivity of fluid, Ω^{-1} m^{-1}
χ_P	specific conductivity of fluid including wall and packing, Ω^{-1} m^{-1}
χ_{KCl}	specific conductivity of KCl solution, Ω^{-1} m^{-1}
χ_{ker}	specific conductivity of kerosene, Ω^{-1} m^{-1}
ε	porosity of packed bed
ε_o	porosity of packed bed before deposition commences
ε_d	porosity of deposit
η	efficiency of packed bed
η_I	efficiency due to interception ($3A_S N_R^2/2$)
η_D	efficiency due to diffusion ($4A_S^{4/3} N_{Pe}^{-2/3}$)
η_G	efficiency due to gravity ($A_S N_G$)
η_S	single collector efficiency
$(\eta_S)_I$	single collector efficiency due to interception ($3N_R^2/2$)
$(\eta_S)_{BM}$	single collector efficiency due to Brownian motion ($4A_S^{1/3} N_{Pe}^{-2/3}$)
$(\eta_S)_G$	single collector efficiency due to gravity (N_G)
κ	inverse Debye length, m^{-1}
λ	filter coefficient, cm^{-1} or m^{-1}
λ_o	initial filter coefficient, cm^{-1} or m^{-1}
λ_{ss}	filter coefficient at steady state, cm^{-1} or m^{-1}
μ	viscosity of fluid medium, $kg\ m^{-1}s^{-1}$
ρ	density of fluid medium, $kg\ m^{-3}$
ρ_p	density of particle, $kg\ m^{-3}$
σ	specific deposit (mass of deposit/volume of empty bed), kg/m^3 or mg/mL

ξ	dielectric constant of medium
ξ_0	permittivity of vacuum, C/mV
ψ	electric potential, V
ψ_s	surface potential, V
ψ_D	potential at the Stern plane, V
ζ	zeta potential, V

Chapter One

Introduction

Granular filtration refers to the process of capture of fine particles from a suspension onto the surface of granules in a packed bed. It is important to note that such a mode of capture results in the removal of particles smaller than the pores of the filter medium, particles which would have otherwise been regarded as non-filterable. This mode of clarification of a suspension differs from cake filtration, which deals with the removal of particles within a wide range of size and from relatively concentrated suspensions. The result is the formation of a cake on the surface of the filter medium which strains particles from the passing liquid. Granular filtration, which is commonly referred to as deep bed filtration, refers to the removal of fine particles from dilute suspensions. In this case, deposition of particles on the granules is more or less uniform within the granular medium (or packed bed).

Reference to granular filtration dates back to as early as 200 B.C (Tien, 1989). The principal application of this process, then and now, is water filtration. Impurities in water can be reduced to levels of 0.1 ppm after deep bed filtration by passage through sand filters. In addition, this process is finding wide applications in waste water treatment and gas cleaning. Although extensive work has been done to understand this phenomenon in aqueous suspensions, granular filtration in non-aqueous liquids is a relatively unexplored topic. However, it would be inappropriate to conclude that deep bed filtration in non-aqueous systems is not of importance. Fine particle deposition is commonly observed in the petroleum industry in hydrotreaters and other packed bed reactors. It is a widespread problem and is of concern in refineries all over the world. In these packed bed reactors, a two phase mixture of the hydrocarbon liquid and hydrogen flows cocurrently in the downward direction. The flow regime is either pulsed or trickle flow. The pulsed flow regime is normally characterized by erratic pressure drop. Due to granular filtration, fine particles from the hydrocarbon liquid feed plug the pores between the pellets of the catalytic reactors resulting in excessive pressure build up.

1

In the Mizushima refinery in Japan, it was found that iron sulfide particles along with coke formed during the reaction plugged the catalytic bed in the resid desulfurization unit (Koyama et al., 1995a). The resulting poor liquid distribution led to the formation of "hot spots", leading in turn to increased conversion rate of heavy molecules thus producing more coke. The problem was partly resolved by improving catalyst loading procedures, changing the shape of the catalyst, improving liquid distribution and implementing a recycle of product oil (Koyama et. al. 1995b).

Similar problems are also observed in Canada. At Syncrude Canada Ltd. in Fort McMurray, clay particles in the hydrocarbon liquid feed deposited in the hydrotreater catalyst beds. The majority of the plugging was due to fine particles in the suspension rather than coke formed during hydrotreating or attrited catalyst. The consequence of this deposition was the premature shutdown of the reactor due to high pressure drop build-up (by a deposit of 4-6%wt of fines on the catalyst) rather than loss of activity of the catalyst. A typical composition of the fines is given in Table 1.1.

	% wt of the fines
Clay particles	65
Coke	5
Attrited catalyst	30

Table 1.1 Typical composition of the fines deposit on the hydrotreater catalyst at Syncrude Canada Ltd.

To study this problem, Chan et al. (1993) at Syncrude Canada Ltd Research performed "cold studies" to investigate capture efficiency and pressure drop build-up due to deposition of clay particles in a catalytic bed, with a gas and liquid feed. They observed that the capture efficiencies increased with increasing gas flux, which is contrary to what one might expect. To understand the effect of hydrotreating conditions on the morphology of the deposit, they carried out "hot tests" in a CSTR with clay particles in gas oil, hydrogen and catalyst. They observed that the clay particles become covered with a layer of coke. The clay particles themselves no longer remained as individual particles, but formed aggregates of particles.

2

In order to understand the features of particle deposition in a comple. environment, we need to break down the problem into its component parts:

(1) Particle capture and pressure drop in a single-phase flow of a non-aqueous liquid.

(2) Particle capture and pressure drop studies for two-phase (gas + liquid) flow.

(3) Role of surface chemistry at reactor conditions in determining particle attachment.

The scope of this thesis is the study of particle deposition in packed beds from non-aqueous media. By selecting a model particle-solvent system, we can understand the mechanisms behind particle attachment and the unexpectedly high pressure build-up. It is also important to understand the role that electrokinetics plays in particle removal.

The experiments undertaken had the following objectives in mind:

(1) To select the model system to study the fundamentals of particle trapping.

(2) To determine the zeta potential of the clean packed bed material and, thereby, the electrokinetic properties of the model system.

(3) To monitor the efficiency of collection in the upward and downward flow of liquid through the packed bed as a function of particle concentration and liquid velocity.

(4) To obtain pressure drop data across the packed bed for both upward and downward flow of liquid as a function of particle concentration in the liquid feed and liquid velocity.

Chapter Two

Literature Review

Fluid-particle separation technology refers to a range of processes for removing, separating, concentrating, and recovering particles from fl··· ·le suspensions. In order to understand the filtration process, it is necessary to view the system at the microscopic level. Electrokinetic phenomena and modeling of particle removal help analyze the system under study at nanometer and micrometer levels. Filtration manifests itself in increased pressure drop as fine particles accumulate on the granular medium. Hence, it becomes necessary to follow the steps leading to capture in order to limit the pressure drop increase to within allowable limits. Throughout this work, the term collector refers to the filter grains, while the term particles refers to fine solids dispersed in the liquid to be filtered.

2.1 Electrokinetic phenomena in non-aqueous media

2.1.1 Existence of charge

The presence of electric charge in non-aqueous media was first inferred from incidents and observations in the electric power industry and the petroleum industry (Klinkenberg and Van der Minne, 1957). An explosion at the Shell industry at Pernis served as an eye opener to the hazards that could be caused by a build-up of static electricity. An accumulation of charge occurs whenever a liquid, such as a hydrocarbon, flows past a solid or another fluid. The extent of accumulation is determined by the type and concentration of trace compounds present in oil products. In flowing hydrocarbons, there is a net charge build-up due to the extremely low conductivities of the fluid. Lack of ability to dissipate this charge may ultimately lead to an explosion.

2.1.2 Solid/Liquid interface

The extent of electrostatic stabilization of charged particles in non-aqueous media depends on the dielectric constant, ξ, of the medium (Van der Hoeven and Lyklema, 1992). It is appropriate to distinguish three regimes of ξ: i) $\xi > 11$, the (semi) polar range, where

4

particle suspensions can be stabilized more or less as in aqueous systems, ii) the intermediate low polar regime (5 < ξ < 11), and iii) the apolar range (ξ < 5), where electrostatic stabilization may be more problematic. Most substances acquire a surface charge when brought in contact with a polar (aqueous) medium, resulting from one or more of a number of mechanisms involving ionization, ion adsorption and ion dissolution. The surface charge influences the spatial distribution of the nearby ions in the polar medium, with ions of the opposite charge (counter-ions) being attracted by the surface and ions of the same charge (co-ions) being repelled away from the surface. This distribution, together with the random thermal motion, leads to the formation of the "electrical double layer" made up of the charged surface with a neutralizing excess of counter-ions, and further from the surface co-ions distributed in the diffuse manner in the polar medium. The concept of an electrical double layer was first introduced by Helmholtz, who envisaged an arrangement of charges in two parallel planes, as shown in Figure 2.1 a) (Hunter, 1981). However, thermal motion causes the counterions to be spread out in space, forming a diffuse double layer. This model for the double layer was proposed by Gouy-Chapman and is shown in Figure 2.1 b). In this model, the charged surface has a potential ψ_S. The surface, consisting of a layer of charge, is surrounded by the compensating ions, which are regarded as point charges in a continuous dielectric medium. The repulsion/attraction between ions coupled with random thermal motion of the ions within the dielectric medium gives rise to an electric diffuse layer. Within this diffuse layer, there is no charge neutrality. Equilibrium is established due to the forces attributed to attraction/repulsion and diffusion due to concentration gradients.

As discussed by Hunter (1981), Debye and Huckel obtained an expression for the variation of the electric potential ψ with distance from the charged surface which is

$$\psi(x) = \psi_o \exp(-\kappa x) \tag{2.1}$$

where the parameter κ, called the inverse Debye length, is regarded as a measure of the thickness of the double layer. This expression is strictly applicable for the case of low potentials. The expression for κ is given as

5
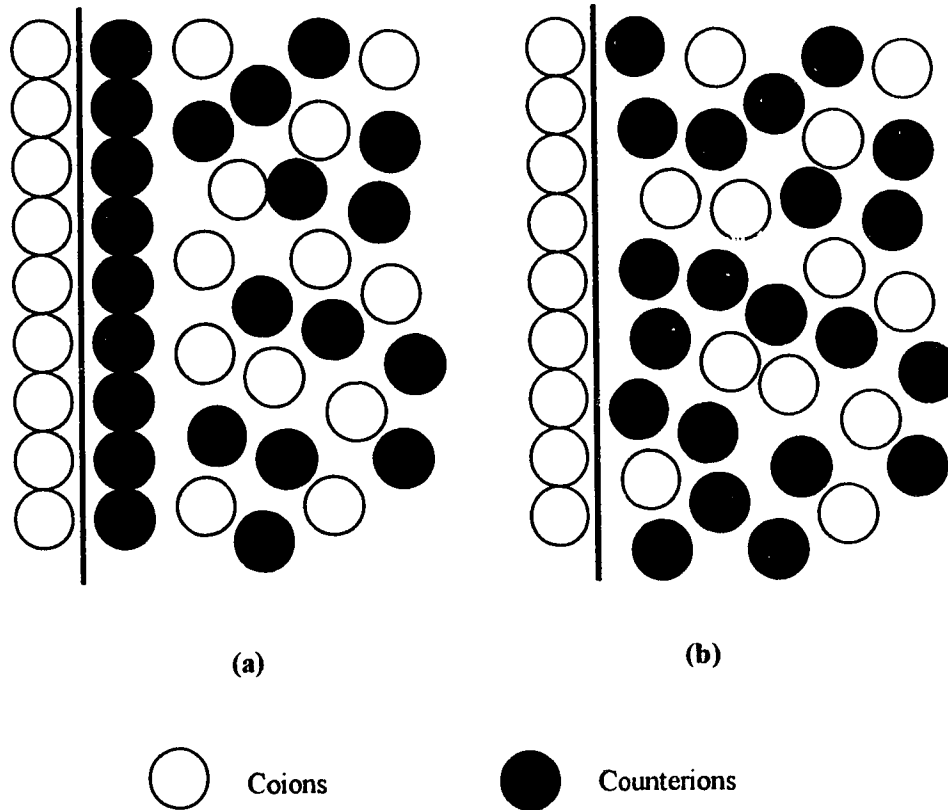
Figure 2.1 Electrical double layer (a) according to Helmholtz model, b) according to Gouy-Chapman's diffuse double layer model (Hunter, 1981)

6

$$\kappa^2 = \frac{e^2}{\xi\xi_o kT} \sum_i z_i^2 n_{io}$$ (2.2)

Stern proposed a model (shown in Figure 2.2) in which the inner boundary of the electrical double layer, referred to as the Stern plane, is at a distance of approximately the radius of a hydrated ion from the solid surface. The electrical potential changes from ψ_S at the surface to ψ_d at the Stern plane and decays to zero far away from the Stern plane. The ions, with their centers attached to the solid surface, are considered to be immobile. Ions whose centers lie beyond the Stern plane form the mobile part of the diffuse layer. Consequently, the mobile inner part of the electrical layer is located one to two radii away from the surface. This boundary is referred to as the shear plane and the potential at the shear plane is referred to as the electrokinetic potential (or zeta potential) ζ. It is possible to measure the zeta potential at a solid surface either by electrophoresis or by streaming potential (Masliyah, 1994). The latter will be discussed in section 2.1.4. Electrophoresis measurements involve measuring the electrophoretic velocity U of a charged particle when it is placed in an electric field of strength E_∞. For extended double layers, i.e. $\kappa a \ll 1$, (which are observed in non-aqueous media), Huckel's equation can be used to evaluate the zeta potential.

$$\zeta = \frac{3}{2} \frac{\mu U}{\xi\xi_o E_\infty}$$ (2.3)

2.1.3 Interaction between double layers

In non-aqueous media with a low dielectric constant, electrolytes are poorly dissociated and often ionic strengths are low ($< 10^{-6}$ M) (Van der Hoeven and Lyklema, 1992). Increased molarity of the electrolyte tends to decrease the value of κ^{-1}. In non-aqueous media, the inverse Debye length κ is very small. Hence, charged particles dispersed in such media are surrounded by extended double layers and the dispersed particles are positioned on each other's double layers. Electrostatic repulsion is a consequence of the interaction of the double layers surrounding the particles. To protect colloids against coagulation, it is necessary that the attraction between particles should be such that a
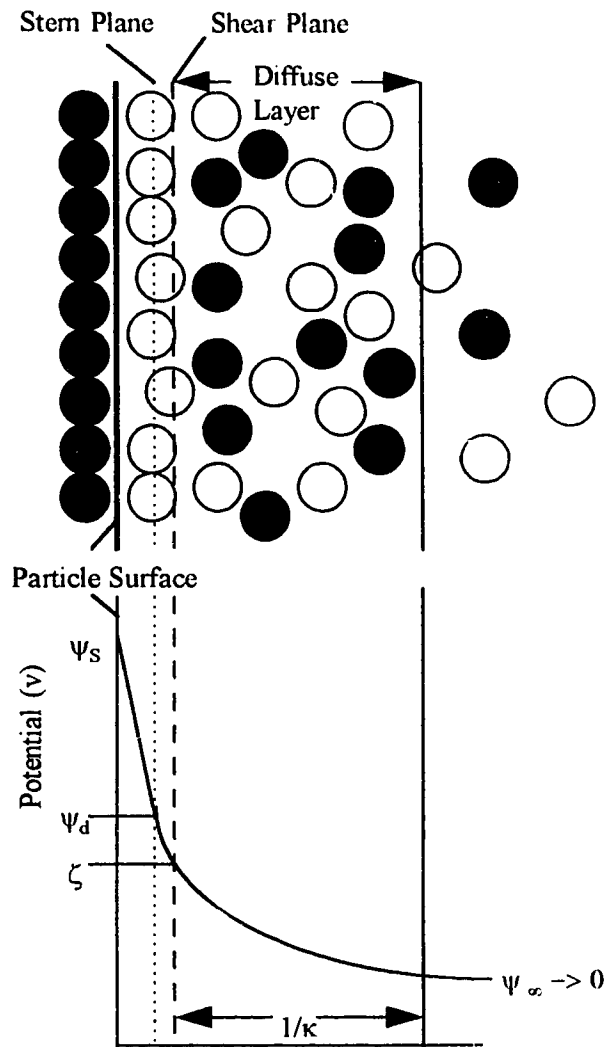
Figure 2.2 Representation of the electric double layer according to Stern's model (Hunter, 1981)

position can be found where the attraction is outweighed by electrostatic repulsion. This concept was developed independently by Derjaguin and Landau in USSR, and Verwey and Overbeek in the Netherlands and is known as the DLVO theory. The magnitude of repulsion is related to the extent of the overlap. With addition of an electrolyte (surfactant), the bulk ion concentration increases and the double layers become thinner.

Since the double layer thickness in non-aqueous systems is of the order of a micrometer, double layer interactions are expected to play an important role in non-aqueous filtration. During filtration, capture occurs when the particles from the suspension attach to the surface of the collector. In order to do so, the electrostatic repulsion between the particles and the collector has to be overcome.

2.1.4 Streaming potential

Streaming potential measurements are a convenient method for characterizing the interfacial charge at a solid-liquid interface. This method is particularly useful for characterizing systems which are unsuitable for electrophoretic measurements. When a liquid is forced through a porous plug, a potential difference, the streaming potential, arises between the ends of the plug. This potential is given by

$$\Delta E = \frac{\xi \xi_0 \zeta \Delta P}{\mu \chi_B} \tag{2.4}$$

Past convention was to insert the bulk specific conductivity, but in recent practice χ_B has been replaced by the pore conductivity χ_P (Kitahara et al., 1971). This term incorporates the surface conductivity due to the packed material as well as the wall of the bed. χ_P is determined by measuring the electrical resistance across the porous plug with the cell constant of the plug having been previously determined with a solution of high conductivity.

2.1.5 Electrokinetics in deposition of particles

Chowdiah et al. (1982) conducted filtration experiments, while simultaneously measuring the streaming potential, for removal of carbon particles from tetralin during flow through a bed of sand. The experiments were conducted at a packed particle Re of 0.004 for

different concentrations of the carbon in tetralin suspension. It was found that the point of breakthrough of the suspended particles from the bed coincided with the neutralization of filtration media for all the runs as can be seen from Figure 2.3. Assuming charge neutralization due to particulate capture alone, a charge balance was made in conjunction with material and rate balance equations of deep bed filtration to model the behavior of the filter. This work has major implications in processes where the surface charges affect the deposition rates. In such situations, the proper choice of a surfactant and a filter medium to obtain desirable surface characteristics can be the key to filtering contaminants from non-aqueous media.
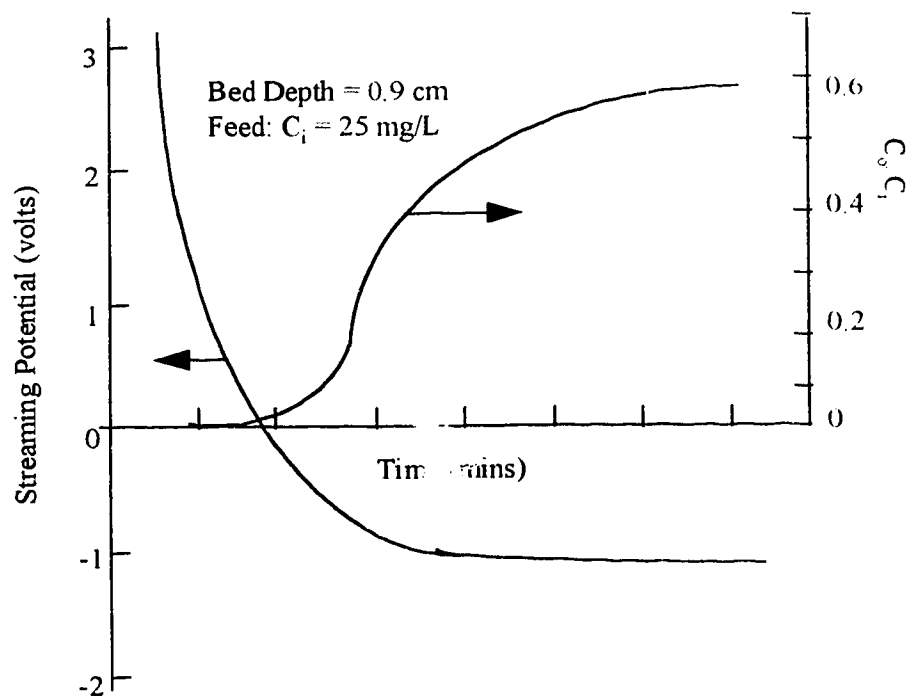
Figure 2.3 Filtrate turbidity and streaming potential curves for the filtration of carbon black from tetralin through a bed of sand.

In the filtration model proposed by Chowdiah et al., particle retention is due to two mechanisms: one due to charge neutralization and the other due to mechanisms like straining, dendrite formation, etc., which are independent of the electrical double layer near the surface of the collector. It is probably due to these mechanisms that the effluent concentration of particles attains a constant value, which is not equal to the feed value

even after the surface charge of the collector has been neutralized, as seen from the Figure 2.3.

Byers and Amarnath (1995) emphasized the significance of electrokinetics in their review paper on the potential uses of electro-separations. The process called dielectric filtration refers to removal of particles from nonconducting liquid streams (non-aqueous media) by applying a strong D electric field across the granular bed. The electric field polarizes particles on the solid packing, causing charged or polarizable particles to be captured on the packing surface with high efficiency. Critical to filter efficiency is the packing dielectric constant, which must be higher than that of the continuous phase. The effectiveness of the filter is approximately proportional to the polarizability of the packing in the liquid phase. This essentially means that the effectiveness of the filter goes up linearly as the dielectric constant of the packing increases. Such an approach to filtration has several advantages, the main ones being economy and reduced environmental impact.

2.2 Prediction of particle removal

Other factors beside electrokinetic phenomena may influence deposition of particles. It is generally accepted that capture of particles by filtration through a porous medium takes place by two principal steps: transport to the surface followed by attachment. A third step, detachment, may possibly take place during filtration, but it mainly occurs during cleaning of the filter medium. Although several factors are responsible for particle transport, often simultaneously, it is convenient and useful to examine them individually (Tien, 1989). These factors will be discussed in detail in Section 2.2.2.

Particle filtration can be described in two different modeling approaches: (1) phenomenological equations, and (2) trajectory theories. These theories are used as background and can be combined with empirical evidence for use as prediction of performance of a filter.

2.2.1 Phenomenological equations

This approach attempts to describe the change in concentration or mass of particles from the influent stream to the effluent stream as a function of time. For a stream with a

concentration C (kg/m³) of fine particles flowing at a flow rate of Q (m³/s) through a bed of cross-sectional area A, the mass balance for the particles in suspension over a depth Δx of bed is given by:

Mass of particles removed from suspension = Mass of particles deposited

$$\Delta C Q \Delta t = \Delta \sigma A \Delta x \qquad (2.5)$$

where σ is the specific deposit in the bed i.e. kg of deposit per m³ empty bed.

In the limit as $\Delta x \to 0$, this equation transforms to

$$\frac{\partial C}{\partial x} = \frac{A}{Q} \frac{\partial \sigma}{\partial t} \qquad (2.6)$$

or

$$\frac{\partial C}{\partial x} = \frac{1}{U_\infty} \frac{\partial \sigma}{\partial t} \qquad (2.7)$$

Based on experimental data, Iwasaki (1937) showed that the particle concentration C at any time throughout the filter can be described by a logarithmic relationship, that is

$$\frac{\partial C}{\partial x} = -\lambda C \qquad (2.8)$$

where λ is the filter coefficient, having dimensions of reciprocal length.

On integrating, we have

$$C(x,t) = C_o(t)\exp(-\lambda x) \qquad (2.9)$$

The expression for filtration rate can be obtained by combining equations (2.7) and (2.8)

$$\frac{\partial \sigma(x,t)}{\partial t} = -\lambda U_\infty C(x,t) \qquad (2.10)$$

The filter coefficient is an important parameter in filtration. Because σ, λ and C are all functions of time, a third equation is necessary to determine concentration as a function of time. Many investigators have proposed a variety of equations of the form $\lambda = \lambda_o \cdot F(\sigma)$ with various empirical coefficients. The selection of a particular form of expression for F(σ) depends on the specific filter and on the suspension to be filtered.

Broadly, there are three types of expressions that can be used (Tien, 1989):

(1) F(σ) is a monotonically increasing function of σ, where the effect of deposition is favorable. In this case, the filter's ability to collect particles improves as the bed becomes increasingly clogged. Examples of this type of expression include $1 + b\sigma$, $1 + b\sigma^2$, etc.

(2) F(σ) is a monotonically decreasing function of σ, where the effect of deposition is unfavorable. In this case, the filter performance is found to deteriorate as particle deposition increases. Examples of this type of expression are $1 - b\sigma$, $1 - b\sigma^2$, etc.

(3) F(σ) exhibits a combination of behaviors in 1 and 2. It may first increase with increase in σ and then decrease after reaching a maximum. Examples of this type of expression are $(1 + b\sigma)^m (1 - a\sigma)^n$ with a, b >0 and m and n of the same sign.

The most general expression is of the form proposed by Ives (1975)

$$\frac{\lambda}{\lambda_o} = \left(1 + b\sigma/\varepsilon_o\right)^y \left(1 - \sigma/\varepsilon_o\right)^z \left(1 - \sigma/\sigma_u\right)^x \tag{2.11}$$

where the empirical parameters b, y, z, σ_u and x are adjusted to give agreement with experimental data; ε_o being the porosity of the clean bed.

The selection of a specific filtration rate expression is, to a large degree, arbitrary. The major weakness of the phenomenological approach is its lack of generality for predictive purposes. Furthermore it does not provide a fundamental understanding of the mechanisms of deposition.

2.2.2 Trajectory theories

Trajectory theories attempt to couple the mechanics of tran   attachment of an individual particle with the observed deposition of particles w.   filter. The principle of trajectory analysis is to view the granular bed as an assembly of collectors and to determine the extent of particle deposition on these collectors as the suspension flows past them (Amirtharajah, 1988). The representation of a filter bed is given in Figure 2.4.

The trajectory of a particle as it moves past a collector, is dictated by the forces acting on the particle. In trajectory analysis, it is necessary to specify (1) the geometry and size of the collectors, (2) the flow field around the collectors, (3) the nature and magnitude of the relevant forces acting on the particles present in the suspension, and (4) the criteria for

UNIT BED ELEMENTS

Filter
Bed

| 1 |
| 2 |
| 3 |

⋮

| N |

Capillaric
Collectors

Constricted
Tubes

Spherical
Collectors

d_{ci} b_i
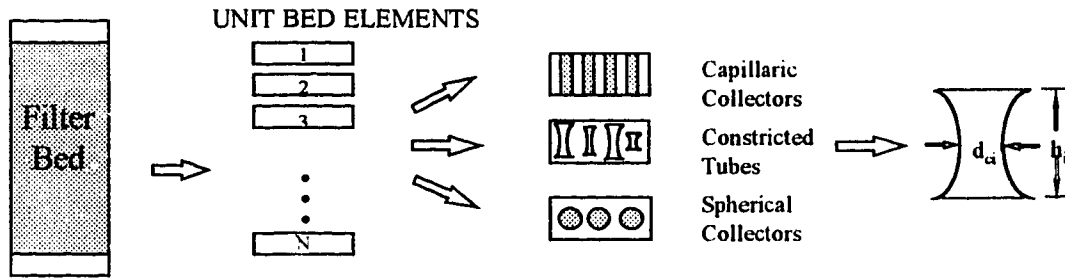
Fig. 2.4 Representation of the filter bed as an assembly of collectors

14

particle adhesion. The application of these specifications is initiated by considering the single-collector efficiency, η_s, defined as the rate at which particles strike the single collector divided by the rate at which the particles approach the collector.

The removal of particles within the pores of a filter is mediated by transport mechanisms that carry the small particles from the streamlines in the bulk of the fluid to distances closer to the collector surfaces. Once transported, the question of whether a particle will stick or not is determined primarily by the surface characteristics of the particles and the collectors (namely, interfacial phenomena). As well as adhering to the collectors, the particles must also adhere to the existing deposits - otherwise the filter will cease to operate as soon as the collectors are all covered with a monolayer of particles. The role of electrokinetics in determining adhesion has already been discussed in the Section 2.1.

2.2.2.1 Particle transport mechanisms

a) Inertial Impaction

Sometimes particles, because of their inertia, change trajectories differently from the way the fluid does. As they deviate from the streamlines of the flowing fluid, some of the particle trajectories may intersect with the collector surface. These intersections, in turn, lead to particle deposition (Tien, 1989). For particles of less than 10μm in liquids, inertial deposition is not considered to be an important mechanism, however, inertial deposition in gases can be very significant.

Inertia is quantified in terms of Stokes number ($St = 2c_s\rho_pU_\infty a_p^2/9\mu a_c$), which is twice the ratio of the kinetic energy of the particle to the work done against the drag force experienced by the particle. The single collector capture efficiency increases with increasing Stokes number. Using different models like potential flow over a sphere, creeping flow over a sphere, etc., different investigators have calculated the collection efficiency due to inertial impaction (George and Poehlein, 1974; Neilsen and Hill, 1976).

b) Interception

Capture by interception assumes that the particles have a finite size and they are non-interacting and non-diffusing. The center of the particle follows exactly the undisturbed

fluid streamline past the collector. When the particle touches the collector, capture or deposition takes place. As the particles follow the fluid streamline, it is possible to evaluate the flux of particles that intercept the collector from the stream function of the flow. A particle is considered to be intercepted by the collector when its center is within one particle radius of the collector surface (Tien, 1989). Capture efficiency is defined as the ratio of the actual captured particles to the idealized capture and the expression for capture is given as

$$(\eta_s)_I = \frac{3}{2}\left(\frac{a_p}{a_c}\right)^2 = \frac{3}{2}N_R^2 \qquad (2.12)$$

where a_p and a_c are the particle and collector radius respectively and N_R is called the relative size group.

The dimensionless parameter A_S can be multiplied to the right hand side of the above expression to modify it to model capture by pure interception through a packed bed of spheres (Happel, 1958). The expression for A_S is

$$A_S = \frac{2\left(1-(1-\varepsilon)^{5/3}\right)}{2-3(1-\varepsilon)+3(1-\varepsilon)^{5/3}-2(1-\varepsilon)^2} \qquad (2.13)$$

c) Brownian Diffusion (without a repulsive barrier)

In the absence of surface interaction forces, the deposition of particles subject to pure Brownian motion can be regarded as a pure mass transfer process, with the Brownian diffusivity D_{BM} replacing the ordinary diffusion coefficient (Tien, 1989). For mass transfer of particles of diameter d_p over a packed bed of spherical collectors of diameter d_c, the Sherwood number for mass transfer is given as

$$N_{Sh} = \frac{d_p}{D_{BM}} \frac{I}{C_\infty(\pi d_c^2)} \qquad (2.14)$$

where I denotes the mass flux over a collector and C_∞ denotes the driving force when there is no surface interaction forces i.e. the concentration of the particles at the interface

16

becomes zero. For particle deposition, the single collector efficiency for a spherical collector can be written as

$$(\eta_s)_{BM} = \frac{1}{\left(\frac{\pi}{4}d_c^2\right)U_\infty C_\infty}$$ (2.15)

For mass transfer in packed beds for the case when the Peclet number ($N_{Pe} = U_\infty d_c/D_{BM}$) >>1, the Sherwood number (Tien, 1989) is

$$N_{Sh} = A_s^{1/3}N_{Pe}^{1/3}$$ (2.16)

The single collector efficiency for a spherical collector can be found by combining the Equations 2.14, 2.15 and 2.16 to obtain

$$(\eta_s)_{BM} = 4A_s^{1/3}N_{Pe}^{-2/3}$$ (2.17)

d) Gravitation

Gravitation deposition can be predicted by calculating the rate at which particles settle onto the collector (Ives, 1975). Settling will take place in the direction of the gravitation force depending on the density difference between the particles and the fluid. The settling velocity of small particles in dilute suspensions can be approximated by Stokes' law as

$$V_s = \frac{2}{9}\frac{a_p^2 g(\rho_p - \rho)}{\mu}$$ (2.18)

For an isolated spherical collector, the collector efficiency attributed to gravitation is

$$(\eta_s)_G = \frac{V_s\pi a_c^2 C_\infty}{\pi a_c^2 U_\infty C_\infty} = \frac{2a_p^2 g(\rho_p - \rho)}{9\mu U_\infty} = N_G$$ (2.19)

e) Electrostatic Forces

Four types of forces can act on particles moving towards a collector:

1. When both the particle and collector are charged, then coulombic forces of attraction or repulsion act, depending on whether the particle and the collector have unlike or like charges.

17

2. A charged collector induces charges on the surface of the particle, opposite in sign to the charge on the collector, which results in an additional force on the particle.

3. If a particle is charged, then it also induces an image charge on the collector. This also results in an additional force on the collector.

4. Particles of the same charge produce a repulsive force among themselves. This mechanism is called the space charge effect.

Besides these forces, there may be other forces of importance, especially in electrically enhanced granular filtration where an external electric field is applied. Such an applied field gives rise to a force on a charged particle in the presence of a neutral collector. The electric dipole interaction gives rise to a force between an uncharged particle and an uncharged collector, where both are polarized by an applied electric field. Expressions for these forces are given by Tien (1989).

f) Straining

If the size of particles in suspension is greater than the pore constriction of the granular media through which the suspension flows, the particles will be retained in the media the way particles are retained on a sieve when the openings are smaller than the particle diameter. This mechanism of particle deposition in a filter bed is called straining or sieving (Tien, 1989). The accumulation of particles on the surface forms a cake which dramatically increases the pressure gradient necessary to maintain a given flow across the filter.

2.2.2.2 Combined mechanisms

During actual filtration, it is probable that many of these mechanisms act simultaneously, although with varying degrees of importance, depending on the nature of the suspension and the filter medium. Different investigators have proposed models to describe the overall deposition process.

a) Spielman and Fitzpatrick model :

Spielman and Fitzpatrick (1973) developed a trajectory equation by performing a force balance which included gravitational and unretarded London-Van der Waals surface

forces. The resulting efficiency was obtained by solving the trajectory equation computationally. Figure 2.5 gives the variation of the capture efficiency with N_{ADS} and $N_{G,S}$, where $N_{G,S}$ and N_{ADS} are defined as follows :

The modified gravity number is

$$N_{G,S} = \frac{N_G}{A_S N_R^2} \tag{2.20a}$$

The Adhesion number is

$$N_{ADS} = \frac{Ha_c^2}{9\pi \mu A_S a_p^4 U_\infty} \tag{2.20b}$$

The authors obtained the following expression for capture efficiency by neglecting gravity and considering the case of $N_{ADS} \gg 1$.

$$\eta / \eta_I = \left(\frac{1}{2} N_{ADS}\right)^{1/2} \tag{2.21}$$

b) Rajagopalan and Tien model :

As straining is not strictly a transport mechanism, Rajagopalan and Tien (1976) included inertia, gravity, surface forces and drag forces and formulated the trajectory equation as a first order differential equation by utilizing Happel's sphere-in-cell model. To solve the trajectory equation, they considered the typical parameters considered in granular filtration, namely N_G, N_R and N_{Lo}. where N_{Lo} is defined as

$$N_{Lo} = N_{ADS} \cdot A_S \cdot N_R^2 \tag{2.22}$$

The theoretical calculations were grouped under a) favorable surface conditions, and b) unfavorable surface conditions (repulsive surface interactions in the vicinity of the collector). Theory predicts negligible or no deposition when a large repulsive barrier exists. Hence, only the first case was considered. Figure 2.6 represents the calculated values for η as a function of N_G and N_R.

19
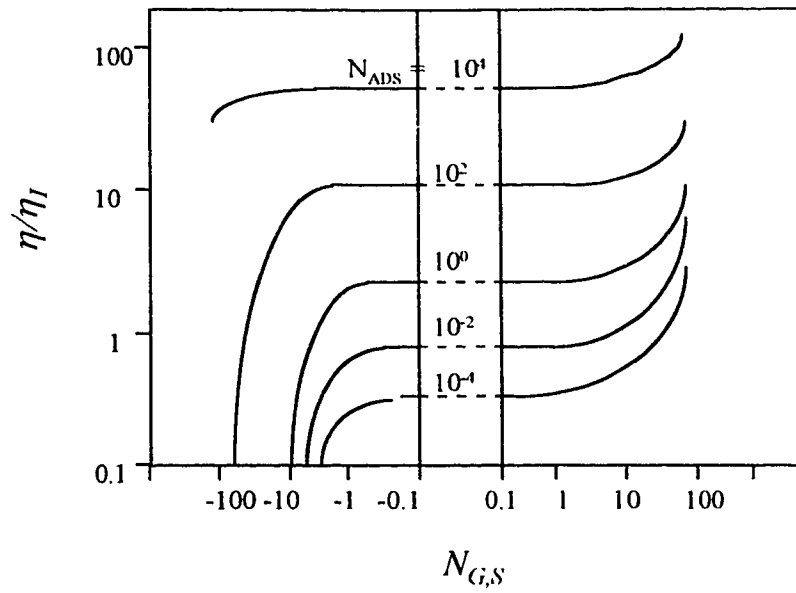
Figure 2.5 *Computed normalized capture efficiency versus gravity numbers for different adhesion numbers according to Spielman-Fitzpatrick's model.*
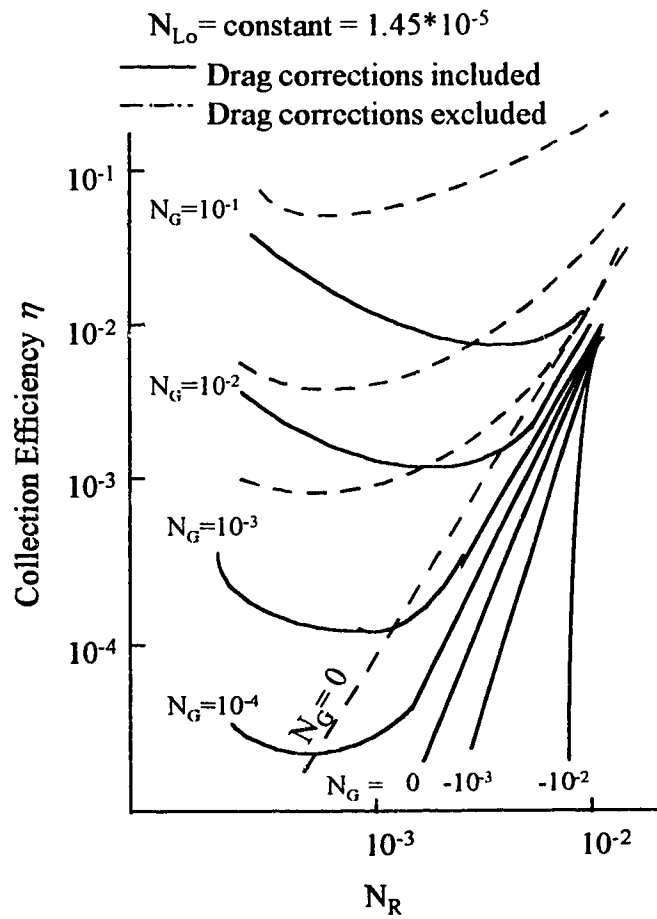
Figure 2.6 *Collector efficiency curves according to Rajagopalan-Tien's model*

When wall corrections were ignored, the collector efficiency of a single spherical collector due to the different mechanisms was simply the sum of the efficiencies of the contributing mechanisms (interception and gravitation). If transport is by diffusion, fluid flow and gravity forces, then the expression for single collector efficiency is

$$\eta = \eta_I + \eta_G + \eta_{BM} \tag{2.23}$$

In order to make extensive calculations unnecessary, Rajagopalan and Tien obtained an empirical expression for removal efficiency for liquid-particle suspensions by keeping two of the dimensionless groups constant and varying the third. The resulting expression for downflow ($N_G > 0$) and for $N_R < 0.18$ is given by

$$\eta = 0.72 A_S N_{LO}^{1/8} N_R^{15/8} + 2.4 \times 10^{-3} A_S N_G^{1.2} N_R^{-0.4} + 4 A_S^{1/3} N_{Pe}^{-2/3} \tag{2.24}$$

This analysis is based on the fact that there is no repulsion potential between the particle and the collector i.e. for favorable surface interactions. Experimental data showed that this expression was adequate when surface interactions were favorable. The key difference between Rajagopalan and Tien's model and Spielman and Fitzpatrick's model, in addition to using a different expression for the stream function, is that Spielman and Fitzpatrick neglected the unretarded London attraction.

A disadvantage of trajectory analysis is that it does not describe the removal efficiencies as particles accumulate within the filter, but simply gives the initial value of the single collector efficiency when its surface is clean. Expressions such as Equation 2.24 indicate the influence of operating conditions on particle deposition, but they do not predict efficiency as a function of the number of particles deposited.

2.3 Pressure drop studies

In a filtration or packed-bed operation, a primary interest is the extent to which the pressure drop will increase over the initial value for a clean bed.

2.3.1 Pressure drop for clean beds : Ergun's equation

In order to estimate the increase in pressure drop during filtration, it is necessary to know the pressure gradient-flow rate relationship for clean filter media. For the flow of an

incompressible fluid through a granular medium composed of spheres of uniform size dimeter d_c), the pressure drop (-ΔP) necessary to maintain a fluid flow at a superficial velocity U_∞ over a distance L in laminar flow is

$$\left(\frac{-\Delta P}{L}\right) = 150\frac{(1-\varepsilon)^2}{\varepsilon^3}\frac{\mu U_\infty}{d_c^2}$$ (2.25)

Equation 2.25 is known as the Carman-Kozeny equation and is derived on the basis that the flow is laminar and the pressure drop results entirely from form-drag loss. As the fluid velocity increases, kinetic energy losses become significant. The pressure drop resulting from kinetic energy losses was found to be

$$\left(\frac{-\Delta P}{L}\right) = 1.75\frac{\rho U_\infty^2}{d_c}\frac{(1-\varepsilon)}{\varepsilon^3}$$ (2.26)

Equation 2.26 was first obtained by Burke-Plummer to predict the pressure drop in turbulent flow through packed beds. The Equations 2.25 and 2.26 can be added to yield a general relationship for flow through porous media which is

$$\left(\frac{-\Delta P}{L}\right) = 150\frac{(1-\varepsilon)^2}{\varepsilon^3}\frac{\mu U_\infty}{d_c^2} + 1.75\frac{\rho U_\infty^2}{d_c}\frac{(1-\varepsilon)}{\varepsilon^3}$$ (2.27)

The above expression is known as Ergun's equation and can be used to estimate the pressure gradient to maintain a given flow at U_∞ for a clean filter (McCabe and Smith, 1985).

2.3.1 Modification of Ergun's equation for deposition in packed beds

The increase in pressure drop in packed beds during deposition can be predicted by an expression relating the transient pressure drop with pressure drop across the clean filter bed (Ives, 1975). If one assumes that the deposition merely changes the porosity of the filter media, and that Carman-Kozeny equation applies to both clean and clogged packed beds, then we have

22

$$G(\sigma) = \frac{(\partial P/\partial x)}{(\partial P/\partial x)_0} = \left(\frac{d_{co}}{d_c}\right)^2 \frac{\varepsilon_0^3(1-\varepsilon)^2}{\varepsilon^3(1-\varepsilon_o)^2} \qquad (2.28)$$

where G is the ratio of the pressure drop due to a clogged packed to that for a clean bed.

The relationship between the change in filter porosity and the extent of deposition can be considered in the following manner. If one assumes that the particle deposition on the outside of the collectors forms a relatively smooth surface on the grain, then the change in the effective diameter of the collector can be given as

$$\frac{d_c}{d_{co}} = \left(\frac{1-\varepsilon}{1-\varepsilon_o}\right)^{1/3} \qquad (2.29)$$

The change in the media porosity can be given by

$$\varepsilon = \varepsilon_o - \frac{\sigma/\rho_p}{1-\varepsilon_d} \qquad (2.30)$$

where ε_d is the deposit porosity.

Combining equations 2.28, 2.29 and 2.30 yields

$$G(\sigma) = \left(\frac{1-\varepsilon_o}{1-\varepsilon}\right)^{2/3} \left(\frac{\varepsilon_o}{\varepsilon}\right)^3 \left(\frac{1-\varepsilon}{1-\varepsilon_0}\right)^2$$

$$= \left[1 - \frac{\sigma/\rho_p}{\varepsilon_0(1-\varepsilon_d)}\right]^{-3} \left[1 + \frac{\sigma/\rho_p}{(1-\varepsilon_o)(1-\varepsilon_d)}\right]^{4/3} \qquad (2.31)$$

This form for G(σ) has been found to grossly underestimate the increase in pressure drop (Tien et al. 1979).

2.3.3 Different studies of transient pressure drop increase

Since theoretical expressions failed to predict the pressure drop increase, different investigators resorted to obtaining empirical expressions from experimental data.

23

For example, Maroudas and Eisenklam (1964) performed experiments to visually confirm different modes for increase in pressure drop. Their model filter bed is shown in Figure 2.7. With different particle sizes and shapes and different flow rates, the following modes of deposition was observed : a) gradual constriction of flow paths : constricting mode, and b) rapid blocking of flow paths : blocking mode.

In the constricting mode, the deposits gradually constricted the channels. The interstitial velocity at any level thus increased until it reached a critical value. Thereafter, no deposition occurred at that level, and so on at each successive level. Eventually, the whole bed became non-retaining, i.e. the inlet and outlet concentrations of particles were equal. At this stage, there were no blocked flow paths; they had all only become narrower. In the blocking mode (as observed with larger irregular particles), there was variation in the deposits in the different channels. Since the channels were all interconnected, the local velocity in the less obstructed paths rose and even swept the path free of any previously deposited particles, while the reduced velocities in the more obstructed paths led to further deposition. Hence, the deposits in some channels gave rise to more and more constricted channels which soon became completely blocked. Other channels remained almost free of deposits. When the junction to the last flow path is blocked, there is a steep but short pressure drop rise. Following this, a uniform cake of solids deposits on the surface of the bed and the pressure drop increases linearly with time. Typical curves for pressure drop increase are given in Figure 2.8 a) and b).
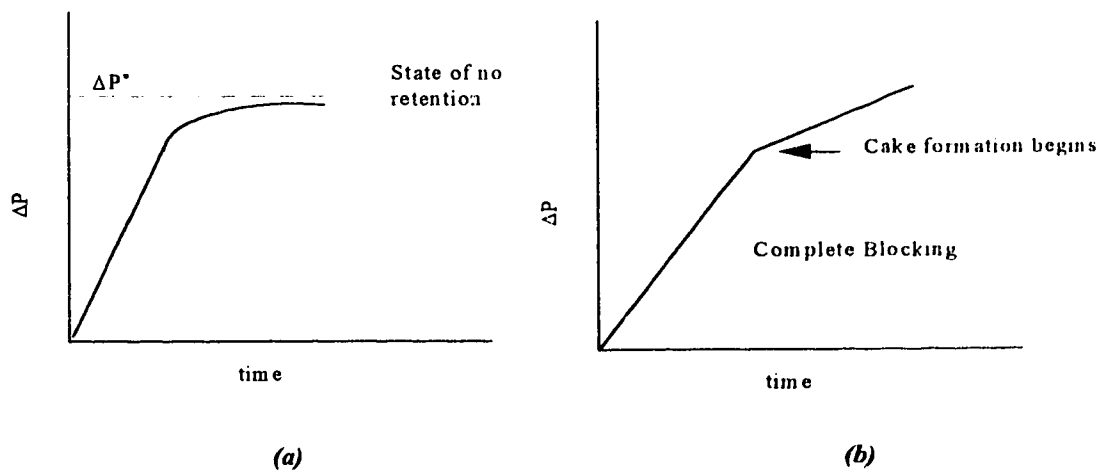
Figure 2.8 Pressure drop for a) no deposition mode, b) complete blocking mode

24
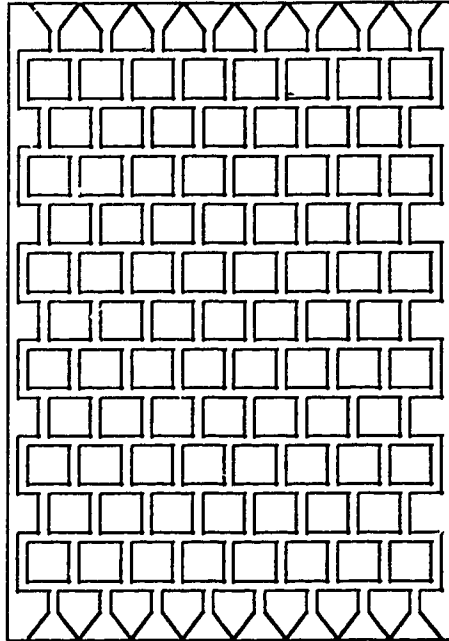
Fig. 2.7 Model filter bed for Maroudas and Eisenklam's experiments

Different investigators obtained empirical correlations for their experimental data. A few examples will be listed.

Mehter et. al (1970) suggested two empirical correlations for their experimental data:

$$G = 1 + d\sigma \; ; d > 0 \tag{2.32}$$

$$G = \left(\frac{1}{1 - d\sigma} \right)^m \; ; d > 0; m > 0 \tag{2.33}$$

Ives (1975) applied mathematical models representing the granular bed as an assembly of individual spheres and as an assembly of individual capillaries to estimate the increase in pressure drop. He combined these two models to obtain a combined specific surface model. The basis for this model was that initially, deposits will form on the surface of spherical collectors. As the deposits become continucus, side spaces will be filled in and flow will be through channels approximating capillaries. The resulting expression for the pressure drop is given below, with the first term on the right contributed by the spherical grain model and the second term contributed by the capillary model.

$$G = \left(1 + \frac{d\sigma}{\varepsilon_o} \right)^m \left(1 - \frac{\sigma}{\varepsilon_o} \right)^n \; ; d > 0; m > 0; n > 0 \tag{2.34}$$

Tian and Guthrie (1995) simulated the distribution and evolution of a specific deposit inside the filter and compared it to experimental data obtained during filtration of a liquid metal. When the filter is relatively clean, the specific deposit follows an exponential decay from inlet to outlet. To study the effect of the specific deposit on the pressure drop, they introduced two models - the smooth coating model and the porosity change model. The smooth coating takes into account an increase in the diameter of the collector as well as a reduction in the porosity of the bed with deposition. The porosity change model only accounts for a change in porosity as the fines accumulate within the bed. The expression to predict the transient pressure drop is as follows :

$$\Delta P = -(\partial P / \partial x)_o \int_0^L G(\sigma)dx \qquad (2.35)$$

where $G(\sigma)$ for the smooth coating model is given by

$$G(\sigma) = \left(1 + \frac{\sigma(t,x)}{(1-\varepsilon_o)(1-\varepsilon_d)}\right)\left(1 - \frac{\sigma(t,x)}{\varepsilon_o(1-\varepsilon_d)}\right)^{-3} \qquad (2.36)$$

and that for the porosity change model is given by

$$G(\sigma) = \left(1 + \frac{\sigma(t,x)}{(1-\varepsilon_o)(1-\varepsilon_d)}\right)^2 \left(1 - \frac{\sigma(t,x)}{\varepsilon_o(1-\varepsilon_d)}\right)^{-3} \qquad (2.37)$$

No general literature is available to effectively model the pressure drop increase with deposition. Most of the models describe the formation of a smooth layer of deposit on the collectors or within the capillaries that constitute the pore spaces of the packed bed and these models have been found to underestimate the pressure drop build-up.

Chapter Three

Experimental Setup and Procedure

3.1 Chemicals

The chemicals used in the experiments were:

(1) Kerosene from Fischer Scientific (Edmonton).

(2) Sodium di-ethyl hexyl sulfosuccinate (technical grade) from Pfaltz and Bauer (Waterbury) as surfactant.

(3) Cyclohexane from Fischer Scientific (Edmonton) as co-solvent to dissolve the surfactant.

(4) Carbon Black from Anachemia Science (Edmonton) as particles to be suspended (5-10 μm, average size = 8 μm as measured by microscopy).

(5) Glass beads (710-1180 μm) from Sigma Chemical company (St. Louis) were used as the packing material. These were sieved to obtain glass beads of the size 850-1000 μm.

(6) Cylindrical extrudate Ni-Mo on γ-alumina hydroprocessing catalyst from Criterion Catalyst (Azusa) of 1 mm diameter and length varying from 4 mm to 10 mm.

3.1.1 Design of model suspension

Kerosene was chosen as the solvent as it has a low vapor pressure. In addition, it is similar in its chemical composition and dielectric constant to hydrotreater products. For the fine particles, carbon black was selected over clay as the latter is a compound without a fixed composition. Also, it was easy to determine the concentration of carbon in kerosene by spectrophotometry, which could not be done using clay. Carbon is also similar to coke which is formed during hydrotreating and is deposited on the catalytic beds. Glass beads were chosen as the primary packing material as they are symmetrical with a well-defined geometry. Hydroprocessing catalyst was also studied to ensure that the same trends in particle collection were observed with the actual catalyst material as with the glass beads.

3.1.2 Preparation of the suspension

The suspension used for the experiments was prepared in the following manner :

1. Surfactant solution.

Various surfactants were tested to determine their ability to stabilize a suspension of carbon black and to increase the conductivity of the solution. Most of the surfactants failed one of the objectives or both. A list of those tried is given in Appendix A1. Finally, the surfactant solution was made by adding sodium di-ethyl hexyl sulfosuccinate (Aerosol OT, also known as AOT) to cyclohexane. This solution was stirred overnight to dissolve the surfactant. For all the experiments, a 6 mmol/L solution of AOT in cyclohexane as a co-solvent was used. Cyclohexane was necessary to help the surfactant dissolve in kerosene. Although, n-heptane and iso-propanol were also tested, they were less effective than cyclohexane.

2. Kerosene Solution

The surfactant solution was added to kerosene to form a 0.3 mmol/L solution of AOT in kerosene. This solution was stirred for half a day before it was used to prepare the carbon suspension.

3. Carbon suspension in kerosene

Carbon black was added in concentrations from 95 to 200 mg/L and homogenized in a commercial blender for half a minute. The suspension was used immediately for the deposition experiments.

3.2 Experimental apparatus

The primary focus of the experiments was to study the ability of the packed bed to remove suspended particles from solution. The flow diagram of the experimental apparatus for upward flow is shown in Fig. 3.1 and that for downward flow is shown in Figure 3.2. The column was made of Plexiglas, 30 cm in length, with an internal diameter of 2.54 cm. Glass beads and hydroprocessing catalyst were used as packing materials. A removable Plexiglas screen with 0.5 mm ID holes was used to hold up the packing. In order to facilitate the easy loading and unloading of the packed material to and from the column, the packed section was made such that two cylindrical sections of Plexiglas, each of ID
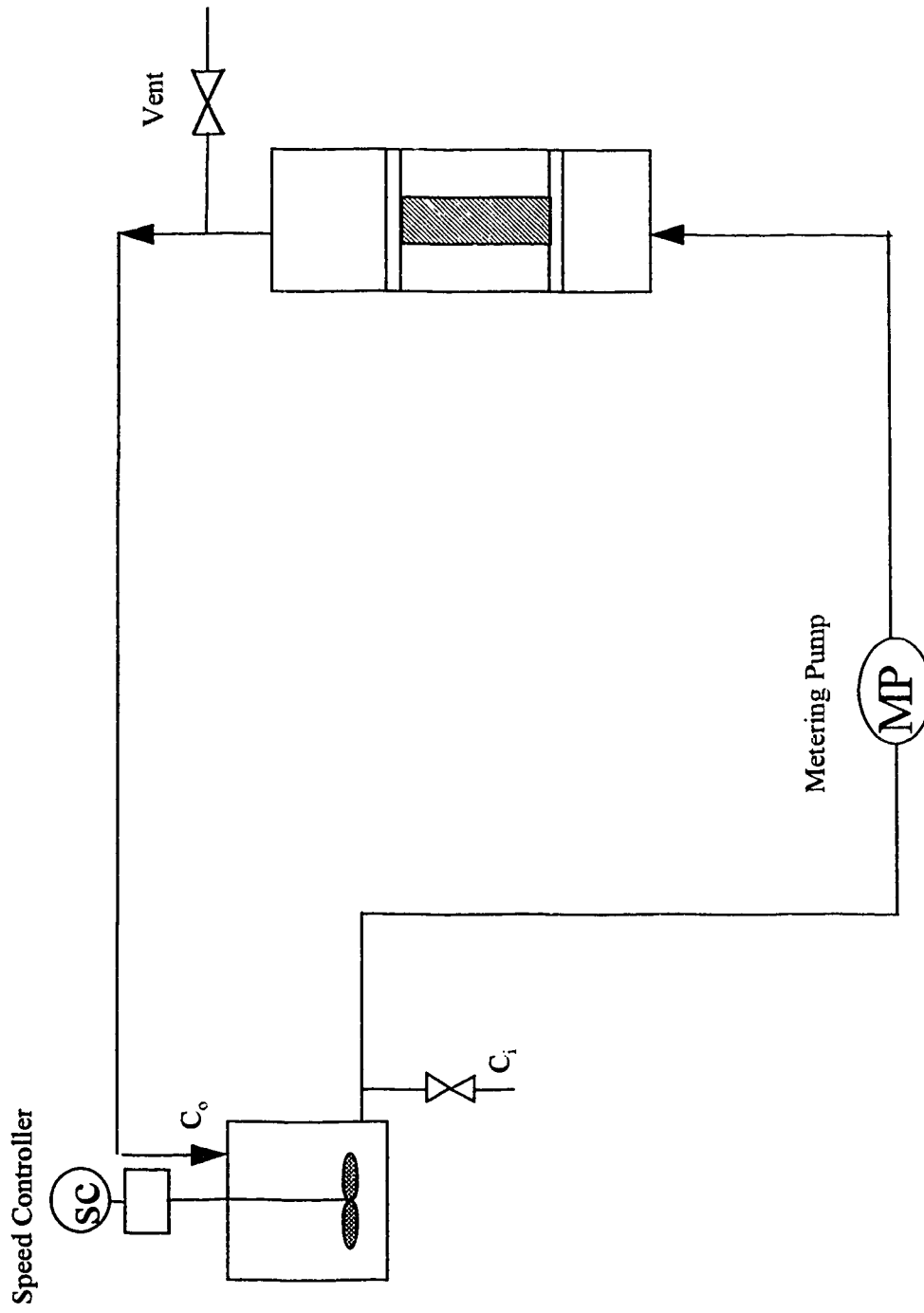
Figure 3.1 Flow diagram for particle capture for upward flow mode
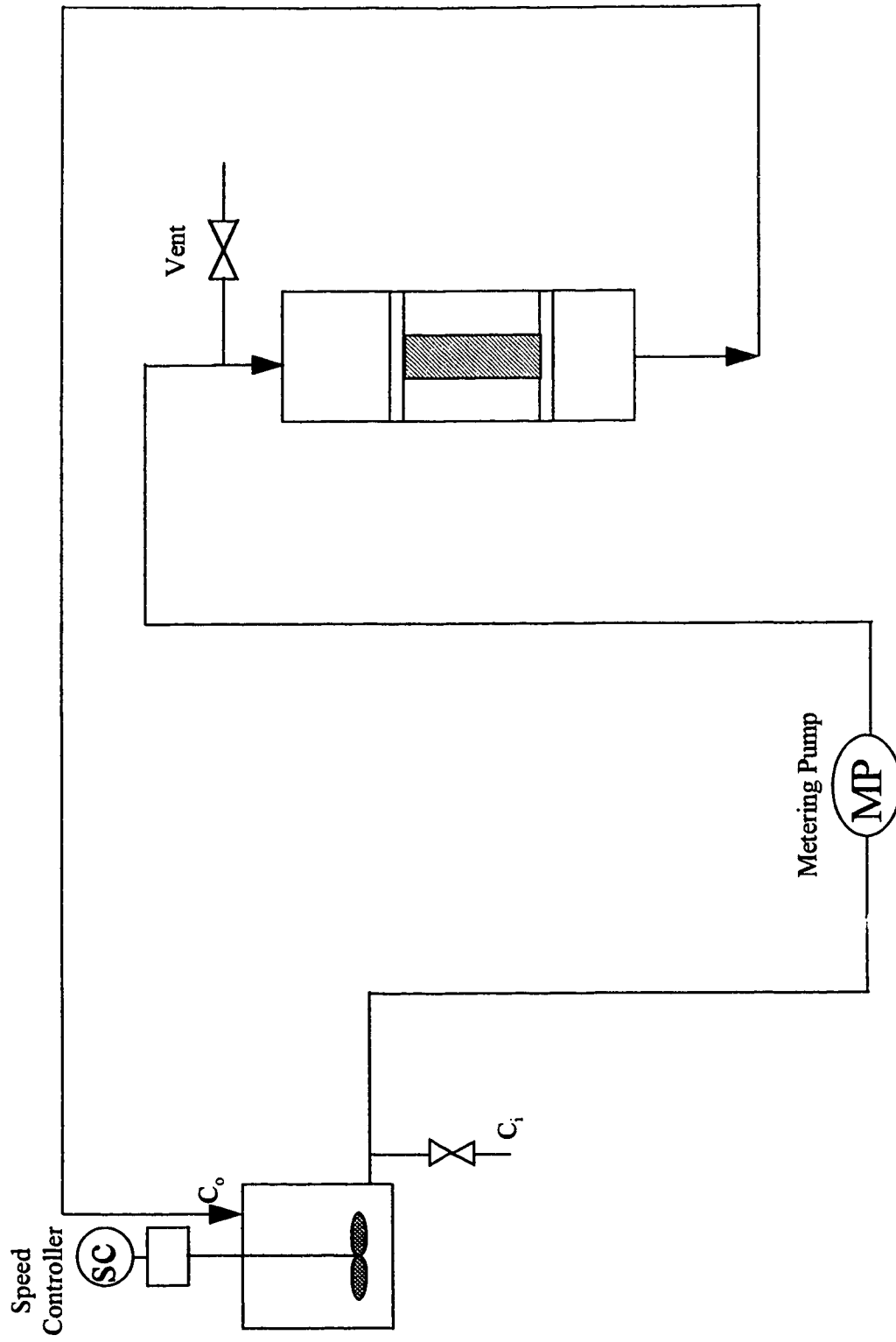
Figure 3.2 Flow diagram fo. particle capture for downward flow mode

3.81 cm and 30 cm length, flanked either end of the packed section. Eight screws and nuts at each end helped to keep the packed section in alignment with adjacent sections. In addition, the packed section had ports at each end for electrodes and connections to a differential pressure (DP) cell (Rosemount Instruments Model 1151-DP-3E-12-D1-B1-C6, Edmonton). A detailed diagram of the packed section is given in Fig 3.3.

The reservoir for the kerosene was a 53 liter tank, which also collected the recirculating kerosene coming out from the packed bed. A metering pump (Fluid Metering Inc., Oyster Bay) was used for pumping the solution through the packed section. It was calibrated from 4-20 mA for a maximum flow of 80 mL/min. The calibration curve is shown in Appendix A3. The pressure drop across the packed bed was measured by the DP cell. The cell was calibrated for 0-7.4 kPa for glass beads and 0-3.7 kPa for the catalyst from 4-20 mA. The calibration data are shown in Appendix A2. Ag-AgCl electrodes from In Vivo Metric (Healdsburg) could be connected to the ends of the packed section. A Keithley 617 electrometer, obtained from Tektronix (Vancouver), could be connected to these electrodes to measure the electrical resistance of the solution. A stainless steel shield was used to enclose the packed section to prevent any stray currents from interfering with the resistance measurements. The concentration samples were withdrawn from the valve at the bottom of the tank (C_i) and from the tubing entering the top of the tank from the column (C_o).

3.2.1 Deposition measurements :

Before starting a run with the carbon suspension in kerosene through the packed bed, it was necessary to ensure that all changes in concentration during the run could be attributed to deposition of carbon black on the packing material itself. Hence, the carbon suspension in kerosene was allowed to circulate overnight through the system without the packing, at the same flow rate as that for the subsequent experiment. The concentration was monitored for an hour the next morning before the packing was introduced, to ensure that there was no further change in concentration. The procedure was then as follows:

(1) A fixed weight of the packing (240 g of glass beads or 90 g of the catalyst) was added to the empty column up to a marked height to ensure that the porosity of the bed remained
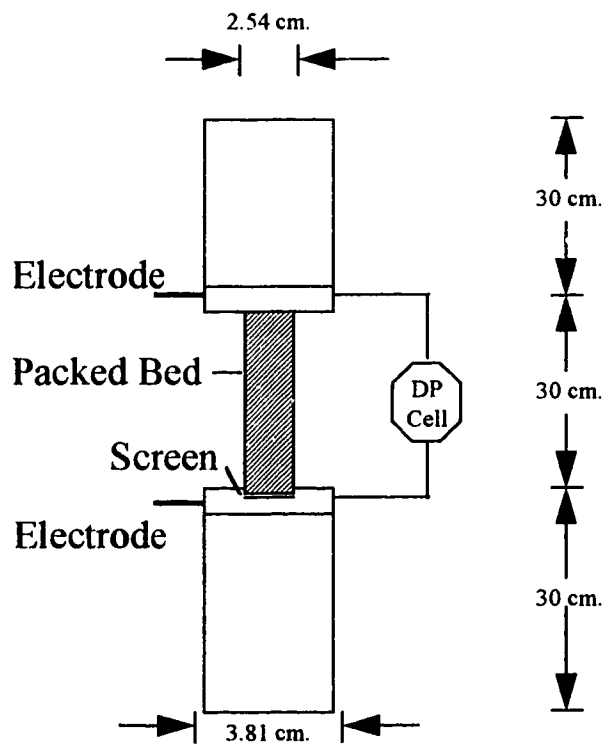
Figure 3.3 Detailed view of the packed section

constant from experiment to experiment. In case of the catalyst, keく ・・ ・・・・・ arbon black was poured into the column after the packing was introduced and before the column was inserted into the apparatus to wet the catalyst, as the catalyst had a tendency to soak up kerosene.

(2) The direction of flow for filling up the column was upward in order to displace any air in the packing. Following the removal of all the air from the system, the vent at the top of the bed was closed.

(3) The suspension was pumped from the tank into the bottom of the column through to the top (or from the top to the bottom as the case may be) and back into the tank.

(4) Zero time for the experiments was the time when the carbon black suspension just began to fill the packed section. The pressure drop when the suspension had completely filled all the lines was noted and this value was recorded as the initial pressure drop.

(5) Samples of the suspension were withdrawn at regular intervals from the tank (i.e. the inlet to the column) and from the top of the column before entering the tank (i.e. the exit from the column). These were analyzed using spectrophotometry, as described in detail in Section 3.3.1. At the same time, the pressure drop across the column was noted.

(6) In case of the single pass experiments, the path of the flow was slightly different. The suspension flowing out from the top of the column was collected in an empty drum, and not returned to the tank. The concentration in the tank was sampled only once, prior to start of the run, while the suspension concentration from the column was withdrawn and analyzed at regular intervals. This procedure gave a constant inlet concentration.

(7) At the end of each run (1 1/2 d for a recirculating run and a few hours for a single pass run), the apparatus was emptied by reversing the flow through the column.

3.2.2 Streaming potential measurements :

Streaming potential measurements were carried out to determine the zeta potential of the collector (glass beads and catalyst). These measurements were carried out at lower flow rates than that for the deposition experiments as it was observed that the potential developed went off the scale of the electrometer at higher flow rates. The packed section was filled with the packing material and clean kerosene solution (with surfactant) was

passed through the packing. The potential difference developed across the packed bed due to the flow was then measured with the electrometer (Keithley 617) by connecting it to the electrodes at the end of the packed section. At the same time, the pressure drop that developed across the bed was also measured. The connections for streaming potential measurements are shown in Fig. 3.4

3.3 Analysis of the samples

3.3.1 Analysis of suspension samples

The analysis of the carbon concentration was done by spectrophotometry at a wavelength of 550 nm with Shimadzu UV Visible Recording Spectrophotometer (UV-160). At this wavelength, the spectrum of kerosene with the surfactant solution showed no peaks, so that any absorbance at this wavelength can be attributed to carbon black. Solutions with different known concentrations of carbon black were made gravimetrically and their absorbance was measured. The calibration curve of absorbance versus concentration of carbon black is shown in Appendix A4.

3.3.2 Photographs of deposits

Initial attempts to view the deposit within the pores of the packed bed failed when the kerosene was withdrawn from the bed even at very low flow rates because the deposit was no longer retained within the pores. This was probably due to the delicate structure of the deposit. Therefore, a different approach had to be taken in order to view the structure of the deposit. After the deposition experiment was carried out in the downflow mode for about 16 h, clean kerosene with surfactant was run through the column to displace the carbon suspension in kerosene from the bed. The kerosene was then withdrawn in the same direction as that for the experiment (i.e. downflow) until the clear kerosene barely covered the surface of the packing material. The top layer of the catalyst was then observed under a microscope to see how the carbon black particles were deposited on the packing. The picture from the microscope was observed on a TV monitor, and recorded using a video recorder. Still images were obtained from the video recording.
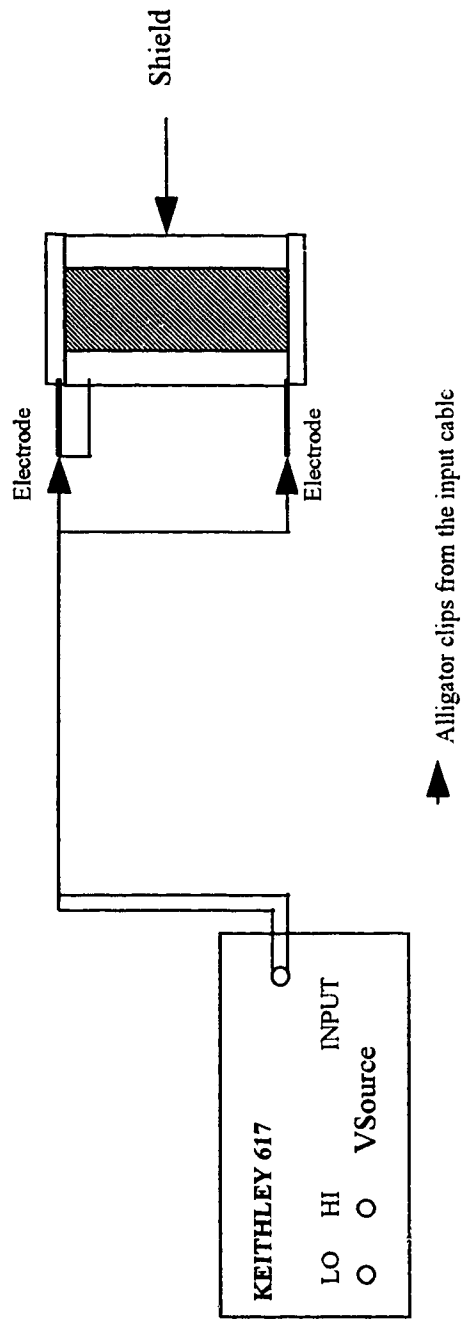
Figure 3.4 Connections for streaming potential measurements

3.3.3 Bulk conductivity measurements :

In order to obtain the bulk conductivity of the kerosene solution, it was necessary to obtain the cell constant of the packed section of the apparatus as well as the resistance of the solution in this section. A 0.1 mho/cm KCl conductivity solution was used to obtain the cell constant (k_{cell}) of the packed section. By measuring the resistance (R_{KCl} in this case) of the solution of known conductivity (χ_{KCl}) while in the packed section, it is possible to calculate the cell constant and, thereby calculate the bulk conductivity of the kerosene solution (χ_{ker}) by measuring its resistance (R_{ker}) as can be seen from the following equations. Calculation of the cell constant is given in Appendix A11.

$$k_{cell} = R_{KCl} \cdot \chi_{KCl} \tag{3.1}$$

$$\chi_{ker} = k_{cell} / R_{ker} \tag{3.2}$$

Equation 3.2 was used to evaluate the conductivity of the kerosene solution with surfactant. The conductivity of the suspension was one of the criteria for the choice of surfactant. The conductivity value was also used in the evaluation of the zeta potential of the collector (by streaming potential measurements) according to Equation 2.4.

The connections for resistance measurements are shown in Figure 3.5.

37
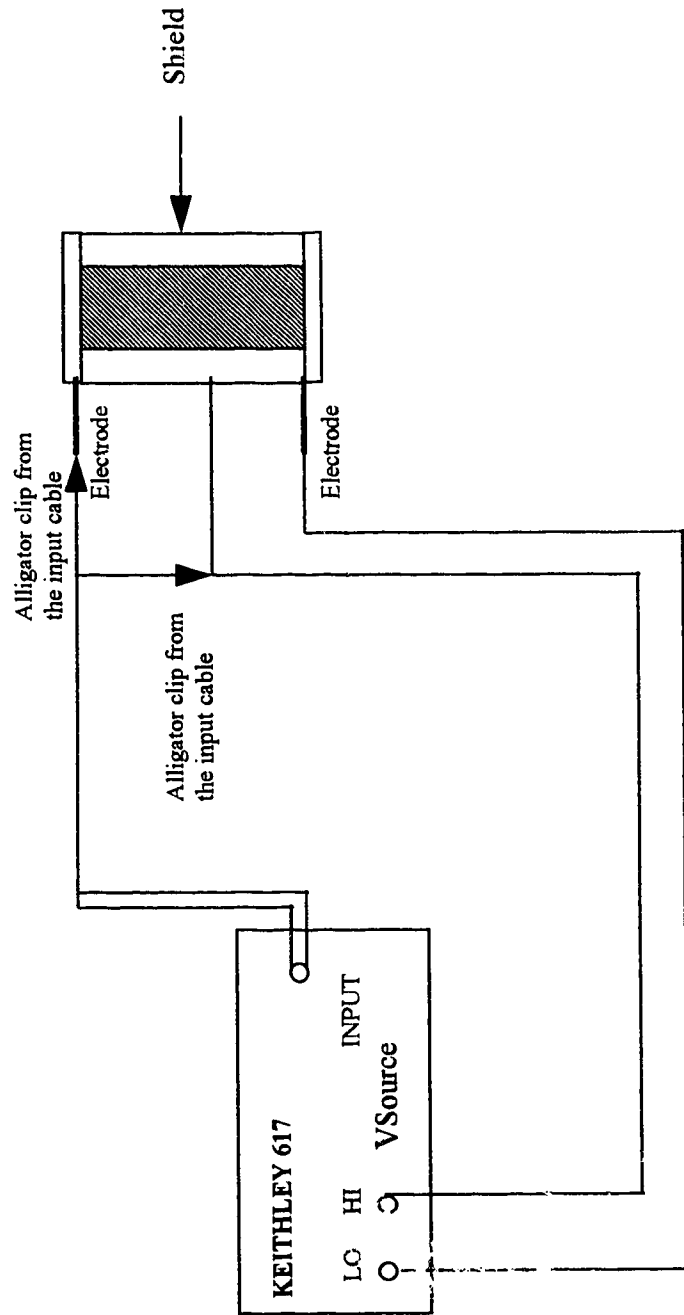
Figure 3.5 Connections for resistance measurement s

38

Chapter Four

Results and Discussion

4.1 Electrokinetic studies

To understand the collection of particles in the bed, it was necessary to know the charge on the collectors and the particles in suspension.

Streaming potential measurements are normally employed for determining the zeta potential of solids in non-aqueous systems and for a porous matrix. Attempts made to monitor the streaming potential during the course of a deposition experiment failed because the developed potential, which was very high, went out of the scale of the electrometer (which was 200 V). It was therefore decided to have kerosene flow without any carbon through the bed at lower velocities in order to determine the zeta potential of the clean bed.

Appendix A12 gives details on how the calculation for zeta potential of the collector was performed. The zeta potential for glass beads was found to be 16 mV and that for catalyst was found to be 31 mV.

Attempts to determine the charge on carbon black particles by electrophoresis failed as the Malvern equipment available was not suitable for non-aqueous media. Literature revealed that carbon black has a negative charge (or negative zeta potential) in non-aqueous media when Aerosol OT is used as a surfactant. Chowdiah et. al. (1982) found that the zeta potential of carbon in 10 mmol/L of Aerosol OT in tetralin was -57.3 mV. Kitahara et. al. (1967) found that the zeta potential of carbon in cyclohexane (14.5 mmol/L of Aerosol OT) was -40 mV; the zeta potential for carbon in n-heptane varied between -40 and -60 mV for varying concentrations of Aerosol OT, while that for carbon in benzene was -80 mV.

4.2 Effect of concentration of the suspension on deposition

Before starting systematic deposition experiments, it was necessary to know the influence of the concentration of the suspension on the key variables of the deposition process.

This study was carried out with glass beads as the packing at a fixed flow rate (superficial velocity U_s = 0.131 × 10^{-2} m/s or Re $\approx$ 0.5) with initial concentrations of carbon black in kerosene ranging from 95 to 200 mg/L. The Reynolds number Re was calculated on the basis of the diameter of the packing i.e. $Re = d_c U_s \rho / \mu$. The different experiments included a single pass mode of operation with the flow in the upward direction through the bed. No downflow single pass experiments were undertaken for any set of experiments. The resulting profiles for the variation of the filter coefficient with the specific deposit are shown in Fig. 4.1. The filter coefficient, λ, was calculated using the inlet and outlet concentrations of the carbon suspension from the packed bed as

$$\lambda = \frac{1}{L} \ln\left(\frac{C_i}{C_o}\right)$$

(4.1)

The data from the various runs collapsed onto a single trend. The data indicate that the transient filter coefficient was not dependent on the initial concentration of the carbon in the kerosene suspension. The filter coefficient is a function of the specific deposit, the chemistry of the suspension and the collector, and possibly the liquid velocity.

All the runs gave rise to a single curve with a bend at a level of carbon in the bed of between 0.6 and 0.8 mg/mL. The data indicated high values of filter coefficient (over 0.01 cm^{-1}) when the amount of carbon in the bed was low. There was a leveling off in the value of the filter coefficient after the bending and this value will be referred to as the steady state filter coefficient.

The filter coefficient calculated from the raw data for all the experiments is one that has been averaged over the entire bed using the concentrations at the inlet and the outlet of the column for this calculation. This averaging is especially severe for the initial times when the transient filter coefficient is strongly dependent on the specific deposit in the bed. The specific deposit itself has been averaged over the entire bed, as can be seen by its definition, according to Equation A5.4 in Appendix A5. The deposition of the carbon on the bed is not uniform. In fact, it was observed that as the carbon suspension passed through the bed in the beginning of an experiment, there was greater deposition near the
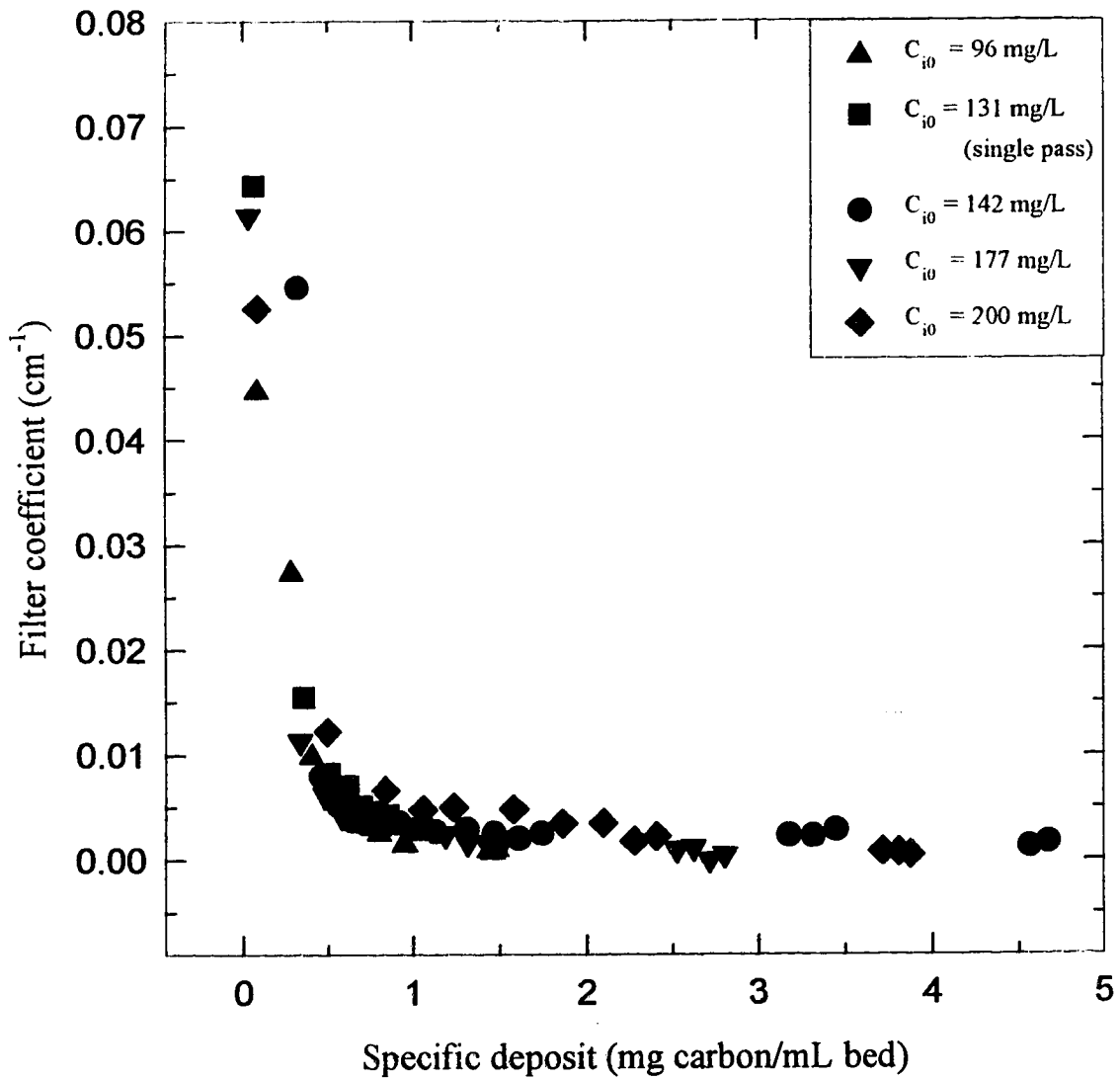
Fig. 4.1 Effect of initial concentration on filter coefficient for glass beads in upward flow at Re = 0.5

41

bed inlet. However, this averaging, probably, does not have any implications on the steady state filter coefficient. As can be seen from the profile, the filter coefficient attains a steady value which is independent of the specific deposit in the bed. Hence, the steady state filter coefficient is not an averaged value although the specific deposit across the bed may vary.

The pressure drop data obtained from this set of experiments is shown in Fig 4.2. With the exception of one group of outlying measurements, the data from the different experiments also collapsed onto a single curve with a slow pressure drop build-up for low specific deposit in the bed and nen a steady, more rapid, increase in the pressure drop once the filter coefficient had re. its steady state value.

The results from this set of experiments were significant in two ways. Experiments did not need the reproduction of the range of concentrations of suspensions observed in industry or that used by another investigator for the purpose of comparing filter coefficients. Secondly, the concentration of the carbon black in the suspension need not be held constant to study the effect of operating variables on the filter coefficient. Filter performance can be normalized with respect to the specific deposit. This result underlies the design of experiments in the following sections of this thesis.

4.3 Particle trapping on glass beads

4.3.1 Upflow of kerosene through the packed bed

In order to evaluate the role of liquid velocity, the transient filter coefficients were determined using glass beads as the packing for different flow rates of kerosene ranging from 0.48 L/h to 4.8 L/h (or Re ranging from 0.1 to 1.0). A plot of the filter coefficient for different Reynolds numbers is shown in Fig. 4.3.

The data of Fig. 4.3 indicated that although the variation of the filter coefficient with specific deposit followed a similar trend for all the velocities, the curves were not superimposable. The leveling off of the filter coefficient at approximately 0.8 mg/mL of specific deposit may indicate a change in mechanism for capture at this point. All the curves for the different velocities bend at around the same point of mass of carbon in the

42

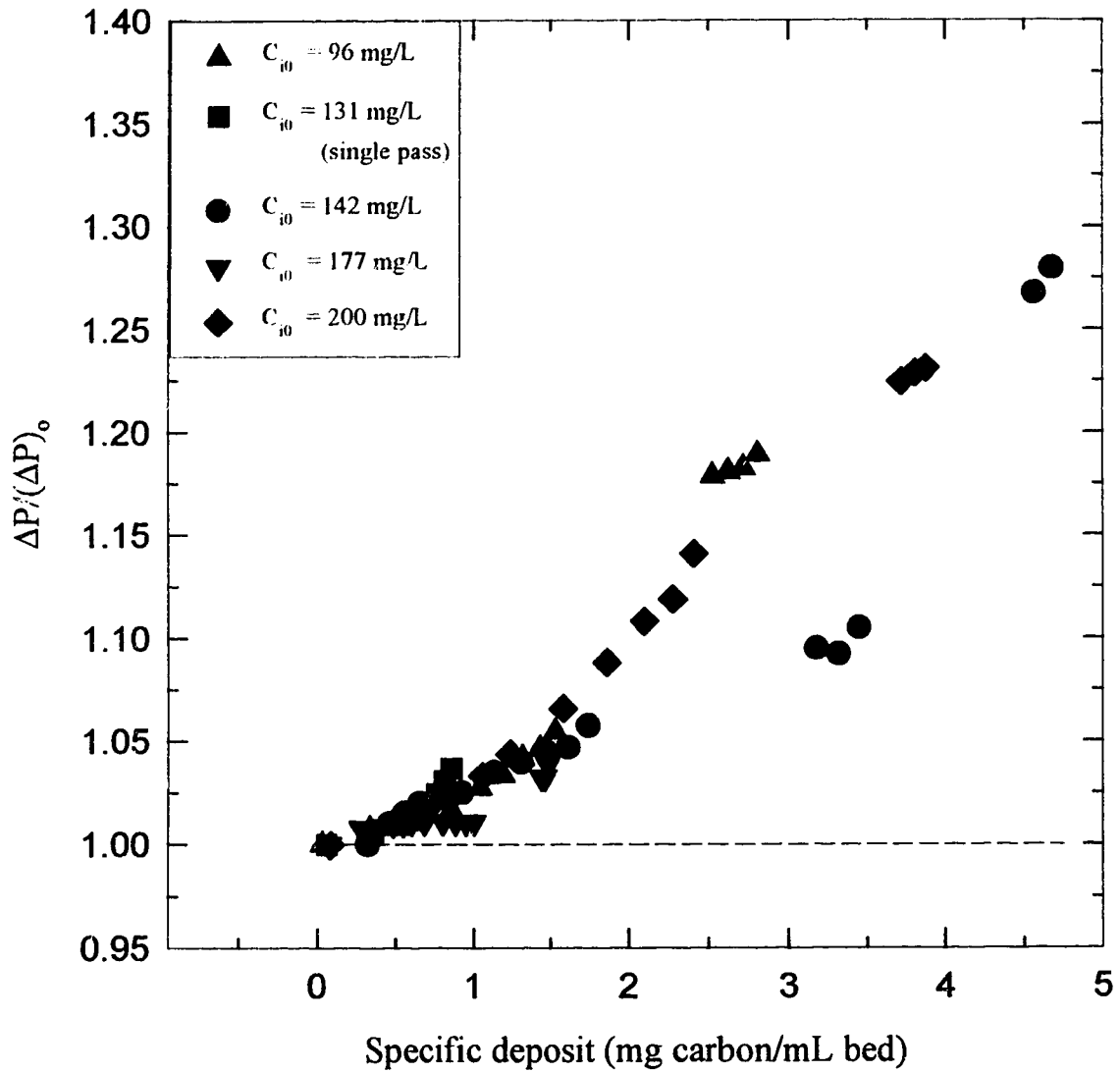*Fig. 4.2 Effect of initial concentration on pressure drop build-up with deposition for glass beads in upward flow at Re = 0.5*

43

bed. It is believed that the high values of filter coefficient before this point i.e. a specific deposit of 0.8 mg/mL may be due to the formation of a monolayer on the packing or due to greater attractive forces between the collectors and the particles in suspension as compared to the those between the carbon and carbon particles. These attractive forces may be due to the Van der Waals forces between carbon and the collector or electrostatic forces due to opposite charges. Beyond a specific deposit of 0.8 mg/mL, carbon adhesion to carbon may be responsible for capture. Monolayer calculations given in Appendix A6 showed that the amount of carbon required for the formation of a monolayer on the packing (10.6 mg/mL) is much higher than that corresponding to a specific deposit of 0.8 mg/mL.

Calculations given in Appendix A10 for the determination of the Hamaker constant showed that the Hamaker constant between the particles and collector is not very different than that between the particles in suspension. Therefore, electrostatic attraction, rather than London-Van der Waals attraction could be probably responsible for capture during the initial period of high filter coefficients. The electrokinetic studies discussed in Section 4.1 which showed that the collector and carbon particles have opposite charges, help confirm that electrostatic attraction was responsible for deposition during initial times.

Chowdiah et al. (1982) monitored the charge on a packed bed by measuring the streaming potential. It was observed that the point of charge neutralization coincided with the point of breakthrough of carbon particles in the effluent. For the sake of comparison, their data from an experimental run has been plotted in terms of the filter coefficient and specific deposit in Figure 4.4. There appears to be a similar trend for the transient filter coefficient in both the cases with a leveling off of the filter coefficient after initial high values. In their case, it was confirmed that the steady state filter coefficient was achieved after the neutralization of charge. Capture continued during steady state as a result of other mechanisms, such as straining or dendrite formation (i.e. carbon deposition on carbon).

For the case of upflow, no deposition took place beyond an initial period of deposition at Reynolds numbers of 0.75 and 1.0. At these values of Reynolds numbers, the concentration in the tank (C_i) merely fluctuated without any significant change i.e. $\lambda \approx 0$
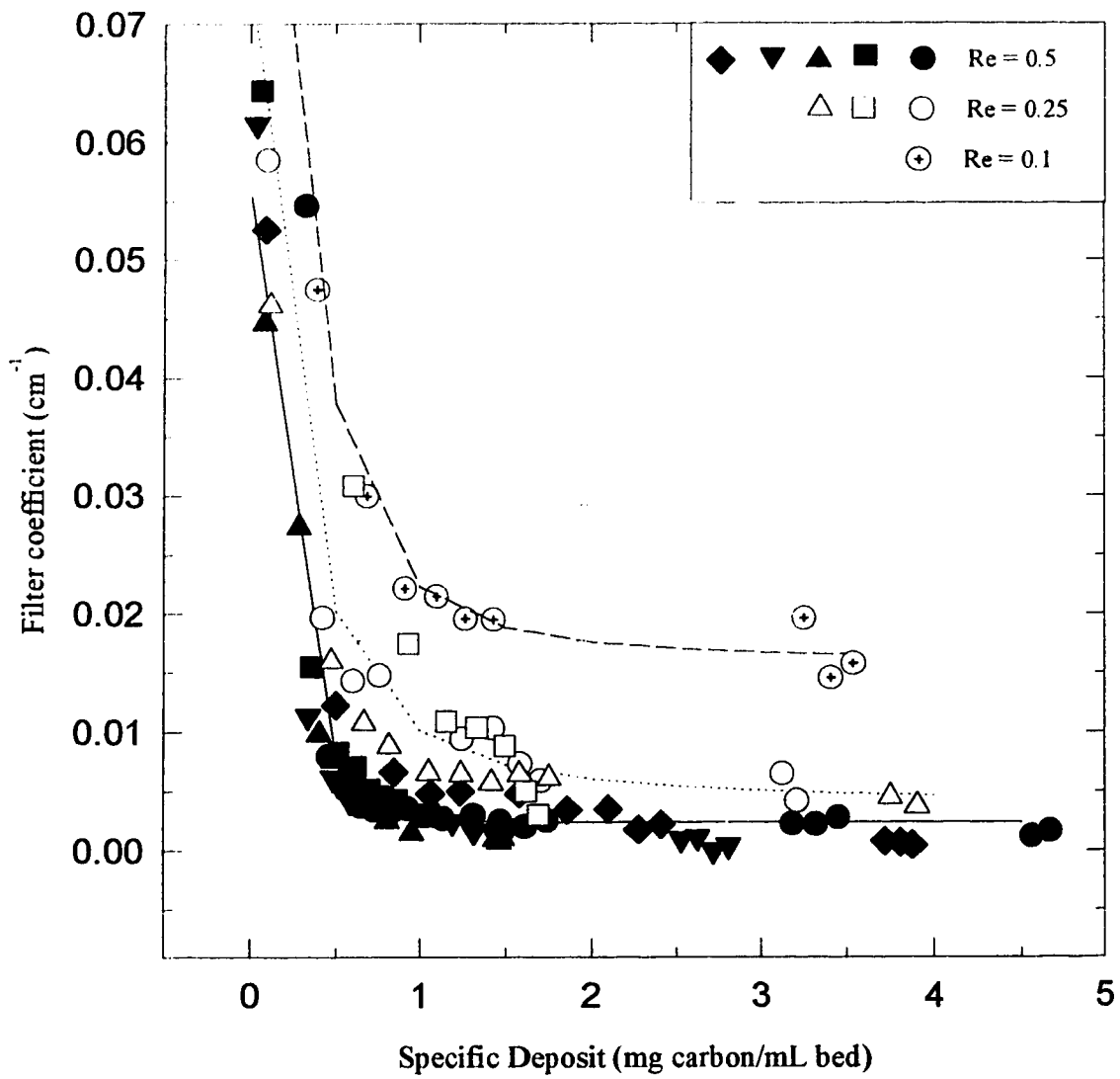
Fig. 4.3 Filter coefficient versus specific deposit for glass beads in upward flow

45
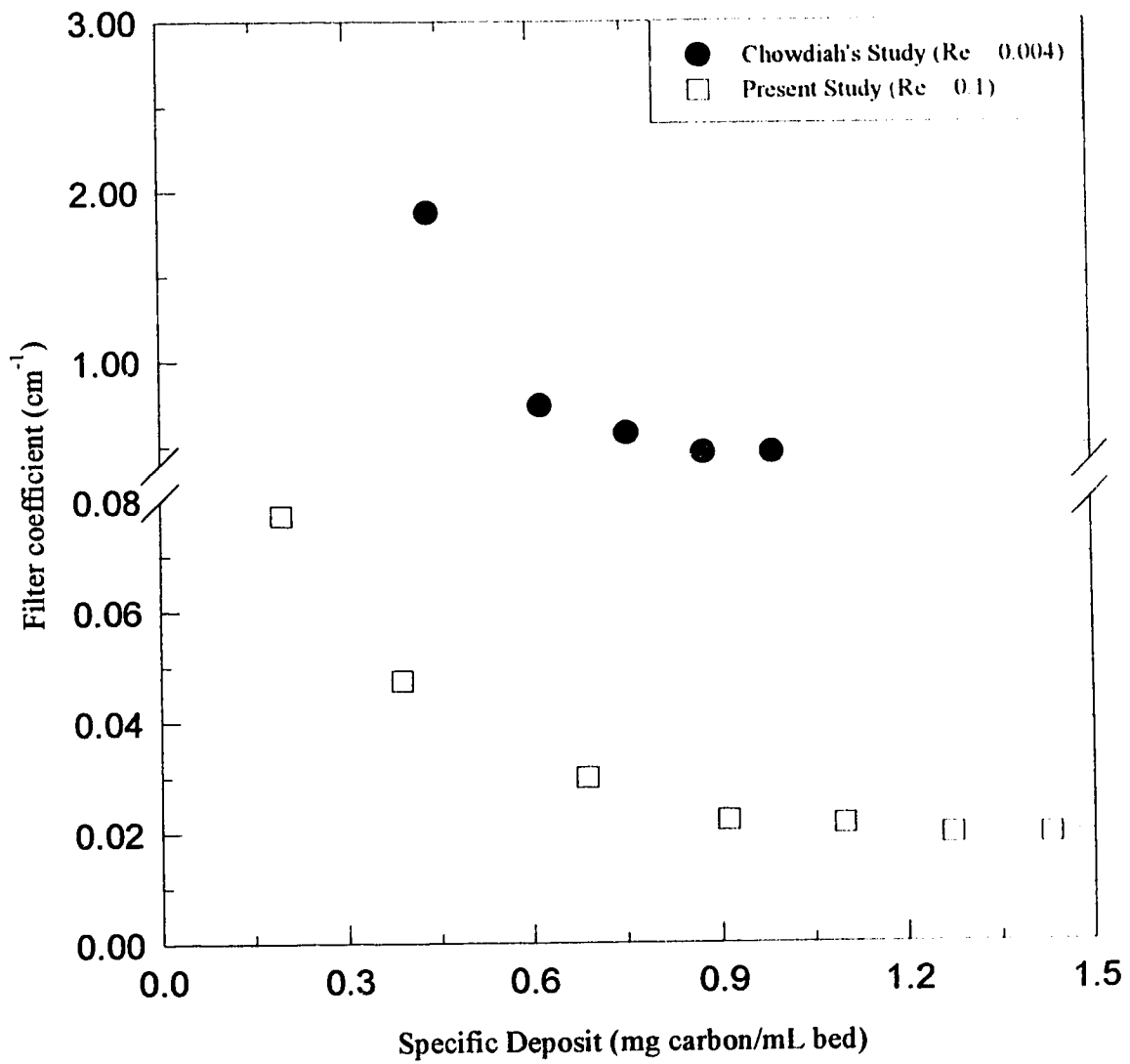
Fig. 4.4 Comparison of transient filter coefficient with Chowdiah et al. (1982)

46

within experimental precision. The same pattern was true for the pressure drop i.e. the pressure drop did not increase with time after an initial increase. These observations imply that there was a critical Reynolds number for upflow between 0.5 and 0.75, beyond which particles no longer remain attached at steady state i.e. when attachment is no longer between particles and collector.

Pressure drop variation with deposition at different velocities is shown in Fig. 4.5 for the case of upward flow. There was a significant difference in the rate of increase at different velocities, with a greater relative increase in pressure drop at lower velocities than at higher velocities. For the two highest values of Re which were studied, the plot $(\Delta P)/(\Delta P)_o$ with specific deposit was a horizontal because there was no deposition and therefore no change in pressure drop. The data of Fig. 4.5 suggest that the structure of the deposit in the pores of the bed was critically dependent on the flow velocity. The structure of the deposits on the catalyst at different flow rates was examined by microscopy in Section 4.4.2. Photographs with glass beads could not be obtained because the surface of the glass beads reflected too much light.

4.3.2 Downflow of kerosene through the packed bed

Experiments carried out for downflow with glass beads gave data similar to those obtained for upflow. A plot of filter coefficient with specific deposit at different velocities is given in Fig. 4.6. The significant difference when the direction of flow was downward, as compared to upward through the packed bed, was that deposition took place even at Reynolds numbers 0.75 and 1.0. At these Reynolds number values deposition had ceased to occur for the upflow case.

The change in pressure drop with specific deposit from Fig 4.7 shows that there was a variation with velocity for downflow, which was similar to that observed for upflow.

4.4 Particle trapping on catalyst

4.4.1 Upflow of kerosene through the packed bed

When catalyst was used as packing, the variation of the filter coefficient with specific deposit (or time) at different velocities of the kerosene stream, given in Fig. 4.8, showed

Fig. 4.5 Pressure drop build-up with deposition for glass beads in upward flow

Fig. 4.6 Filter coefficient versus specific deposit for glass beads in downward flow

49

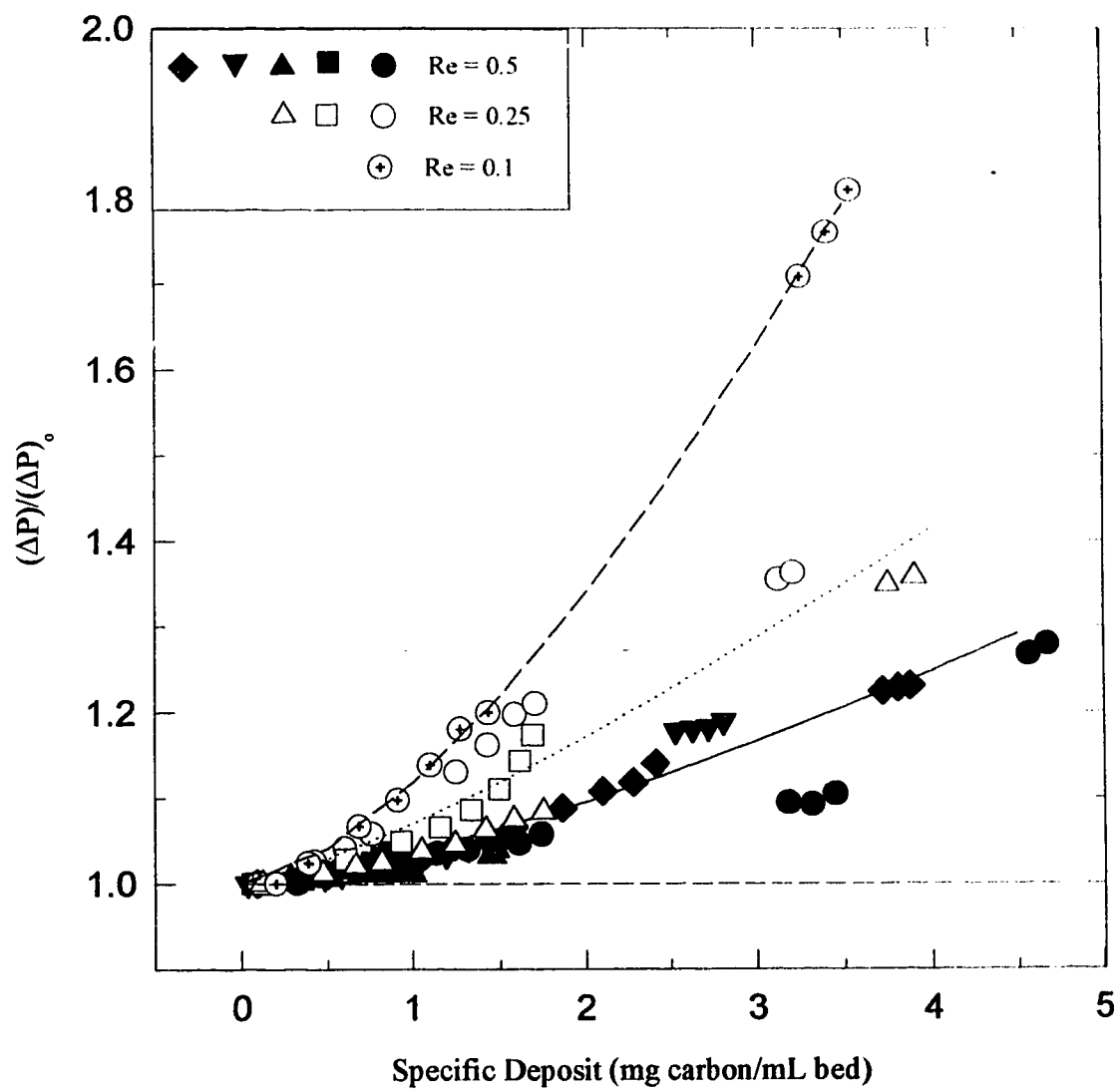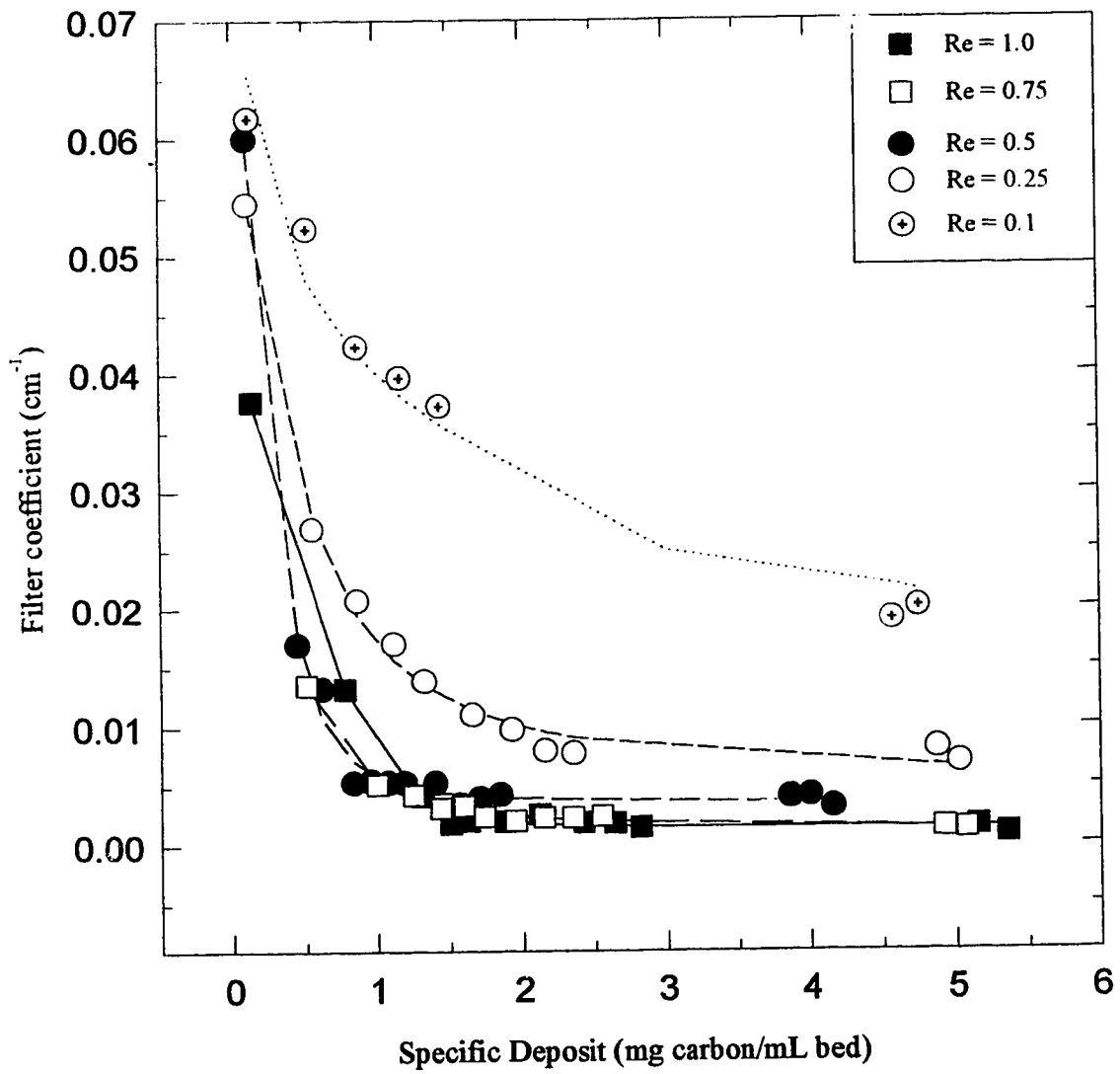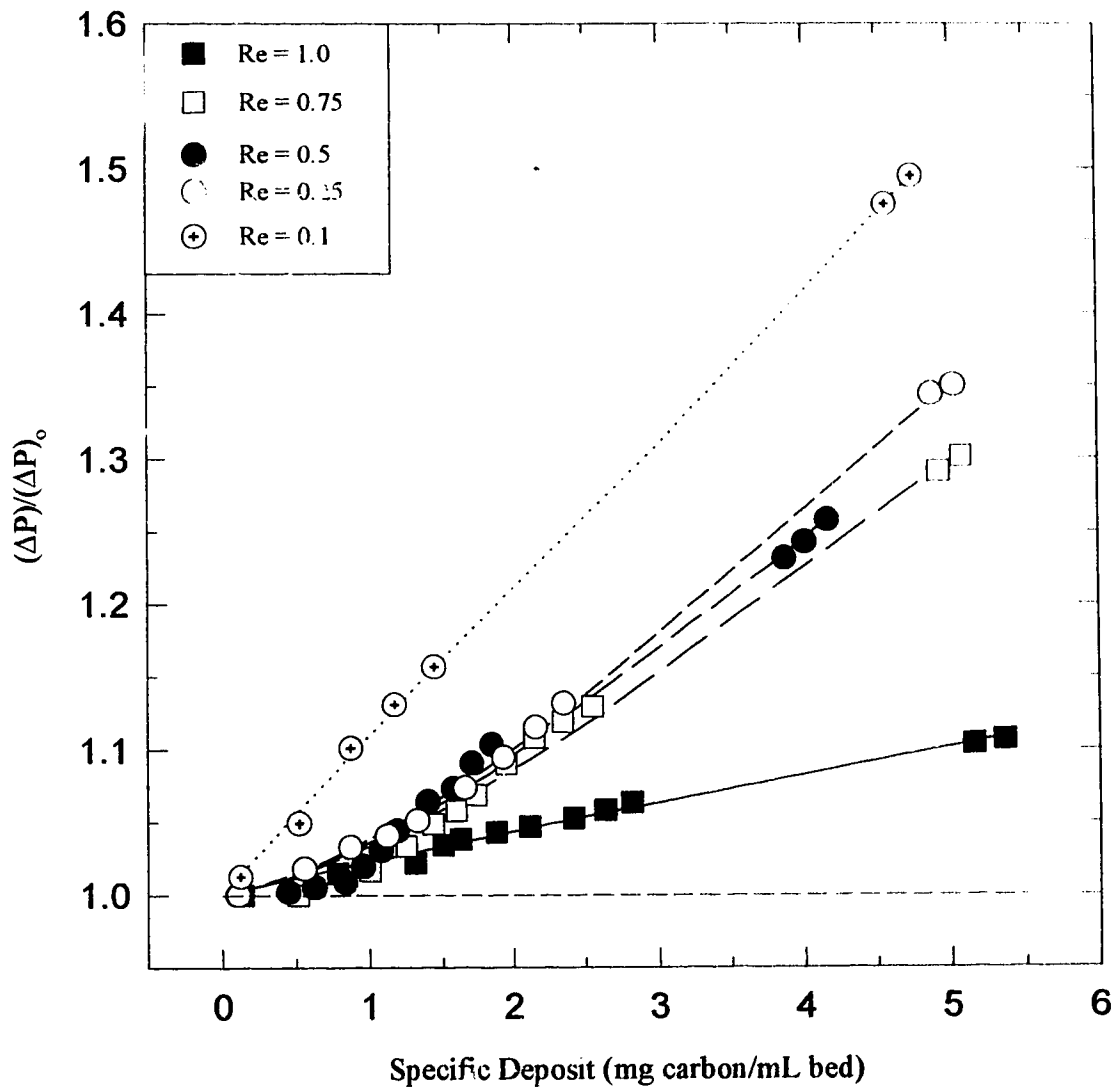*Fig. 4.7 Pressure drop build-up with deposition with glass beads for downward flow*
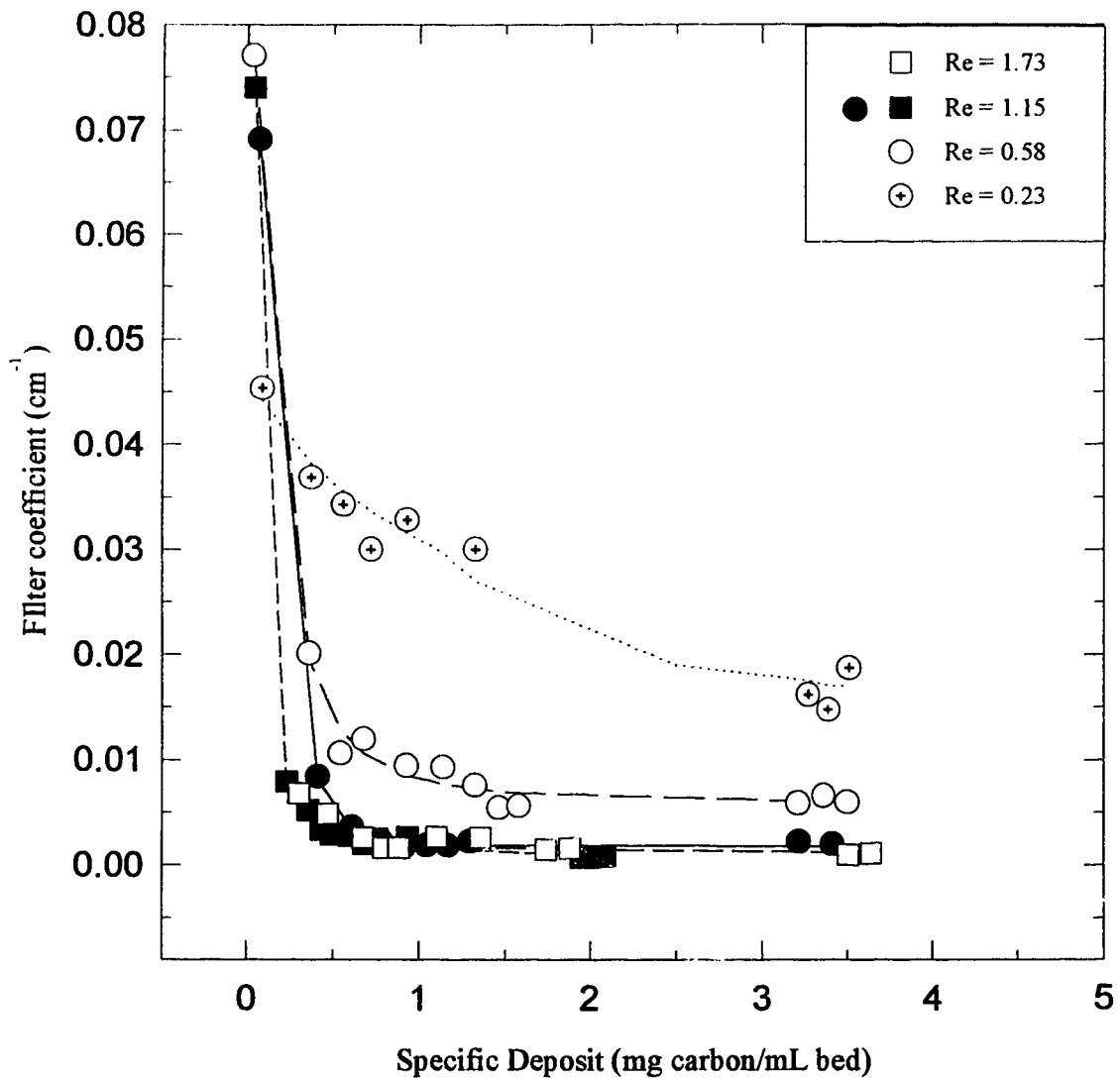
Fig. 4.8 Filter coefficient versus specific deposit with catalyst in upward flow

similar trends as with glass beads. Re was varied from 0.23 to 2.3; the velocities corresponding to Re from 0.1 to 1.0 with glass beads. However, some differences were observed when using catalyst as packing as opposed to glass beads.

Deposition did not cease to occur at velocities of 0.197 cm/s (Re 1.73 for catalyst and 0.75 for glass beads) and 0.263 cm/s ($Re = 2.3$ for catalyst and 1.0 for glass beads), when catalyst was used. Experiments by Maroudas and Eisenklam (1964) showed that deposition ceases when the interstitial velocities are greater than a certain critical value. Since the diameter of glass beads was smaller than the effective diameter of the catalyst, the diameter of pores within the bed of catalyst were larger than the diameter of pores within the bed of glass beads. The interstitial velocities were, therefore, higher for the case of glass beads at the same superficial velocity as compared to those for the bed of catalyst. This difference could be the reason why deposition continued to occur at a Re of 2.3 for the catalyst but did not occur with glass beads at a Re of 1.0.

The pressure drop build-up with deposition of carbon on the catalyst is shown in Fig. 4.9. The normalized pressure drop did not follow a definite trend with liquid velocity as was observed for the case of the glass beads. Although there appears to be a definite difference in pressure build-up between different velocities, there was no pattern for the variation of this build-up with velocity. This anomaly can be explained on the basis of Fig. 4.10, where the pressure drop for a clean bed (from the repeated experiments for upflow and downflow) has been plotted against Re. Pressure drop data from glass beads are also shown. There was a greater variation in the initial pressure drop (i.e. the pressure drop developed across the bed when the bed is clean) at a particular velocity with catalyst than for the case of glass beads. The ratio of the length of the catalyst pellets to the diameter of the column was 0.28 which is greater than 0.125, the recommended value (Treybal, 1980) necessary to ensure good liquid distribution and the absence of wall effects. In the case of glass beads, d_c/D_{col} was equal to 0.04. The difficulty in packing the catalyst uniformly along the length of the column prevented reproducible initial pressure drops from experiment to experiment. This variability could be the reason why the build-up did not follow a regular trend with velocity.
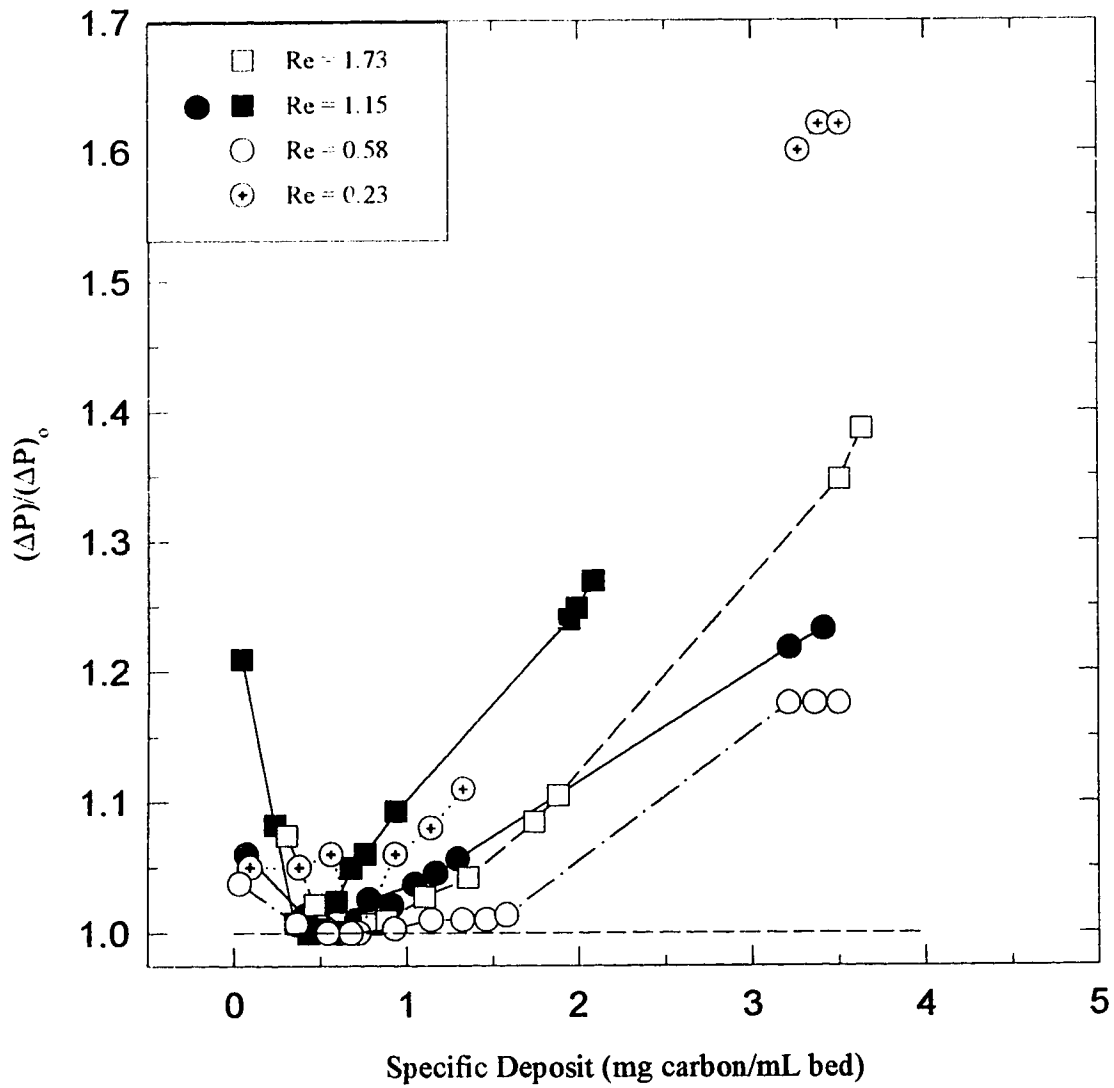
Fig. 4.9 Pressure drop build-up with deposition for catalyst in upward flow
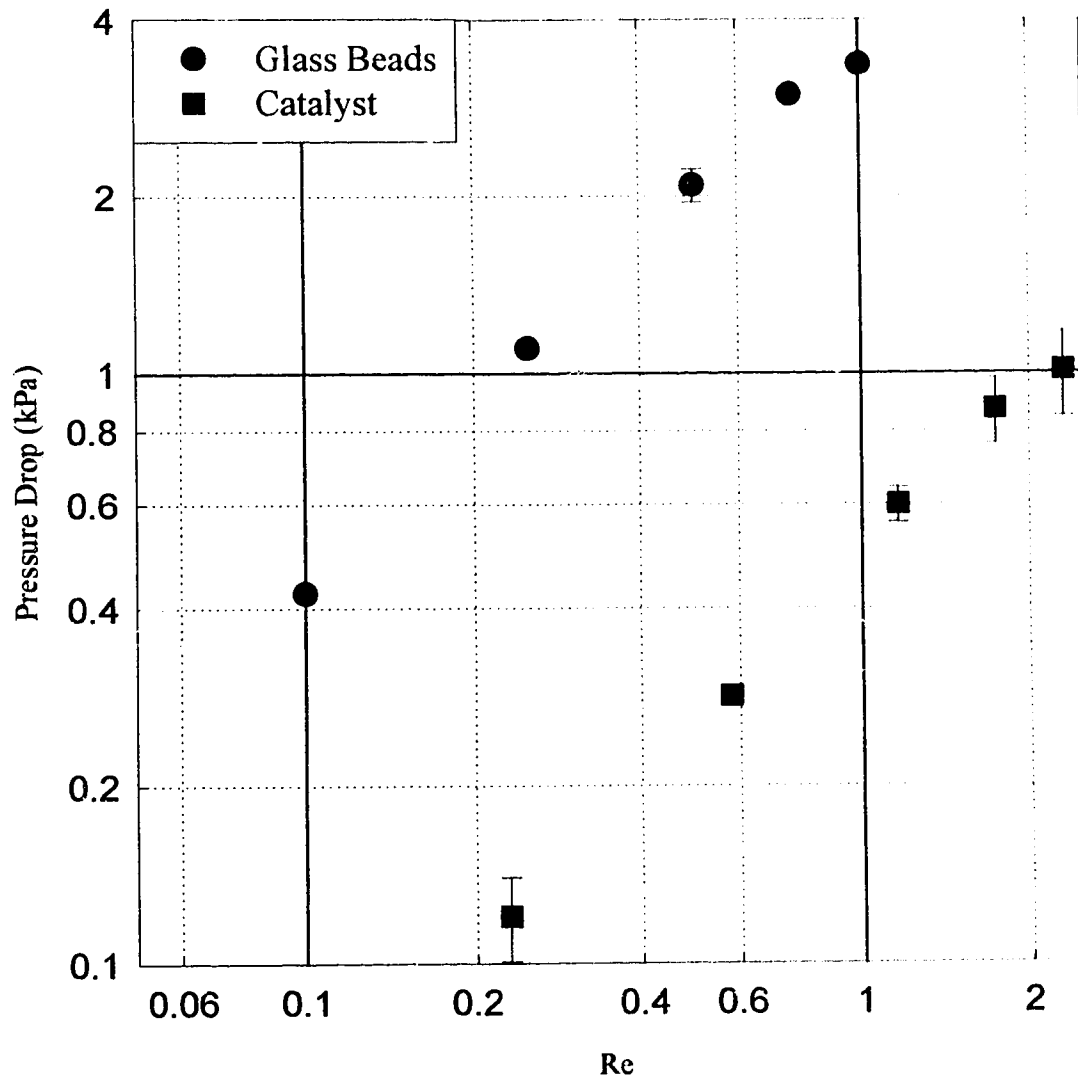
Fig 4.10 Pressure drop versus Re

54

Moreover in the case of catalyst it was observed that although there was definite trapping of carbon black in the bed (as indicated by the decreasing tank concentration), there was an initial period of decreasing pressure drop. The microporosity of the catalyst prevented complete removal of air from the packing during start-up. Higher pressure drops occurred, therefore, when air bubbles were trapped within the bed. With time, air was displaced from the bed till there was no more air visible within the packed section. Subsequently, the pressure drop showed an increase. The combination of variability in packing the catalyst and transient changes due to air bubbles can account for the lack of a trend in $(\Delta P)/(\Delta P)_o$ as a function of liquid velocity.

4.4.2 Downflow of kerosene through the packed bed

When catalyst was used as packing with flow downward, similar variation of filter coefficient with specific deposit was observed as with the glass beads (Fig. 4.11). The pressure drop profiles for downward flow are illustrated in Fig. 4.12. The experiments with catalyst gave few initial points for the filter coefficient. At the beginning of each experiment, the direction for filling the column with kerosene was always upward in order to displace the air from the bed. When the direction of flow was reversed to begin the experiment, there was some 'backwashing' of the deposit giving rise to a transient increase in column concentration. These changes at the beginning of each experiment prevented measurements of filter coefficients at low specific deposit (i.e. at short times).

Figs. 4.13 and 4.14 show typical images of the structure of deposit formed on the catalyst during downflow for $Re = 2.3$ and $Re = 0.23$ respectively. Lower velocities permitted the formation of a web of carbon particles within the pore, while there was a conspicuous absence of such a structure within the pore at $Re = 2.3$. Fig. 4.13 shows an uneven distribution of lumpy deposits. Microscopy revealed that the carbon particles in suspension before and after deposition were stable and did not flocculate. Hence, the formation of lumpy deposits on the collector surface was due to carbon adhesion to carbon. This type of a lumpy deposit differs from a monolayer in that a monolayer is an even layer of carbon black all over the surface of the collectors. The mode of deposition,
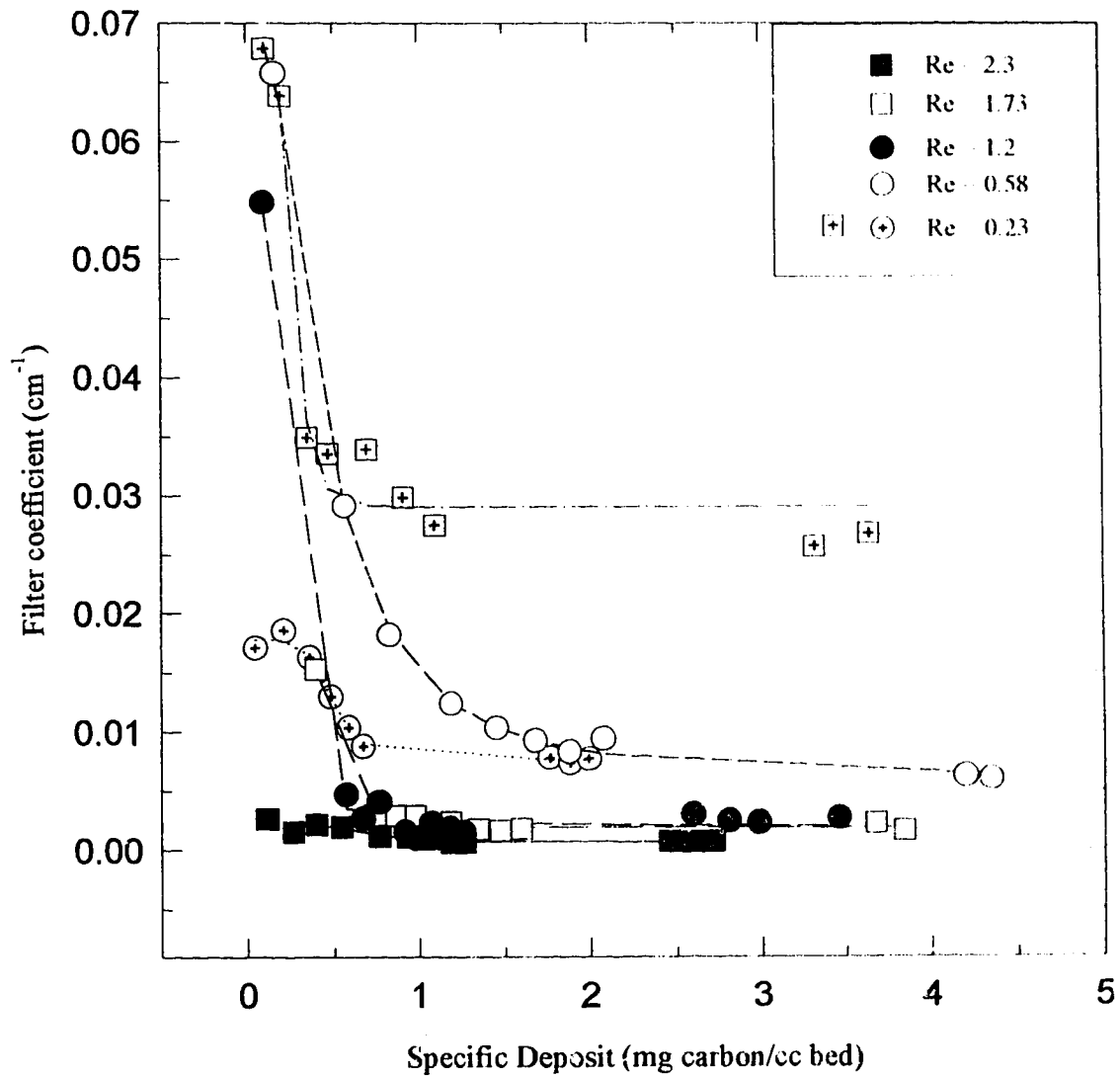
Fig. 4.11 Filter coefficient versus specific deposit for catalyst in downward flow
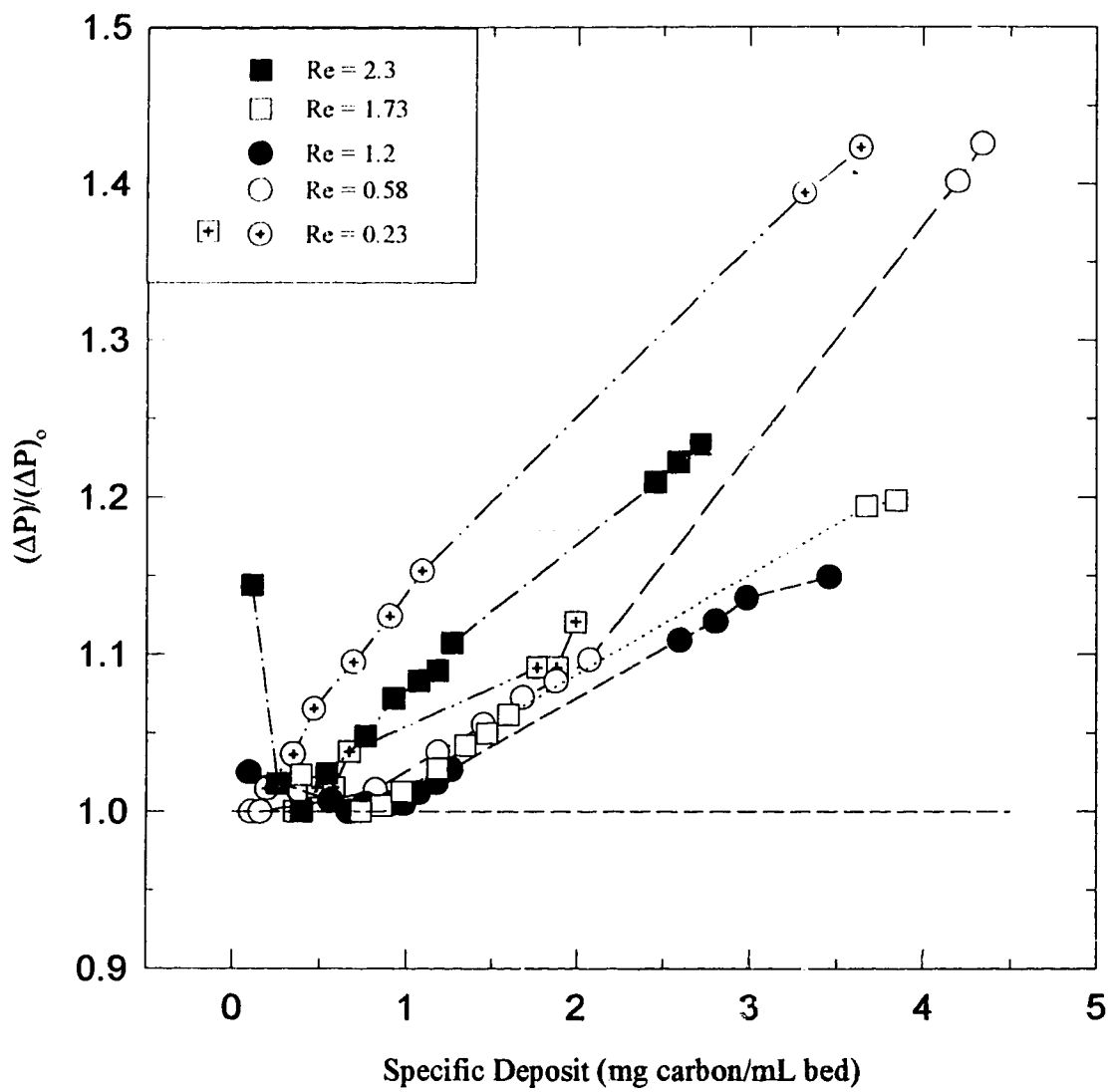
*Fig. 4.12 Pressure drop build-up with deposition with catalyst for downward flow*
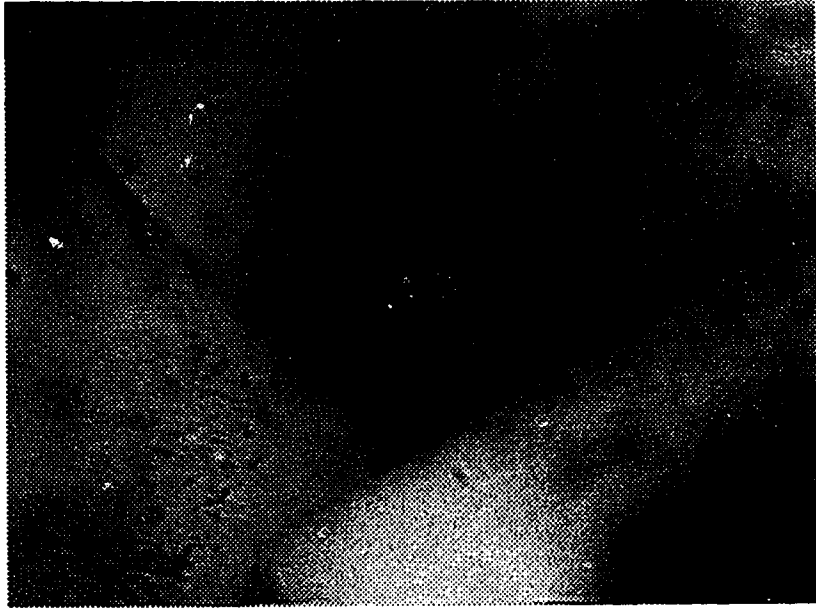
Fig. 4.13 Photograph of structure of deposit with catalyst at Re = 2.3
Scale : 1 cm = 0.33 mm
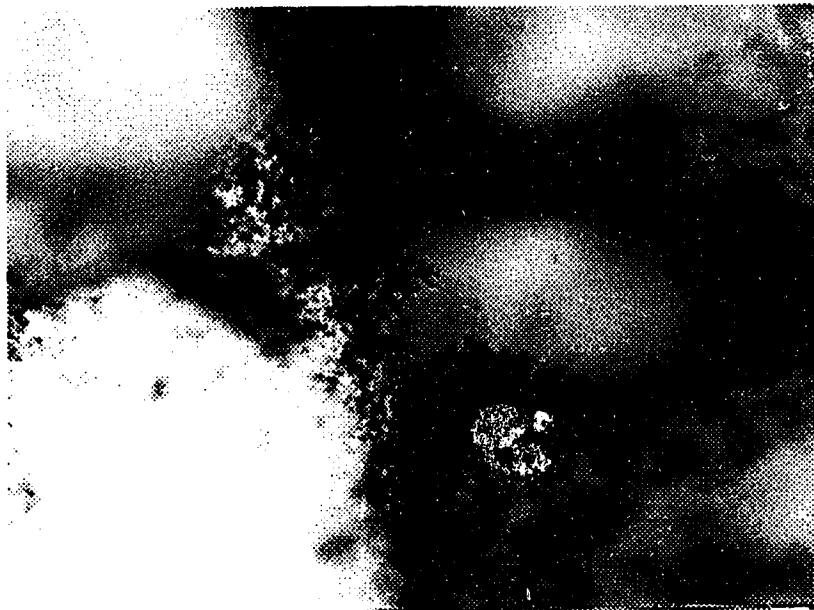
Fig. 4.14 Photograph of structure of deposit with catalyst at Re = 0.23
Scale : 1 cm = 0.33 mm

therefore, was likely starting with initial deposition on the surface followed by subsequent deposition of carbon black onto carbon black.

4.5 Interpretation of steady state filter coefficients

The steady state filter coefficient was the value of the filter coefficient that was attained after the initial transient period. This value was verified as remaining unchanged even after 40 h of continued deposition. The steady state filter coefficient was likely due to capture of carbon black particles on the carbon that was already deposited on the packing. As illustrated in Fig. 4.13 and Fig. 4.14, these deposits would range from domains on the surface of the collector at high Re to web-like structures in the pores at low Re.

4.5.1 Effect of velocity and direction with glass beads

Steady state filter coefficients (λ_{ss}) for deposition with upflow and downflow were plotted against the superficial velocity on a log-log plot for the glass beads, as illustrated in Fig. 4.15. The steady state filter coefficient showed power-law behavior with respect to the superficial velocity. Deposition did not take place for upward flow at $Re = 0.75$ and Re 1.0, however, deposition continued at steady state for these Reynolds numbers with downward flow.

The steady state filter coefficients for the case of downflow were higher than for the case of upflow (Fig. 4.15). This observation can be explained as follows :

$$\text{Flux of particles towards collectors} \approx Flux_{\text{Lon-Van derWaal}} + Flux_{\text{gravity}} + Flux_{\text{diffusion}} \quad (4.2)$$

The flux due to the three mechanisms are additive when flow is in the downward direction. When the flow of kerosene is upward, the flux due to gravity (g being a vector) and those due to the other mechanisms are opposite, as the density of carbon black is higher than that of kerosene. Hence, the net flux for the case of downflow is higher than that for upflow, resulting in increased capture when the flow of the carbon suspension in kerosene is downward as opposed to when the flow is upward. Table 4.2 shows the relative contributions of efficiencies due to London-Van der Waals attraction, gravity and diffusion. Calculations have been performed according to Equation 2.24. It is noteworthy
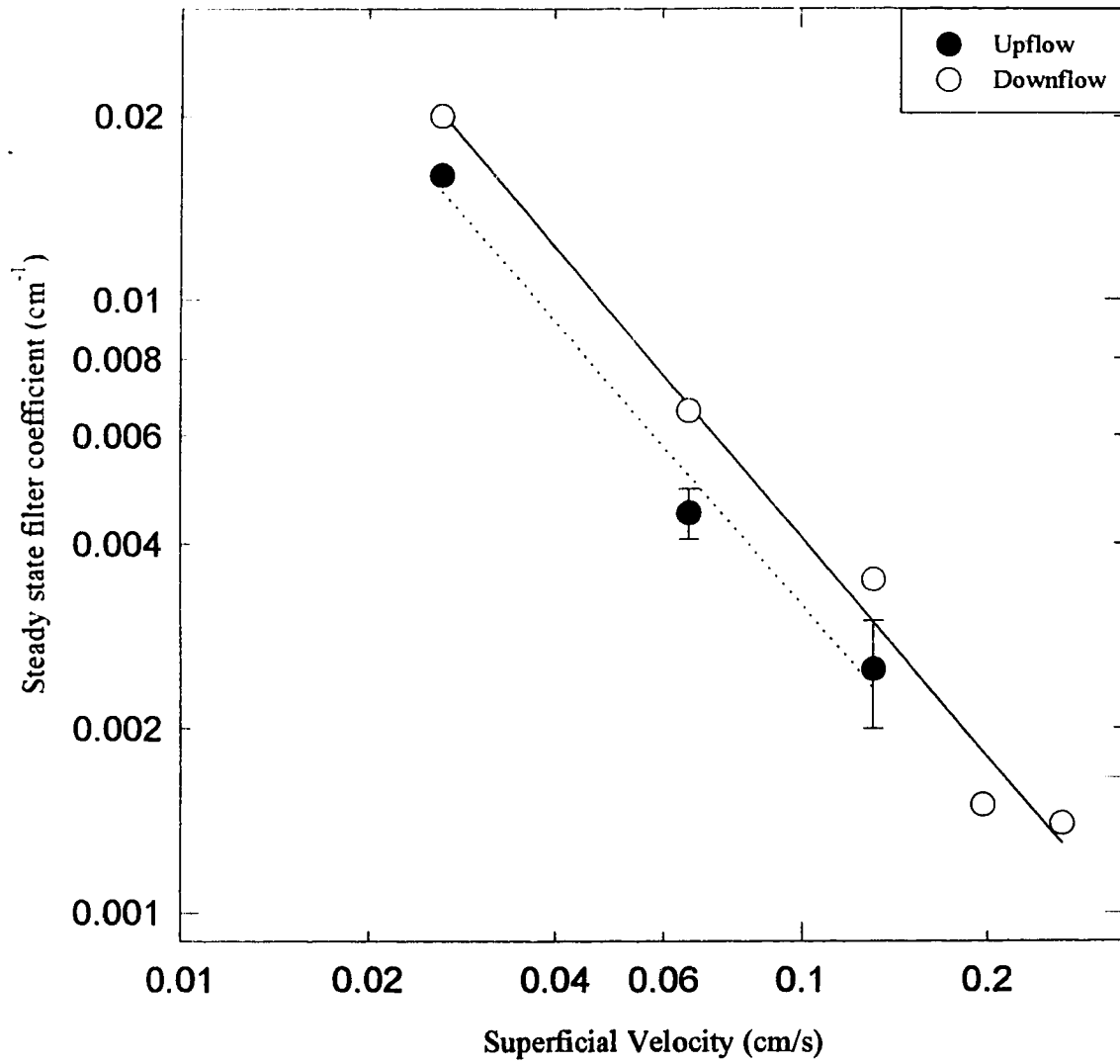
Fig. 4.15 Steady state filter coefficient versus superficial velocity for glass beads

that at higher velocities η_G is comparable to η_{LO}. This also leads to our experimental observation that deposition ceased to occur at high velocities in upflow.

	London-Van der Waals attraction	Gravity	Diffusion-Convection
Re	η_{LO}	η_G	η_{diff}
0.1	1.38×10^{-3}	0.032	3.45×10^{-4}
0.5	1.5×10^{-3}	4.6×10^{-3}	1.17×10^{-4}
1.0	1.04×10^{-3}	2.01×10^{-3}	7.38×10^{-5}

Table 4.2 Effect of different mechanisms on the overall efficiency at different velocities

Work by Thomas and Yoder (1956) for aqueous systems in which the particle density was greater than that for the liquid, also showed that particle trapping was greater with flow in the downward direction than in the upward direction.

The steady state filter coefficients were higher for lower flow rates or lower superficial velocities of the liquid stream. Various mechanisms may be responsible for the capture of particles from the suspension onto the packed bed. Forces due to gravity, Van der Waals attractions and diffusion are inversely dependent on the superficial velocity of the liquid stream, as discussed in Section 2.2.2.1. Filter coefficient values are related to efficiency as (Tien, 1989)

$$\lambda = \frac{3(1 - \varepsilon_o)\eta}{2d_c} \tag{4.3}$$

The functional dependence of the filter coefficient, following from Equation 2.24 and Equation 4.3, is of the form :

$$\lambda = AU_\infty^{-0.12} + BU_\infty^{-1.2} + CU_\infty^{-0.67} \tag{4.4}$$

where the first term is the contribution due to Van der Waals attraction, the second term is due to gravity and the third due to diffusion-convection. If one term is dominant, then we can approximate this relationship as

$$\lambda = DU_\infty^{-\beta} \tag{4.5}$$

The overall dependence of the filter coefficient on the velocity depends on the relative magnitude of these three forces, the variation being between $\beta = 0.12$ (for only Van der Waals attraction) and $\beta = 1.2$ (for only gravitational forces). A regression analysis for λ_{ss} versus velocity for glass beads gave $\beta = 1.16$ for upflow and $\beta = 1.19$ for downflow indicating that gravity was more significant for this system than Van der Waals forces. Other investigators have observed a similar functional dependence, for example, Fitzpatrick and Spielman (1973) observed an inverse dependence of filter coefficients on velocity ranging from $\beta = 0.2$ for low velocities to $\beta = 0.5$ at higher velocities for filtration experiments conducted with latex suspensions in aqueous media through a bed of glass spheres. The value of β, and the dominant force for capture, would depend on the chemistry of the liquid medium and the particles being deposited.

4.5.2 Effect of velocity and direction with catalyst

When catalyst was used as the packing material, it was observed that the dependence of the steady state filter coeff cients on velocity was similar to the glass beads, as illustrated in Fig. 4.16. The filter c fficient values were found to decrease with increasing superficial velocity of the liqu d. The dependence of the steady state filter coefficient on velocity was $\beta = 1.41$ for upflow and $\beta = 1.2$ for downflow. However, it must be noted that there was a greater variation of the steady state filter coefficient at a particular velocity with the catalyst as compared to the glass beads. This can be attributed to lack of uniformity of packing of catalyst within the bed for reasons cited in Section 4.4.1.

Statistical analysis showed that the confidence interval for β for the plot of downflow ($1.95 > \beta > 0.83$) was within the confidence interval for that of upflow ($1.75 > \beta > 0.90$). Details of how the calculations were performed are given in Appendix A7. These values

63

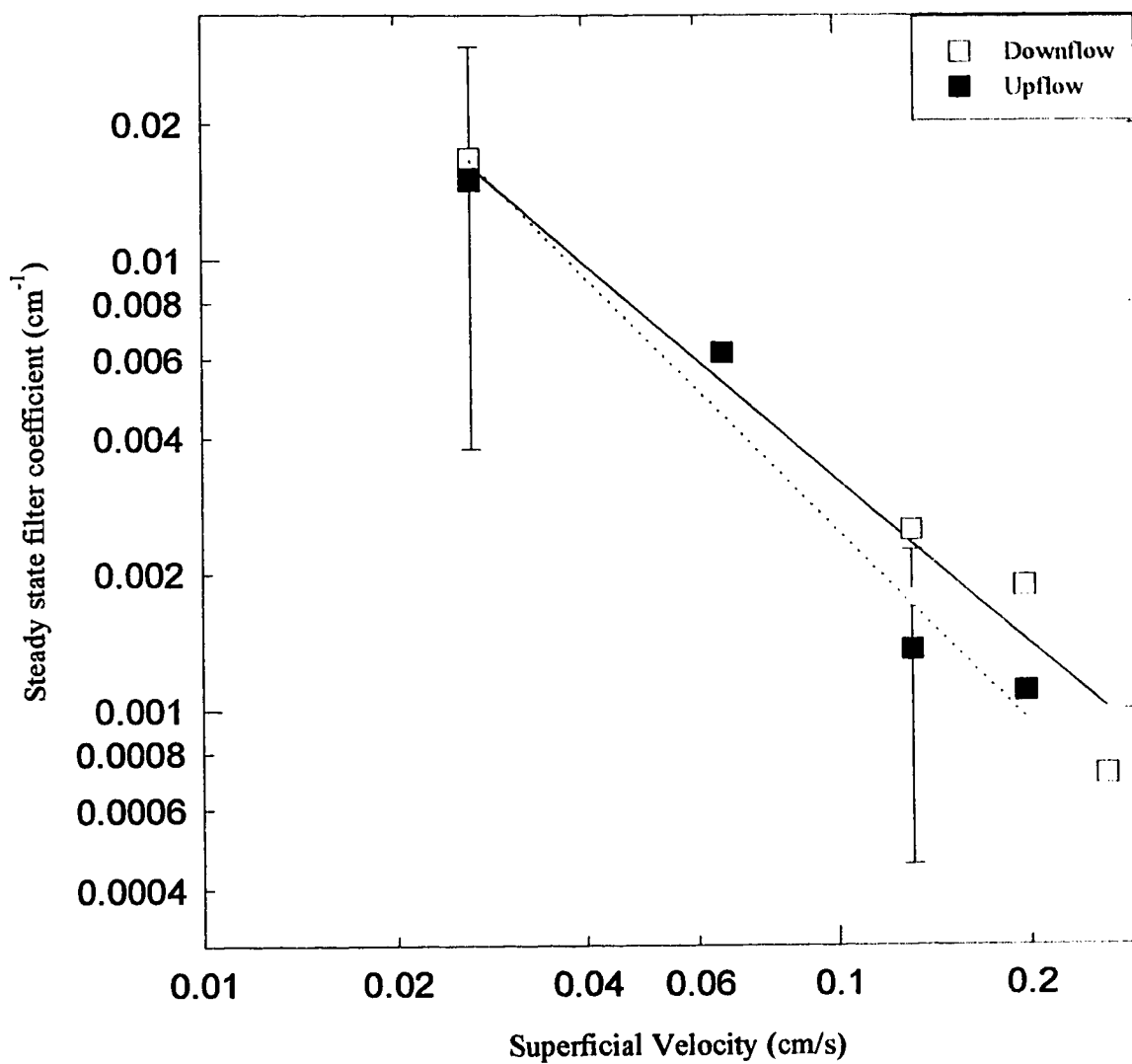*Fig. 4.16 Steady state filter coefficient versus superficial velocity for catalyst*

of β for $λ_{ss}$ indicated that gravity was the dominant force for capture in the case of catalyst as compared to other forces, the same as for the glass beads.

4.5.3 Comparison of experimental and predicted values of filter coefficients

Comparison of the experimental steady state filter coefficient values with those predicted for downflow by Rajagopalan and Tien's trajectory approach (Rajagopalan and Tien, 1976; Section 2.2.2.2) is shown in Fig. 4.17. Although the dependence of the filter coefficients on velocity was similar (for glass $β_{pred}$ = 1.02 as compared to $β_{expt}$ = 1.19; for catalyst $β_{pred}$ = 1.17 as compared to $β_{expt}$ = 1.2), the predicted values are higher than those obtained from experiments by one order of magnitude. This modeling approach predicts values of filter coefficients during initial periods of deposition i.e. when the filter is relatively clean. The experimental filter coefficient values which have been used are those for the steady state. The transient filter coefficient curves indicated higher values of filter coefficients at early times, therefore, the magnitude of the observed values of filter coefficients were similar to the theoretical predictions at short times. For example, Fig. 4.3 illustrates that the first measured value of λ as 0.045-0.065 cm^{-1} at Re = 0.5, compared to λ = 0.003 cm^{-1} at steady state. Experiments conducted in our study did not provide enough data at short times to compare the initial filter coefficients at different velocities.

No predictions could be obtained for upflow as neither of the two modeling approaches discussed in Section 2.2.2.2 provide an expression for the case of negative gravitational numbers. Values for filter coefficients for upflow and downflow could not be extrapolated from the plots obtained by computational simulations with the Spielman-Fitzpatrick approach because the Van der Waals attraction number (N_{ADS}) for our system had extremely low values of the order of 10^{-14} due to the fact that gravity was the dominant mechanism for capture in our experiments. The numerical calculations by Spielman and Fitzpatrick (1973) covered N_{ADS} from 10^{-6} to 10^{7}. However, a qualitative comparison can be made between this work and Spielman-Fitzpatrick's model as summarized in Fig 2.5. It is seen from the figure that with decreasing N_{ADS}, there is a larger difference in the values of efficiency between upflow and downflow for the values of $N_{G,S}$ of this study. $N_{G,S}$, following Equation 2.20a, ranges from 0.2 to 2 for glass beads and 1.5 to 15 for catalyst.
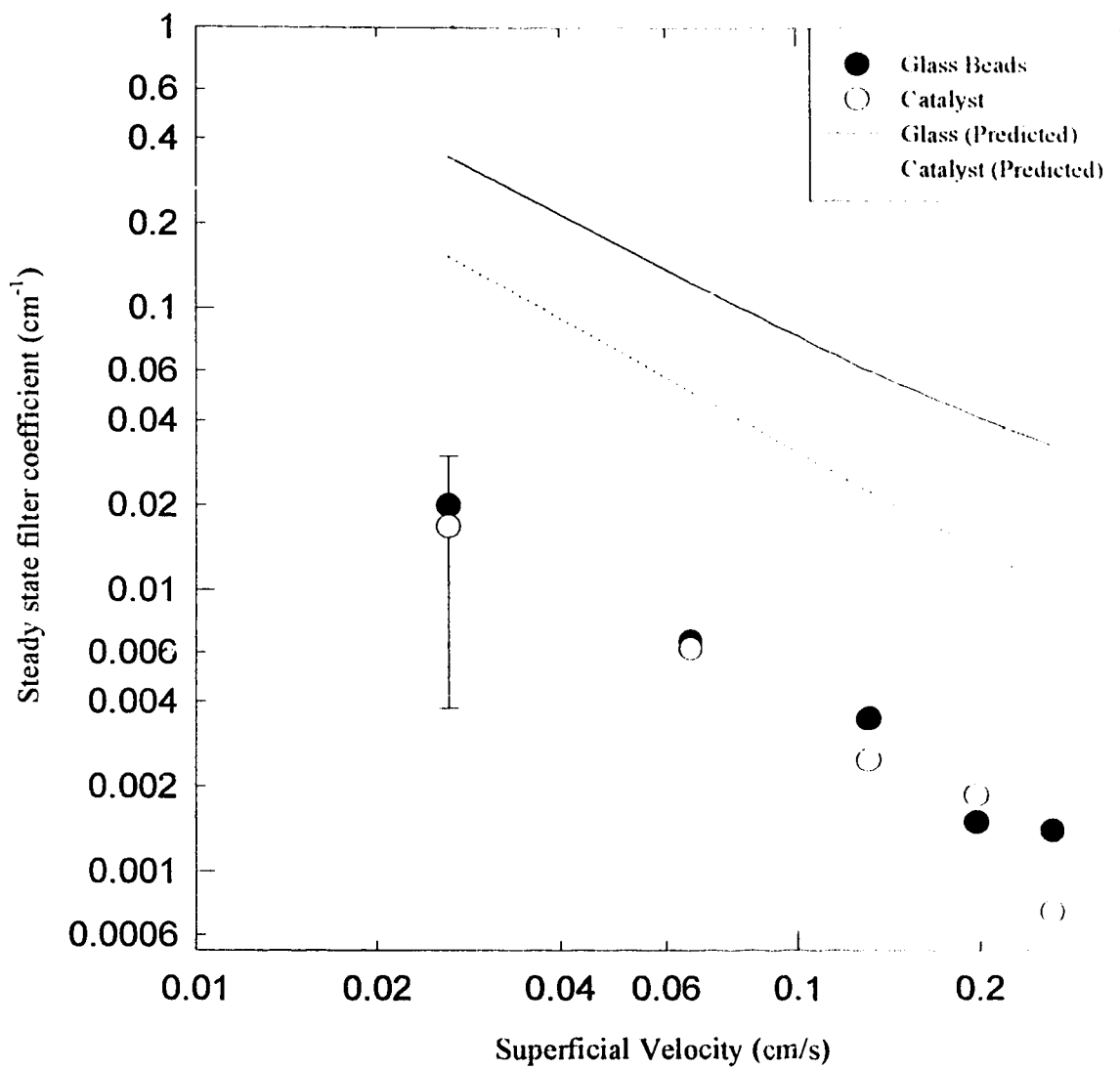
Fig. 4.17 Comparison of experimental steady state filter coefficients with predicted values for glass beads and catalyst for downflow

Figure 2.6, which shows the predicted values of capture efficiency from Rajagopalan and Tien's approach (Rajagopalan and Tien, 1976; Section 2.2.2.2), was for a constant value of N_{Lo} 1.45×10^{-5}. N_{Lo} for our experiments varied from 0.13×10^{-5} to 1.3×10^{-5} for glass beads and 0.25×10^{-5} to 2.5×10^{-5} for catalyst. Hence, predicted values for upflow could not be obtained from this modeling approach either. Either approach could be used in principle, but the equations would have to be solved numerically for the appropriate range of values of the dimensionless groups.

4.6 Modeling pressure drop behavior

A plot of the dimensionless pressure drop build-up versus specific deposit with glass beads for upflow and downflow operation is shown in Fig. 4.18. These data show that there was a difference in build-up of the pressure drop at the same velocity for opposing directions. This difference was greatest for the lower values of Re, with almost no difference for Re = 0.5. Note that there was no capture for Re = 0.75 and 1.0 for upflow. Ison and Ives (1964) conducted experiments for removing kaolinite particles from an aqueous medium in a bed of gravel for both upflow and downflow operation. Gravity was found to be the dominant mechanism for particle removal. Although, there was no mention of pressure build-up in their work, photographs of the deposit in the upflow and down indicated that the pattern of deposition we different for the two cases. In general, gravity and Van der Waals attraction are more i   t lower velocities than at higher velocities, as can be seen by the definition of N_G in Equation 2.19. The data of Fig. 4. along with the results of Ison and Ives (1964), suggest that the structure of deposits, and hence the change in pressure drop increasing with the specific deposit, depends on the magnitude of the gravity number.

Several researchers have reported the inability of Ergun's equation to predict the change in pressure drop due to deposition. For the purpose of comparison, a modified Ergun's equation (smooth coating model), given by Equation 2.36, was used to compare with the experimental data. As can been seen from Fig. 4.19, the smooth coating model predicts only a 5% increase in the pressure drop over the initial value, compared to the observed increase of up to 30% (and upto 80% for Re = 0.1).
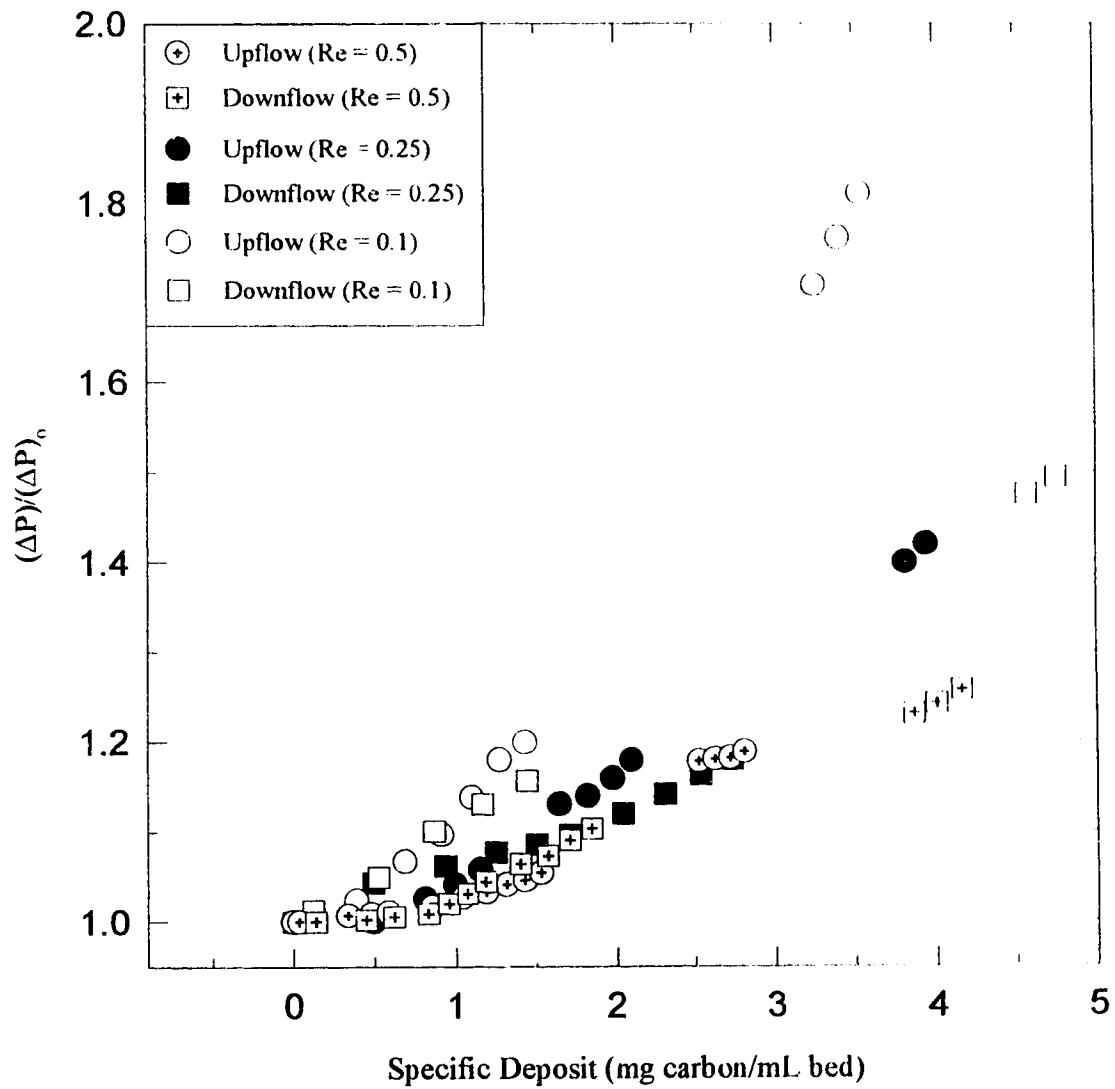
Fig. 4.13 Effect of flow direction on pressure drop build-up with glass beads
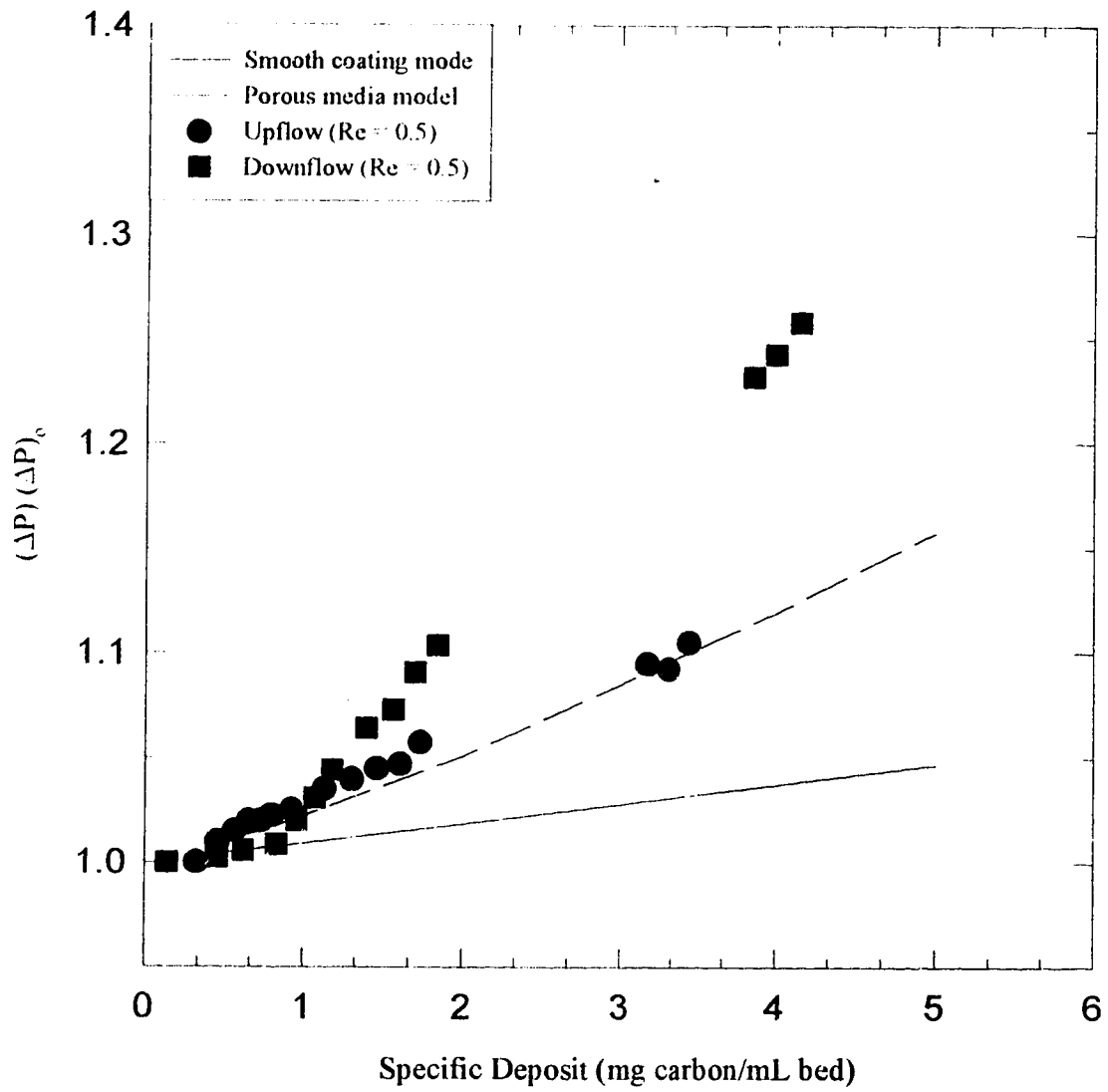
Fig. 4.'9 Comparison of experimental data to smooth coating model (Equation 2.31)
and porous media model (Equation 4.9) for glass beads at Re = 0.5

An attempt was made to correct the pressure drop for deposition of particles by modeling the pore spaces within the packed bed as a porous medium. Darcy's law relates the permeability of the porous medium, k, to the pressure drop across it as

$$\frac{\Delta P_{deposit}}{L} = \frac{\mu U_\infty}{k}$$

(4.6)

This pressure drop corresponds to that developed within the pore spaces and therefore due to the deposit within these spaces. In the absence of any deposit, the permeability k tends to infinity, thereby reducing $(\Delta P)_{deposit}$ to zero.

The total pressure drop across the bed is assumed to be a linear combination of the pressure drop due to the deposit and due to the packed bed.

$$\frac{\Delta P}{L} = \frac{\Delta P_{packing}}{L} + \frac{\Delta P_{deposit}}{L}$$

(4.7)

The pressure drop due to the packing is given by Ergun's equation for a clean bed. Therefore, to evaluate the total pressure, we require an expression to predict permeability as a function of the mass of deposit within the porous medium. This was achieved using Happel's model (Happel, 1958) to predict the permeability, which is given as

$$k = \frac{-d_p^2}{16c}[\ln c + (1 - c^2)/(1 + c^2)]$$

(4.8)

where c is the volume fraction of the deposit within the pores and d_p is the diameter of the particles in the suspension.

Combining equations 4.6 and 4.7, the normalized pressure drop build-up was calculated as

$$\frac{(\Delta P)}{(\Delta P)_o} = 1 + \frac{\mu U_\infty / k}{(\Delta P)_o / L}$$

(4.9)

where $(\Delta P)_o$ is $(\Delta P)_{packing}$ from Ergun's equation.

A comparison of the prediction of the porous media model with experimental data shows that although the developed model is an improvement over the smooth coating model, it still however underestimates the change in pressure drop.

Another approach was to model the change in the pressure drop by modifying Ergun's equation. In the smooth coating model, the deposit was assumed to form a layer on the collector, thereby increasing the diameter of the collector. By such an assumption, we assume that there is no liquid flow in the spaces between the deposited particles, when in fact there would be flow and concomitant pressure drop due to flow of liquid in this space (as seen from Fig. 4.20).

Following this view of particle deposits, the effective diameter of the collector was defined as the 'hydraulic' diameter, based on the ratio of volume to surface area of the collector.

$$d_{co} = \frac{6V_{co}}{S_{co}} \tag{4.10}$$

When carbon black particles deposit on the collector, we have

$$d_c = 6\frac{V_{co} + V_d}{S_{co} - \alpha S_d + (1 - \alpha)S_d} \tag{4.11}$$

where α is the fraction of the surface of a particle that is occluded due to contact with the collector and other particles. The occlusion parameter α ranges from 0 to 0.5.

Deposition of carbon black onto carbon black would further increase the hydraulic diameter, following Equation 4.11. The volume occupied by the deposit V_d and surface area of the deposit S_d can be calculated from the specific deposit of the bed. Derivations of the expressions of the four terms (V_{co}, S_{co}, V_d and S_d) in Equation 4.11 are shown in Appendix A8. The extent of occlusion is unknown, therefore, the estimated increase in pressure drop due to carbon deposits on the surface of the collector by this approach is represented by a region where the higher bound of the pressure drop assumes no occlusion of the active surface area by the depositing particles ($\alpha = 0$) and the lower bound for the increase in pressure drop is for greater occlusion of the available surface area by the deposited particles (in this case $\alpha = 0.25$). It has been assumed that up to half the surface

71
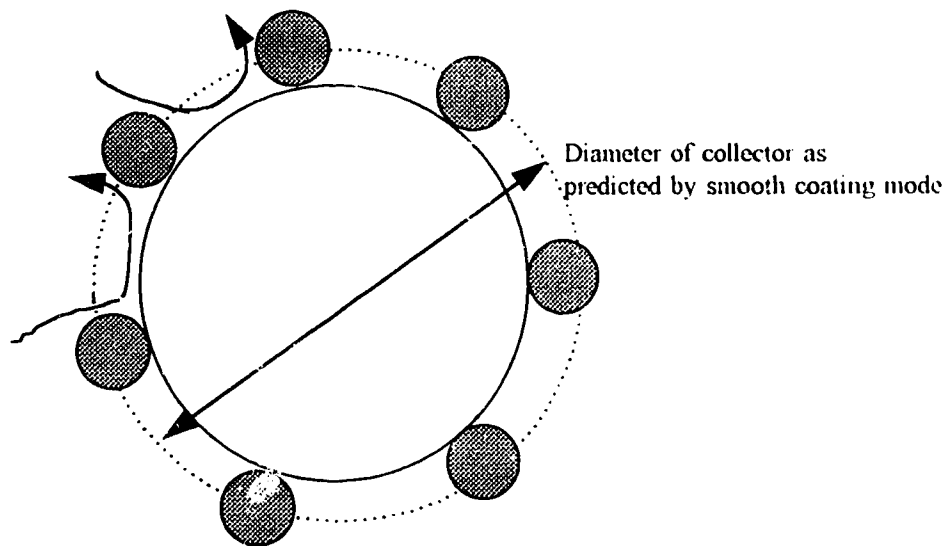
Fig. 4.20 Surface available for liquid contact for calculation of hydraulic ۔ameter

area of a single particle may not be in contact with the flowing fluid because a single particle of carbon may occlude surface (on the collector or on another carbon particle) equal to a quarter of its own surface. This model, called the 'hydraulic diameter' model, has been compared to the experimental data in Fig. 4.21.

None of the three models predicted any dependence of $\Delta P/(\Delta P)_o$ on velocity, because none of the models allowed for the kind of structure obtained, as illustrated in Fig. 4.14. The deposits at higher values of Re had an appearance similar to Fig 4.20, and the hydraulic diameter model was able to span the observed data at $0.25 \leq Re \leq 0.5$ depending on the choice of the occlusion parameter α.

The limitations of the hydraulic parameter could be overcome by adding another term for pore blockage by deposits as illustrated in Fig. 4.14, for example :

$$\frac{\Delta P}{L} = \frac{\Delta P_{packing}}{L} + \frac{\Delta P_{deposit}}{L} + \frac{\Delta P_{pore}}{L} \qquad (4.12)$$

The data of Fig. 4.18 suggest that the contribution due to formation of structural deposits in the pores would be negligible for specific deposit < 0.8 mg/mL. Such a model would require more adjustable parameters in addition to α. In order to model the data of Fig. 4.18 completely, the expression would need to include dependence on the gravity number N_G, thereby including the dependence of $\Delta P/(\Delta P)_o$ on both direction and velocity of liquid flow.

73
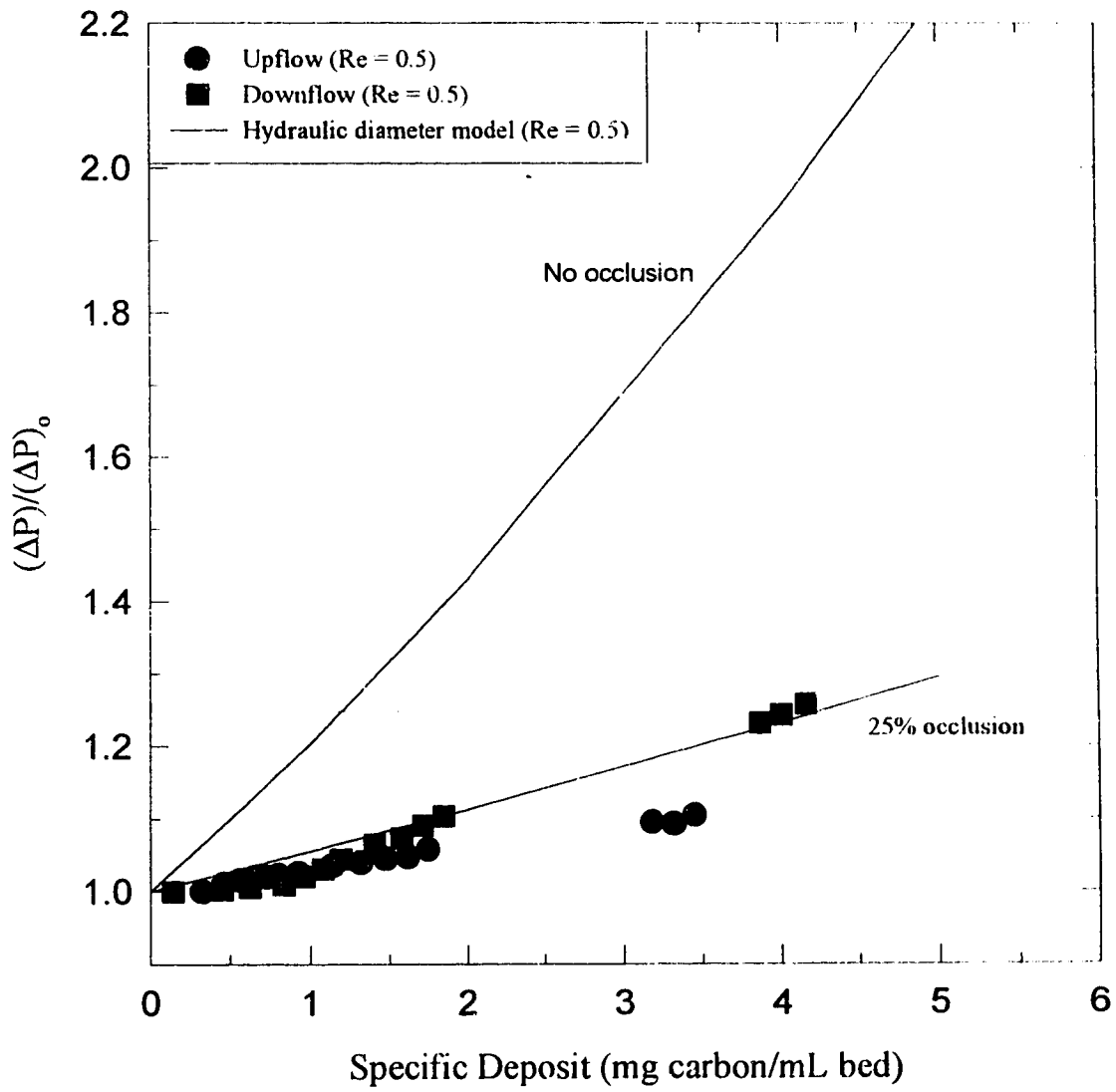
Fig. 4.21 Comparison of 'hydraulic diameter' model to experimental data with glass beads at Re = 0.5

Chapter Five

Conclusions and Recommendations

This final chapter summarizes the results of this study.

The first conclusion is that the filter coefficient and pressure drop data are independent of the concentration of the suspension when other operating variables were held constant from experiment to experiment.

The steady state filter coefficient was found to increase with decreasing fluid velocity. The capture of particles from a single phase liquid feed can be reduced by increasing the liquid flow rate.

The direction of flow of the liquid stream through the packed bed also affected the particle capture. It was observed that the efficiency of capture of the particles in a suspension (as shown by the steady state filter coefficients) was greater when the direction of flow was downward as opposed to upward flow, at the same liquid velocity. The capture for downflow was aided by gravity, since the gravitational force and the flow are in the same direction.

The increase in the pressure drop during each experiment was unexpectedly high for the amount of carbon deposited in the bed. Attempts to use Ergun's equation to model the change in the pressure drop were found to be inadequate. The porous media model was found to be an improvement over Ergun's equation. The use of the 'hydraulic diameter' model to predict the pressure drop increase seemed to be more successful in modeling the change in pressure drop at high flow rates.

The experiments revealed that the increase in the pressure drop is dependent on the liquid velocity. Photographs of the deposits disclosed a 'web-like structure' in the pores at low velocities. Such a structure was absent at high velocities. The presence of the 'web-like' structure would give rise to an additional pressure drop. This study did not attempt to model the pressure drop contribution due to such a structure. The structure of the deposit with catalyst as packing was viewed only for downflow. In order to be able to model the

pressure drop, it is necessary to know the effect of flow direction and velocity on the structure of the deposit, and how the structure of the deposit affects the pressure drop. Further experiments need to be planned for the purpose.

This work has given an insight into the capture of particles from a liquid hydrocarbon feed onto a packed bed. In order for this work to be applicable to the hydrotreaters, when the problem was first observed, experiments have to be performed for a two-phase feed and subsequently at hydrotreater conditions.

Bibliography

Amirtharajah, A. (1988) "Some theoretical and conceptual views of filtration", *J. Am. Water Works Assoc.*, 80(12), 36-46.

Byers, C.H. and Amarnath, A. (1995) "Understand the potential of electro-separations", *Chem. Eng. Prog.*, 91(2), 63-69.

Chan, E., Chung, K., Schiewe, W and Anderson, S (1993) "Packed Bed Pressure Drop Studies", Syncrude Canada Ltd. Research Report 93-5, June 1993.

Chowdiah, P., Wasan, D.T. and Gidaspow, D. (1982) "Electrokinetic phenomena in the filtration of colloidal particles suspended in non-aqueous media", *AIChE J.*, 27, 975-984.

George, H.F. and Poehlein, G.W. (1974) "Capture of aerosol particles by spherical collectors", *Env. Sci. Tech.*, 8, 46-48.

Fitzpatrick, J.A. and Spielman, L.A. (1973) "Filtration of aqueous latex suspensions through beds of glass Spheres", *J. Colloid Interface Sci*, 43(2), 350-369.

Happel, J. (1958) "Viscous flow in multiparticle systems : Slow motion of fluids relative to beds of spherical particles", *AIChE J.*, 4, 197-201.

Hunter, R.J. (1981) "Zeta Potential in Colloid Science", Academic Press, London, .

Ives, K.J.(1975) "Capture mechanisms in filtration" in *The Scientific Basis for Filtration*, ed. Ives, K.J., Noordhoff International Publishing, Leyden.

Ison, C.R. and Ives, K.J. (1964) "Removal mechanisms in deep bed filtration", *Chem. Eng. Sci.*, 24, 717-729.

Iwasaki, T. (1937) "Some notes on sand filtration", *J. Am. Water Works Assoc.*, 29, 1591-1602.

Kitahara, A., Fujii, T. and Katano, S. (1971) "Dependence of ζ-potential upon particle Size and capillary radius at streaming potential study in nonaqueous media", *Media. Bull Chem Soc Japan*, 44, 3242-3245.

Klinkenberg, A. and Van der Minne, J.L. (1957) "Electrostatics in the Petroleum Industry", Elsevier Publishing Company, Amsterdam.

Koyama, H., Nagai, E., Torii, H., and Kumagai, H. (1995a) "Japanese refiner solves problems in resid desulfurization unit", *Oil Gas J.*, 93(46), 82-90.

Koyama, H., Nagai, E., Torii, H., and Kumagai, H. (1995b) "Simple changes reduce catalyst deactivation, pressure-drop buildup", *Oil Gas J.*, 93(47), 68-71.

Maroudas, A. and Eisenklam, P. (1964) "Clarification of suspensions: a study of particle deposition in granular media-Part I", *Chem. Eng. Sci.*, 20, 867-873.

Masliyah, J.H. (1994) "Electrokinetic Transport Phenomena", Alberta Oil Sands Technology and Research Authority, Edmonton.

McCabe, W.L. and Smith, J.C. (1985) "Unit Operations of Chemical Engineering", McGraw-Hill Inc., New York.

Mehter, A.A., Turian, R.M., and Tien, C. (1970) "Filtration in deep beds of granular activated carbon", Research Report No. 70-3, FWPCA Grant No. 17020, OZO, Syracuse University.

Nielsen, K.A. and Hill, J.C. (1976) "Collection of inertialess particles on spheres with electrical forces", *Ind. Eng. Chem. Fund.*, 15, 149-157.

Rajagopalan, R. and Tien, C. (1976) "Trajectory analysis of deep-bed filtration with the sphere-in-cell porous media model", *AIChE J.*, 22, 523-533.

Spielman, L.A., and Fitzpatrick, J.A. (1973) "Theory for particle collection under london and gravity forces", *J. Colloid Interface Sci.*, 43, 606-623.

Tian, C. and Guthrie, R.I.L. (1995), "The dynamic process of liquid metal filtration", *Light Met.* 1995, 1263-1272.

Tien, C.(1989), "Granular Filtration of Aerosols and Hydrosols", Butterworths, Boston.

Tien, C., Turian, R.M., and Pendse, H. (1979) "Simulation of the dynamic behavior of deep bed filters", *AIChE J.* 25, 385-395.

Thomas, J.W and Yoder, R.E. (1956) "Aerosol size for maximum penentration through fiberglas and sand filters", *AMA Arch. Ind. Health*, 13, 545-550.

Treybal, R.E. (1980) "Mass-Transfer Operations", McGraw-Hill Book Co., Singapore.

Van der Hoeven, PH.C. and Lyklema, J. (1992) "Electrostatic stabilzation in non-aqueous media", *Adv. Coll. Inter. Sci.*, 42, 205-277.

Vogel, A.I. (1961) "Textbook of Quantative Inorganic Analysis", Longmans Gressn and Co. Ltd., London.

Appendix A1

Surfactants Tested

This appendix lists the surfactants used and their effect in terms of stability of the carbon suspension in kerosene as well as the electrical resistance of the surfactant with kerosene. The effect of stability of the carbon suspension was checked only when there was a significant reduction in the electrical resistance of the kerosene. Stability was indicated by the fact that little or no carbon settled to the bottom of a beaker containing the suspension.

Name of Surfactant	Electrical Resistance of Surfactant + Kerosene solution (Ω-m)	Effect on Stability of Carbon in Suspension
No surfactant	6.13×10^9	Stable upto 6 hr.
Tetrabutylammonium Iodide (5 mmol/L)	2.71×10^9	Unstable
Champion X897 (15mL/L)	3.02×10^9	Unstable
Antarox PGP 18-2(15mL/L)	15.13×10^9	-
Antarox PGP 18-	93×10^9	-
Antarox L-6	11×10^9	-
AOT (4	$\times 10^9$	-
AOT in mmol/L)	$)^9$	Stable for 10 hr.
AOT in Decane (6 mmol/L)	9.55×10^9	-
AOT in n-Heptane (6 mmol/L)	16.31×10^9	-

Table A1 Surfactants tested and their properties

Appendix A2

Calibration of Differential Pressure Cell

This appendix gives the calibration of the differential pressure (DP) cell. The DP cell was calibrated for 0-38 cm. water in terms of 4-20 mA when glass beads were used as packing. For catalyst, where lower pressure drops were obtained, the DP cell was calibrated for 0-19 cm. The linear regression for two cases is shown in Fig. A2.
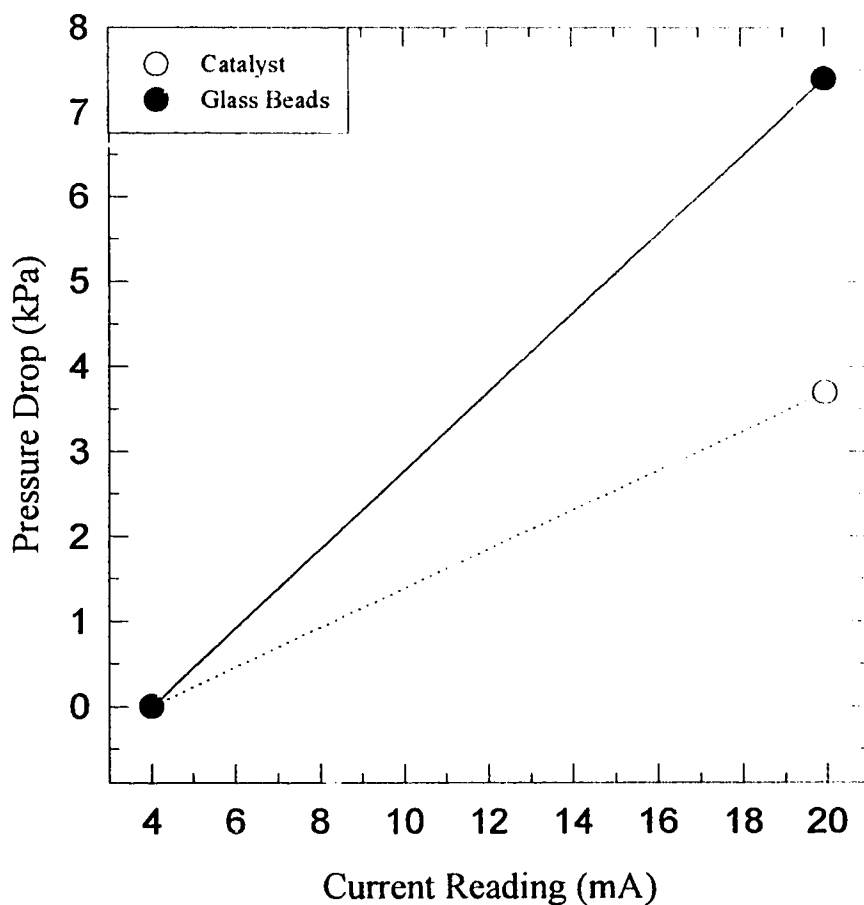
Fig. A2 Calibration of differential pressure (DP) cell

$(\Delta P)_{glass\ beads}$ (cm. water) = 4.763 × (mA) - 19.05

$(\Delta P)_{catalyst}$ (cm. water) = 2.382 × (mA) - 9.525

Appendix A3

Calibration of Metering Pump

The flow rate of the metering pump could be adjusted using the current input signal from 4-20 mA or the adjustment ring which was calibrated from 0-4.5 turns for the maximum flow rate. For convenient control of the flow rate, the adjustment ring was turned to its maximum (i.e. 4.5) and only the current signal was used to adjust the flow rate. The flow rate was evaluated by measuring the volume of the liquid collected for a given time interval. This was repeated three times for each input current signal. The calibration curve is shown in Figure A3.
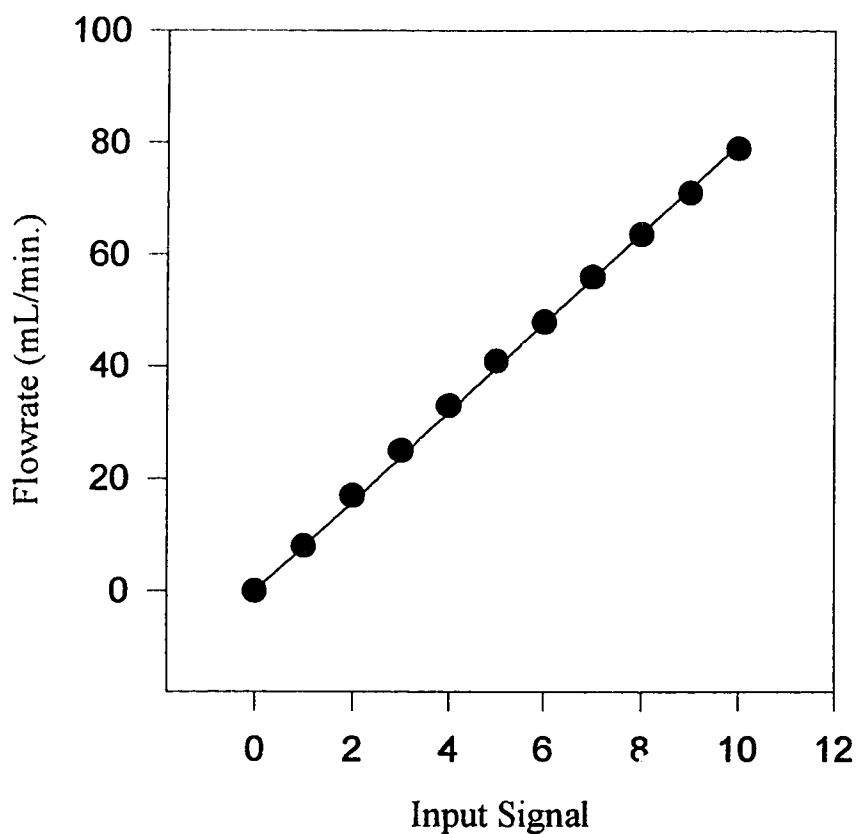
Fig. A3 Calibration curve for metering pump

The regression for the curve is

Flow rate (mL/min.) = 8 × Input signal

Appendix A4

Analysis of Carbon Cu .entration in Suspension

The concentration of the carbon suspension was monitored by using UV spectrophotometry at a wavelength of 550 nm. It was based on the principle of turbidimetry. Particles in suspension may absorb and/or reflect light which is incident on it. The intensity of the transmitted light is a measure of the amount of light absorbed which in turn is related to the number of particles in the suspension as

$$ln\left(\frac{I_t}{I_i}\right) = -\delta Cl \qquad (A4.1)$$

where δ is the extinction coefficient which is a characteristic of the system, C is the concentration of suspension and l is the length of the cell in which the suspension is taken. Equation A4.1 is called Beer-Lambert's Law (Vogel, 1961). δ and l can be lumped together as δ'. The term $-ln(I_t/I_i)$ is called the absorbance A. Therefore, one can write

$$A = \delta' C \qquad (A4.2)$$

It is possible to evaluate δ' by measuring the absorbance of solutions of different known concentrations. The calibration curve in Fig. A4 is a plot of A versus C where the concentration of the solutions were known because the solutions were prepared gravimetrically.

δ' was found to be 82.724 $(mg/L)^{-1}$.
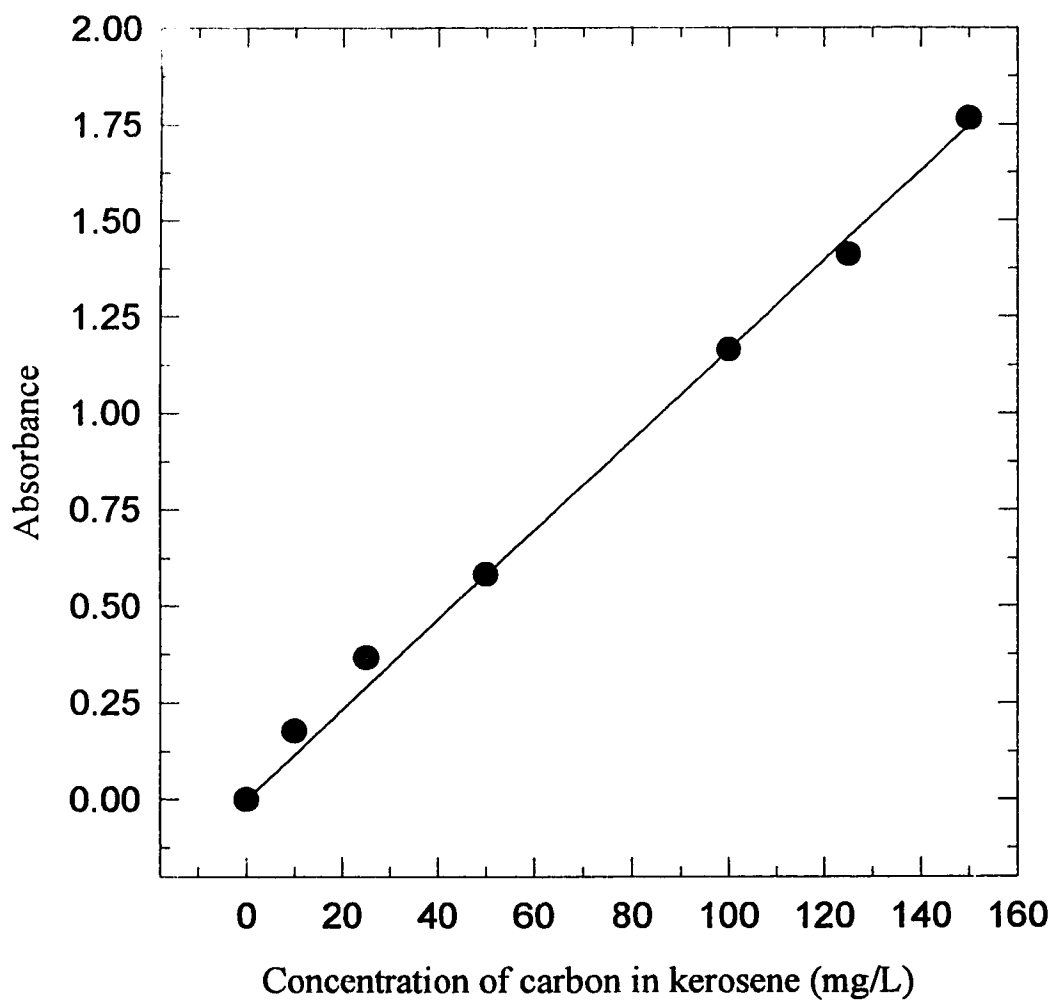
Fig. A4 Calibration curve for suspension of carbon in kerosene using spectrophotometry

Appendix A5

Calculation of Specific Deposit from the Raw Data

The specific deposit is the mass of particles deposited per unit volume of the bed. The specific deposit is, therefore, a function of time and the concentration of the streams entering and leaving the packed section.

A mass balance for the entire packed column is given by

Mass entering the column during a time Δt - Mass leaving the column during the same time = Mass deposited in the packed column

$$QC_i\Delta t - QC_o\Delta t = V\Delta\sigma \qquad (A5.1)$$

$$Q(C_i - C_o)\Delta t = V\Delta\sigma \qquad (A5.2)$$

Taking the limit as $\Delta t \to 0$

$$\frac{d\sigma}{dt} = \frac{Q}{V}(C_i - C_o) \qquad (A5.3)$$

On integrating with respect to time, we obtain

$$\sigma = \frac{Q}{V}\int_o^t (C_i - C_o)dt \qquad (A5.4)$$

The integral term can be evaluated by plotting $(C_i - C_o)$ against time. The area under the curve up to a time t gives the mass that has been deposited in the bed upto that time.

The following table gives the raw data for an experiment for the simple case of single pass with upward flow through the packed bed under the following conditions :

Packing = Glass beads

Re = 0.5

C_{io} (Concentration of inlet stream at time t = 0) = 131 mg/mL

85

Time(hr.)	C_o(mg/L)	C_i-C_o(mg/L)	σ(mg/mL)
0.25	19.0	112.02	0.00
0.50	82.21	48.81	0.3217
0.75	102.21	28.81	0.4769
1.00	105.87	25.15	0.5848
1.25	112.21	18.81	0.6727
1.50	116.41	14.61	0.7396
1.75	118.13	12.89	0.7516
2.00	115.21	15.81	0.8520

Table A5 Raw data from an experiment for calculation of specific deposit
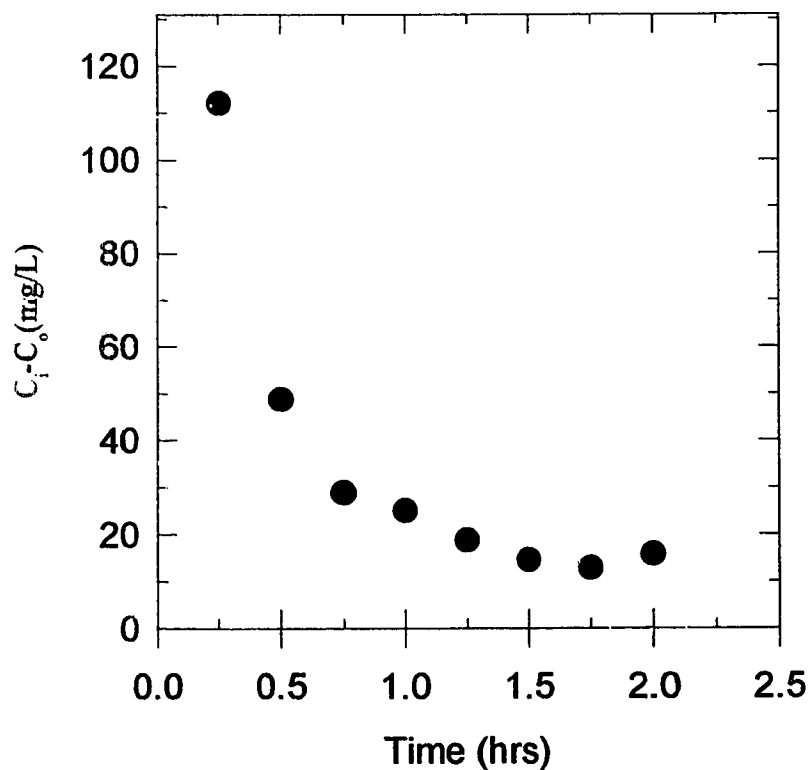
Figure A5 Plot of $(C_i$-$C_o)$ versus time for calculation of specific deposit

Appendix A6

Monolayer Calculation for Carbon Particles on Glass Beads

Diameter of column, D_{col}	= 0.0254 m.
Length of column, L	= 0.30 m.
Diameter of glass beads, d_c	= ?.?) × 10^{-3} m.
Diameter of carbon particles, d_p	= 8 × 10^{-6} m
Porosity of clean bed, ε_o	= 0.37
Density of carbon black, ρ_p	= 1900 kg/m^3

a) Surface area of glass beads

Volume of glass beads = Volume of Packed column × $(1 - \varepsilon_o)$

$$N \frac{\pi}{6} d_c^3 = \frac{\pi}{4} D^2 L \times (1 - \varepsilon_o)$$

$$N = \frac{3D^2 L (1 - \varepsilon_o)}{d_c^3}$$

Surface area of glass beads = $N \pi d_c^2$

b) Mass of carbon for monolayer

Crosssectional area of a particle = Area of the collector that is occluded

Figure A6 Area occluded by depositing particles

Assuming that the carbon particles are spherical, one can write

Surface area of one glass bead $\approx$ n (cross sectional area of one carbon particle)

$$\pi d_c^2 = n \frac{\pi d_p^2}{4}$$

$$n = \frac{4 d_c^2}{d_p^2}$$

Mass of carbon particles per bead = n (Mass of one carbon particle)

Total mass of deposit in bed = N (Mass of carbon particles/bead)
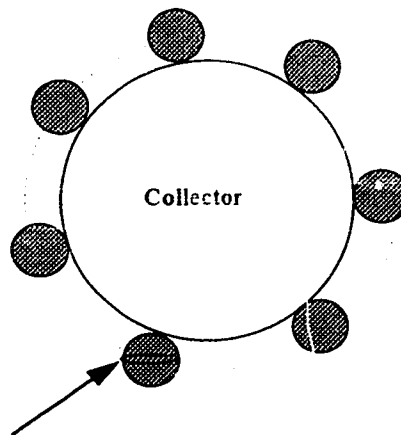
Specific deposit = Total mass of deposit in bed/Volume of bed

$$\text{Specific deposit} \quad = \frac{Nn\left(\rho_p \pi d_p^3/6\right)}{V_{bed}} = \frac{\left(3D^2 L(1-\varepsilon_0)/2d_c^2\right)\left(4d_c^2/d_p^2\right)\left(\rho_p \pi d_p^3/6\right)}{\pi D^2 L}$$

$$= \frac{(1-\varepsilon_0)\rho_p d_p}{d_c}$$

$$= 10.6 \text{ mg carbon/mL bed}$$

The value for specific deposit corresponding to a monolayer is much less than the value of 0.8 mg/mL at which the steady state filter coefficient is attained.

Appendix A7

Statistical Analysis on Steady State Filter Coefficient Versus Specific Deposit Plot for Catalyst

Calculations for upflow :

U_∞(cm/s)	X(ln(U_∞))	λ_{ss}(cm^{-1})	Y_1(ln(λ_{ss}))	$\hat{Y}_1$
0.0263	-3.6382	0.015	-4.1997	-4.1
0.0658	-2.723	6.2e-3	-5.0832	-5.37
0.1315	-2.0287	1.36e-3	-6.6003	-6.334
0.1973	-1.623	1.1e-3	-6.8124	-6.897

Y_1 is regressed versus X to get the slope $\beta_{1,1}$ and intercept $\beta_{1,0}$.

$\beta_{1,1} = -1.388; \beta_{1,0} = -9.15$

$\hat{Y}_1$ is defined as $\beta_{1,0} + \beta_{1,1} X$

$\overline{X}$ = average of X = -2.5032

$$SS_{xx} = \sum_{i=1}^{n}(X_i - \overline{X})^2 = 2.3364$$

$$SSE = \sum_{i=1}^{n}(Y_{1,i} - \hat{Y}_{1,i})^2 = 0.17$$

$$s = \left(\frac{SSE}{n-2}\right)^{1/2} = 0.292$$

$$S_{\beta_1} = \frac{s}{(SSE)^{1/2}}$$

For a confidence of $(1-\alpha)$, the confidence interval is $\beta_1 \pm t_{\alpha/2}(n-2) \cdot S_{\beta_1}$

Confidence	80%	90%	95%	98%
$t_{\alpha/2}$	1.8857	2.9200	4.3027	6.9646
Interval	(-1.75,-1.03)	(-1.95,-0.83)	(-2.21,-0.566)	(-2.67,-0.109)

Calculations for downflow

U_α(cm/s	$X(\ln(U_\alpha))$	λ_{ss}(cm^{-1})	$Y_2(\ln(\lambda_{ss}))$	$\hat{Y}_2$
0.0263	-3.6382	0.0168	-4.086	-3.991
0.0658	-2.723	6.2e-3	-5.083	-5.157
0.1315	-2.0287	2.5e-3	-5.991	-6.0416
0.1973	-1.623	1.88e-3	-6.276	-6.5584
0.263	-1.336	7.2e-4	-7.236	-6.9241

Y_2 is regressed versus X to obtain the slope $\beta_{2,1}$ and intercept $\beta_{2,0}$.

$\beta_{2,1} = -1.27218; \beta_{2,0} = -\varkappa$

$\hat{Y}_2$ is defined as $\beta_{2,0} + \mu$

$\overline{X}$ = average of X = -2.2698

$SS_{xx} = \sum_{i=1}^{n}(X_i - \overline{X})^2 = 3.43$

$SSE = \sum_{i=1}^{n}(Y_{2,i} - \hat{Y}_{2,i})^2 = 0.194$

$s = \left(\dfrac{SSE}{n-2}\right)^{1/2} = 0.254$

$S_{\beta_1} = \dfrac{s}{(SSE)^{1/2}} = 0.137$

For a confidence of (1-α), the confidence interval is $\beta_{21} \pm t_{\alpha/2}(n-2) \cdot S_{\beta_1}$

Confidence	80%	90%	95%	98%
$t_{\alpha/2}$	1.6377	2.3534	3.1824	4.5407
Interval	(-1.75,-1.03)	(-1.95,-0.83)	(-2.21,-0.566)	(-2.67,-0.109)

Appendix A8

Hydraulic Diameter Model

Ergun's equation for calculating the pressure drop is given by

$$\frac{\Delta P}{L} = \frac{150(1-\varepsilon)^2 \mu U_\infty}{\varepsilon^3 d_c^2} + \frac{1.75 \rho U_\infty^2 (1-\varepsilon)}{d_c \varepsilon^3} \tag{A8.1}$$

The only variables that change with time are ε and d_c. Change in ε can be incorporated knowing the specific deposit in the bed.

$$\varepsilon = \varepsilon_o - \frac{\sigma/\rho_d}{1-\varepsilon_d} \tag{A8.2}$$

If the deposit forms a smooth coating on the collector, then the change in d_c is

$$\frac{d_c}{d_{co}} = \left(\frac{1-\varepsilon}{1-\varepsilon_o}\right)^{1/3} \tag{A8.3}$$

With increasing time, and decreasing porosity, one can predict the increase in the diameter of the collector. Fig. 4.19 in Chapter Four showed that the net result was a small decrease in $(\Delta P)/L$, well below the observed values. Furthermore, microscopy did not support the deposition of a smooth layer. As can be seen from Ergun's equation, an increase in the diameter results in a decreased pressure drop and hence this modification does not help account for the increase in pressure drop.

As discussed in Section 4.6, there is an effective decrease in the 'hydraulic diameter' of the collector due to an increase in surface area due to the deposited particles which accounts for the increase in pressure drop. The volume and surface area of the collector glass beads are given as :

$$V_{co} = V_{bed}(1-\varepsilon_o) \tag{A8.4}$$

$$S_{co} = \frac{V_{co}}{\pi d_{co}^2/6}\pi d_{co}^2 = \frac{6V_{bed}(1-\varepsilon_o)}{d_{co}} \tag{A8.5}$$

The volume occupied by the deposit in the bed is given by

$$V_d(t) = \frac{\sigma(t)V_{bed}}{\rho_d}$$

(A8.6)

The surface area occupied by the particles in the bed is given by

$$S_d(t) = \frac{6V_{bed}\sigma}{\rho_d d_p}$$

(A8.7)

Therefore, the hydraulic diameter of the collector, when α is the fraction of the surface of a particle that is occluded due to contact with the collector and the other particles, is

$$d_c = 6\frac{V_{co} + V_d(t)}{S_{co} - \alpha S_d(t) + (1-\alpha)S_d(t)} = 6\frac{V_{co} + V_d(t)}{S_{co} + (1-2\alpha)S_d(t)}$$

$$d_c = 6\frac{\left(V_{bed}(1-\varepsilon_o)\right) + \left(\sigma(t)V_{bed}\big/\rho_d\right)}{\left(6V_{bed}(1-\varepsilon_o)\big/d_{co}\right) + (1-2\alpha)\left(6V_{bed}\sigma(t)\big/d_p\rho_d\right)}$$

$$d_c = d_{co}\left(\frac{(1-\varepsilon_o) + \left(\sigma\big/\rho_d\right)}{(1-\varepsilon_o) + (1-2\alpha)\left(\sigma d_{co}\big/d_p\rho_d\right)}\right)$$

(A8.8)

92

Appendix A9

Porosity of a Clean Bed

To find the porosity of the clean bed, the following procedure was adopted:

1. A measuring cylinder was filled with packing (glass beads or catalyst) up to a volume of 20 mL.

2. Kerosene solution from a measuring cylinder was poured into the section containing the packing. From the volume of kerosene solution remaining, it was possible to know the amount of kerosene required to fill the pore space of the packing.

3. The porosity of clean bed is calculated by

$$\varepsilon_o = \frac{V_{soln.\,in\,pores}}{V_{packing\,in\,cylinder}}$$

4. For the case of catalyst as packing, it was found that kerosene was absorbed by the catalyst due to its internal porosity. Therefore, once kerosene was poured into the measuring cylinder till it covered the packing, the volume of the kerosene that could be poured back out was measured and this was used in the numerator of the above equation to evaluate porosity.

$$\varepsilon_o \text{ (glass beads)} = 0.37$$

$$\varepsilon_o \text{ (catalyst)} = 0.42$$

Appendix A10

Hamaker Constant Evaluation

The dispersive interaction between two separate particles is given by the Hamaker constant (Masliyah, 1994). The Hamaker constant between two particles of the same material is positive, which means that the potential energy of interaction given by Equation A10.1 is always attractive (2 and 1 indicate the same material in this case).

$$V_A = \frac{-H_{12}}{12\pi r_{12}^2} \tag{A10.1}$$

The Hamaker constant between two dissimilar particles may be positive or negative indicating that a repulsive potential can occur in the presence of an intervening medium. The Hamaker constant is needed to evaluate the London-Van der Waal's dispersive force between two particles in the presence of an intervening medium.

The Hamaker constants for the pure components of the system under study are (Masliyah, 1994):

H_{11} (Kerosene) = 5.2×10^{-20} J

H_{22} (Carbon) = 45×10^{-20} J

H_{33} (Glass) = 8.8×10^{-20} J

H_{44} (Catalyst of oxides of metals) = 13.0×10^{-20} J

The Hamaker constant for interaction of a carbon particle with a carbon particle, glass and catalyst, respectively, in the presence of kerosene is

$$H_{212} = \left(H_{22}^{1/2} - H_{11}^{1/2}\right)^2 = 1.96 \times 10^{-19} \, J$$

$$H_{213} = \left(H_{33}^{1/2} - H_{11}^{1/2}\right)\left(H_{22}^{1/2} - H_{11}^{1/2}\right) = 3.04 \times 10^{-20} \, J$$

$$H_{214} = \left(H_{44}^{1/2} - H_{11}^{1/2}\right)\left(H_{22}^{1/2} - H_{11}^{1/2}\right) = 5.87 \times 10^{-20} \, J$$

The values for Hamaker constant were used to evaluate N_{Lo} in order to predict the filter coefficients according to Rajagopalan and Tien's equations. However, it was found that

since gravity was the dominant mechanism for deposition, it did not matter whether H_{212} or H_{213} (or H_{214}) was used in calculating λ_{pred}.

.

Appendix A11

Evaluation of Cell Constant

k_{cell} can be calculated from Equations A11.1.

$$k_{cell} = R_{KCl} \cdot \chi_{KCl}$$
(A11.1)

Specific conductivity of calibrating s 'lution χ_{KCl} = 10 Ω^{-1} m^{-1}

Measured properties :

R_{KCl} = 285 Ω

$\therefore k_{cell}$ = 2.85 × 10^3 m^{-1}

k_{cell} is used to find the specific conductivity of any solution by measuring the resistance of that solution within the packed bed.

Appendix A12

Calculation Of Zeta Potential Using Streaming Potential

Table A12.1 shows the data obtained during these measurements with glass beads and catalyst as packing. It was found that the voltage reading did not become completely steady but fluctuated within the range shown. The zeta potential by streaming potential measurements can be calculated according to Equation A12.1.

$$\zeta = \frac{\mu \chi_p}{\xi \xi_o} \frac{\Delta E}{\Delta P} \qquad (A12.1)$$

k_{cell} was found to be 2.85×10^3 m^{-1} from Appendix A11. Therefore, χ_p can be evaluated from the resistance of the solution within the packed bed as

$$\chi_p = k_{cell} / R_p \qquad (A12.2)$$

The physical properties of the system can be obtained from Appendix A14.

	Glass beads	Catalyst
Potential ΔE (volts)	11-14	94-100
Pressure drop ΔP (kPa)	0.0156	0.007
Re	0.05	0.023
Total Resistance R_p (Ω)	12.9×10^{12}	11.5×10^{13}
Zeta Potential (mV)	16	31

Table A12.1 Streaming potential results for glass beads and catalyst

97

Appendix A13

Evaluation of Diameter of Collector

Since the size of the glass beads and the catalyst varied within a large range, the diameter of the collector was calculated as follows :

The glass bead diameter was taken as the average within the range 850 - 1000 μm

d_c (glass beads) = 9.25 × 10^{-4} m

The catalyst diameter was calculated by equating the volume of a cylinder to that of a sphere :

$$\frac{\pi}{4} d_{cyl}^2 l = \frac{\pi}{6} d_{sph}^3 \qquad (A13.1)$$

The diameter of the catalyst is 1 mm while the length of catalyst ranges between 4 and 10 mm (average = 7 mm)

∴ d_c (catalyst) = 2.2 × 10^{-3} m

Appendix A14

Physical Properties of System

Temperature of system = 20 °C

Kerosene :

Density ρ = 800 kg m^{-3}

Viscosity μ = 2 × 10^{-3} Pa-s

Dielectric constant ξ = 2.5

Carbon Black :

Density ρ_p = 1900 kg m^{-1}

Particle diameter d_p = 8 × 10^{-6} m

Glass Beads :

Collector diameter d_c = 9.25 × 10^{-4} m

Happel's parameter A_S = 45.95

Catalyst :

Collector diameter d_c = 2.23 × 10^{-3} m

Happel's parameter A_S = 37.98

Appendix A15

Sample Calculation of Dimensionless groups

Sample calculations are shown for glass beads with flow at a superficial velocity of 2.63 × 10^{-4} m/s

Happel's parameter for an initial porosity of 0.37

$$A_s = \frac{2\left[1 - (1 - \varepsilon)^{5/3}\right]}{2 - 3(1 - \varepsilon)^{1/3} + 3(1 - \varepsilon)^{5/3} - 2(1 - \varepsilon)^2} = 45.95$$

Reynolds number

$$Re = \frac{d_c U_\infty \rho}{\mu} = \frac{(0.925 \times 10^{-3}) \times (2.63 \times 10^{-4}) \times 800}{2 \times 10^{-3}} = 0.098 \approx 0.1$$

Relative Size Parameter

$$N_R = \frac{d_p}{d_c} = \frac{8 \times 10^{-6}}{0.925 \times 10^{-3}} = 8.65 \times 10^{-3}$$

London Number

$$N_{Lo} = \frac{H}{9\pi\mu U_\infty a_p^2} = \frac{(3.04 \times 10^{-20})}{9\pi(2 \times 10^{-3}) \times (2.63 \times 10^{-4}) \times (4 \times 10^{-6})^2} = 12.8 \times 10^{-4}$$

Gravity Number

$$N_G = \frac{2a_p^2(\rho_p - \rho)g}{9\mu U_\infty} = \frac{2 \times (4 \times 10^{-6})^2 \times (2900 - 800) \times 9.8}{9 \times (2 \times 10^{-3}) \times (2.63 \times 10^{-4})} = 1.46 \times 10^{-4}$$

Brownian Diffusivity

$$D_{BM} = \frac{c_s kT}{3\pi\mu d_p} = \frac{1.16 \times (1.38 \times 10^{-23}) \times 293}{3\pi(2 \times 10^{-3}) \times (8 \times 10^{-6})} = 3.11 \times 10^{-14} m^2 / s$$

Peclet Number

$$N_{Pe} = \frac{U_\infty d_c}{D_{BM}} = \frac{(2.63 \times 10^{-4}) \times (0.925 \times 10^{-3})}{3.11 \times 10^{-14}} = 7.82 \times 10^6$$